Numerical Simulation of Heat Treatment Processes on Industrial Steel Parts

B. Lax
M. Cervera
M. Chiumenti

Monograph CIMNE Nº-84, March 2003

Numerical Simulation of Heat Treatment Processes on Industrial Steel Parts

B. Lax
M. Cervera
M. Chiumenti

Monograph CIMNE Nº-84, September 2003

INTERNATIONAL CENTER FOR NUMERICAL METHODS IN ENGINEERING
Gran Capitán s/n, 08034 Barcelona, Spain

INTERNACIONAL CENTER FOR NUMERICAL METHODS IN ENGINEERING
Edificio C1, Campus Norte UPC
Gran Capitán s/n
08034 Barcelona, Spain
www.cimne.upc.es

First edition: September 2003

NUMERICAL SIMULATION OF HEAT TREATMENT PROCESSES ON INDUSTRIAL STEEL PARTS
Monograph CIMNE M84

ISBN: 84-95999-40-4

Depósito legal: B-40327-2003

Contents

Chapter 1

Introduction

1.1 Motivation and Background

The business of philosophers, students and practical men today is to recreate a vision of the world.

The english mathematician and philosopher *A.N. Whitehall* made this remark more than fifty years ago. His image of those three groups stands for an idea which today is more discussed than ever: Application orientated science and - as the corresponding counterpart - a working reality which is eager to learn.

Whitehall's remark is an appeal not to assess technology merely by the meaning of its short-term costs and benefits. Instead, we have to consider its implication on a wide range of general drafts for the framework of the futural industrial and scientific developments. Cooperation between generalists and specialists, between scientist and technologists, between research and industry is demanded.

The great challenge of todays technology is it to work with constant relation to practice orientated problems, developing general solutions which can be applied to various problems. On the other hand, new developments in technology shall be transparent and easy to handle so that the idea is realizable by the applicants in the industry.

This is especially important for new developments in computational mechanics. New programs, developed by highly specialized scientists, will be adaptable to a wide range of industrial problems and will also be usable by

people specialized for example in manufacturing fields, who want to use these programs for their specific problems.

The aim of this work is to fullfill the given requirements: A finite numerical program, originally developed to solve a great variety of thermo-mechanical problems, was adapted to a specific industrial problem by a user who was confrontated for the first time with both the industrial problem and the developed computer program.

The International Center for Numerical Methods in Engineering (CIMNE) in Barcelona has developed a finite numerical model for coupled thermo-mechanical problems, focusing in the simulation of solidification processes of industrial metal parts. The program COMET (COupled MEchanical and Thermal analysis), developed by *Cervera*, *Agelet de Saracibar* and *Chiumenti* now will be used for the simulation of heat treatment processes.

Heat treatment is the operation of heating and cooling metal in its solid state to change its physical properties. Some heat treatments, such as rapid cooling (*quenching*), evoke high internal stresses due to the differential cooling of the metal piece. The basic requirement of successful design is to plan shapes and treatments in such a manner that the variation in temperature over the cross-section of the part is kept at a minimum during the heat treatment. The simulation of the heat treatment processes will help to find a suitable design for the metal piece of interest.

The Spanish company *Metalogenia* is producing high quality steel-teeth for excavators. The final microstructure *martensite*, reached by quenching the metal, is an extremely hard material. The process of quenching the special steel, used by *Metalogenia*, is simulated with COMET. The results give an insight into the material behaviour at any time of the proccess.

As a first step, the microstructural problem of the production of martensite has to be examined. To apply the program to the problem, the microscopic characteristics have to be expressed by the macro-characteristics material properties.

1.2 Overview

Chapter-2 gives a short introduction to the terminology used in Materials Science. The basic explanations reach as far as it is necessary to understand the microstructural processes taking place within the heat treatment

processes of interest. The special heat treatment processes which are used for the production of martensite are described.

Chapter-3 deals with the theoretical basis of the thermo-mechanical numerical program. It is shown how the heat treatment process is split into two parts, the thermal and the mechanical part, and how the coupling of the splits produces the final results.

Chapter-4 and *Chapter-5* show the numerical simulation of the cooling of a metal cylinder. This geometry is chosen to assess the applications of the program to the problem. The example is examined for several variations on the application for the elastic (*chapter 4*) and the elastoplastic case (*chapter 5*) to get information on the material behaviour and the program.

Chapter-6 contains a closer examination of the elasto-plastic case, the behaviour of a cube is observed.

In *Chapter-7* and *Chapter 8* the quenching process is applied to the geometry of various different excavator teeth. The geometrical characteristics are focussed in this chapter and an aditional example for the effects of design variation is given.

Chapter-9 contains some concluding remarks, summarizing the major results of this work. Moreover, suggestions for future research directions are presented.

Chapter 2

Heat Treatment

Heat treatment is the operation of heating and cooling metal in its solid state to change its physical properties. According to the procedure used, steel can be hardened or it can be softened. With the proper heat treatment internal stresses may be removed, toughness increased, or a hard surface produced over a ductile interior. The composition of the steel must be known since small percentages of certain elements, for instance carbon, greatly change the physical properties.

With heat treatment, the rate of cooling is the controlling factor; rapid cooling results in a hard structure, whereas very slow cooling produces the opposite effect.

Here, only three forms of heat treatment, *normalizing*, *hardening* and *tempering*, will be described, as they are used for the production of *tempered martensite*, the material, which is examined in this work.

2.1 Iron-Iron-Carbide Diagram

Under equilibrium conditions, the knowledge of steel and its structure is best summarized in the iron-iron-carbide diagram shown in *Figure 2.1*. Ranges in which structural changes occur are known as critical ranges.

Certain changes which take place at these critical ranges are called *allotropic changes*. Although the chemical content of the steel remains the same, its atomic structure is changed, and therefore, some properties dependent on this change as well. Principal among these are changes in electrical resistance, atomic structure and loss of magnetism. By definition, an al-

lotropic change is a reversible change in the atomic structure of the metal with a corresponding change in the properties of the steel. These critical ranges should be known, as most heat treating processes require heating the steel to a temperature above these ranges. Steel cannot be hardened unless it is heated to a temperature above the lower critical range and in certain instances above the upper critical range.

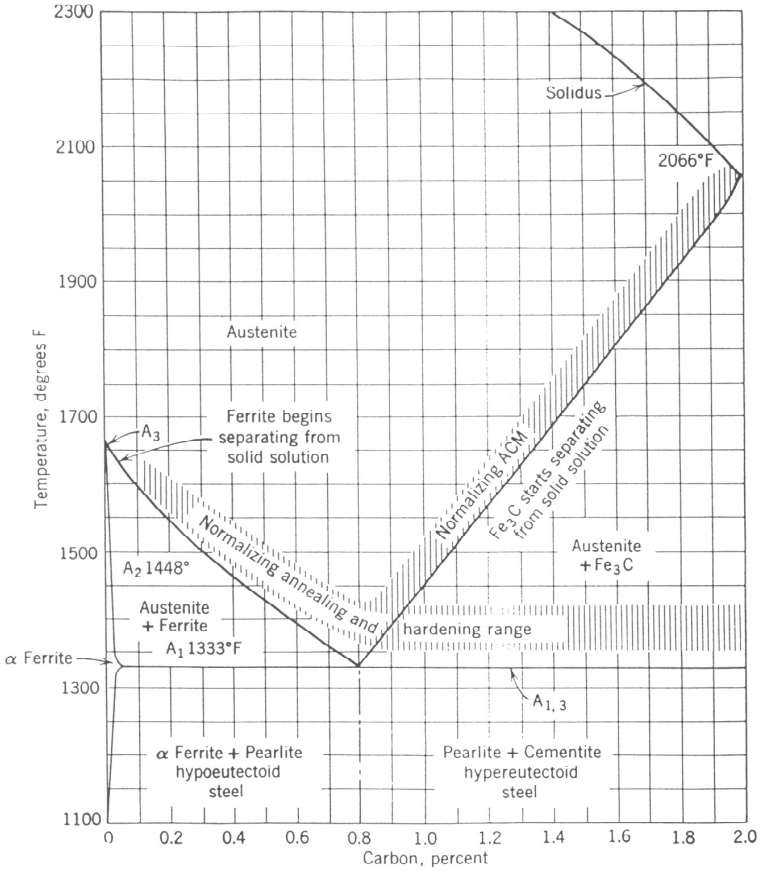

Figure 2.1: Partial Iron-Iron Carbide Diagram

This diagram (*Fig.2.1*), which applies only under slow cooling conditions, is known as a *partial iron-iron-carbide diagram.* The proper quenching temperatures for any carbon steel may be observed in this diagram.

So far as steel treating is concerned, the partial diagram is sufficient, since 2.0 % is the limit of carbon content in steel.

Consider a piece of 0.20 % carbon steel which has been heated to a temperature of around 900 °C. Above the A_3 range this steel is a solid solution of carbon in gamma iron and is called *austenite*. The iron atoms lie in a face-centered cubic lattice and are nonmagnetic. Upon cooling, the iron atoms start to form a body-centered cubic lattice below the A_3 range. This new structure being formed is called alpha iron or *ferrite* and it is a solid solution of carbon in alpha iron. The solubility of carbon in alpha iron is very much less than in gamma iron. As the steel is cooled to the A_1 line, it becomes magnetic and additional ferrite is formed. At the A_1 line the austenite that remains is transformed to a new structure called *pearlite*.

As the carbon content of the steel increases above 0.20 %, the temperature at which the ferrite is first rejected from the austenite drops until, at about 0.80 % carbon, no free ferrite is rejected from the austenite. This steel is called *eutectoid* steel and its structure is 100 % pearlite. The eutectoid point for any metal is the lowest temperature at which changes occur in a solid solution.

If the carbon content of the steel is greater than the eutectoid, a new line is observed in the diagram labeled A_{cm}. The line denotes the temperature at which iron carbide is first rejected from the austenite instead of ferrite. The iron carbide (Fe_3C) is known as *cementite* and it is extremely hard and brittle. Steels containing less carbon than the eutectoid are known as *hypoeutectoid* steels, and those with more carbon content are called *hypereutectoid* steels. All these iron-carbon alloys must be cooled slowly to produce the constituents just described.

2.2 Martensite

The essential ingredient of any hardened steel is martensite. A. Martens, a German scientist, first recognized this constituent about 1878. Martensite is obtained by rapid quenching of carbon steels and it is the transitional substance formed by the rapid decomposition of austenite. It is a supersaturated solution of carbon in alpha iron.

The hardness of martensite depends on the amount of carbon present and varies from Rockwell C47 to C67. It cannot be machined, it is quite brittle and strongly magnetic.

The maximum hardness obtainable for a given piece of steel depends on the carbon content. The maximum hardness obtained in any steel represents

the hardness of martensite and is approximately Rockwell C 66. A carbon content equal to, or close to 0.60 % is necessary to achieve this level.

To obtain maximum hardness, the carbon must be completely in solution in the austenite when quenched. The critical quenching rate, which is the slowest rate of cooling that will result in 100 % martensite, should be used.

2.3 The Time -Temperature -Transformation Diagram

The iron-iron-carbide phase diagram is useful in selecting temperatures for parts to be heated for various treating operations, and it also shows the type of structure to expect in slowly cooled steels. On the other hand, it does not give much information concerning effects of cooling rate and temperature on the final microstructure.

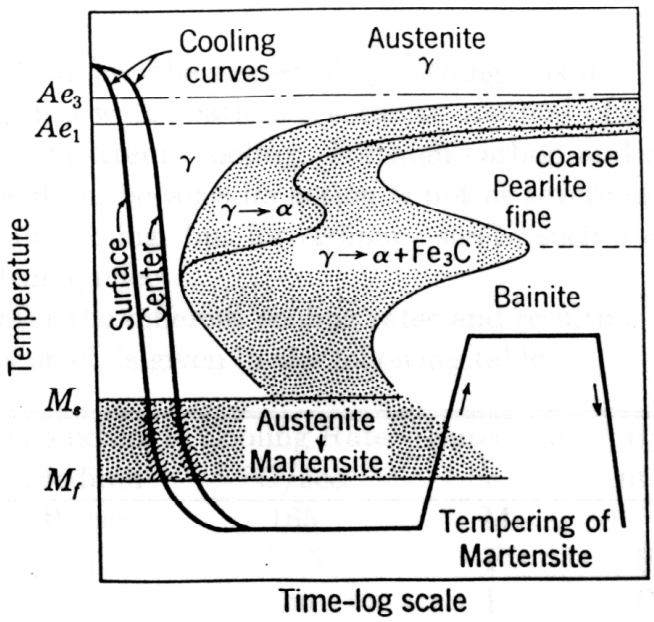

Figure 2.2: Transformation Diagram illustrating the formation of tempered martensite

Time-temperature-transformation diagrams have been developed which show this information. Figure 2 shows one of these diagrams, in it the way

austenitized steel changes if held at a constant temperature is indicated. Knowing this temperature, the times at which the transformation starts and ends may be determined and the resulting structure is indicated on the diagram. To obtain a martensitic structure, the steel must be quenched with sufficient speed so that the cooling curve does not intersect the "nose" of the transformation curve.

The general shape of the time-temperature-transformation curve differs for each steel depending on the carbon content, alloys present and austenitic grain size. Most alloying elements in steel shift the curves to the right, thus allowing more time to harden the steel fully without hitting the bend in the curve.

Hardenability is a measure of the ease with which martensite can be formed in a given steel. The increase in hardenability of the steel allows the hardening of thicker sections than would otherwise be possible. Common examples for alloying elements which increase hardenability, are carbon, manganese, molybdenum, chromium, silicon and nickel. Alloying elements other than carbon have negligible influence on the mechanical properties of martensite. The primary purpose of these elements is to slow the formation of perlite by interfering with diffusion and thus to enable martensite to be produced at slower cooling rates, with the nose of the diagram being shifted to the right.

The time available for transformation of austenite to pearlite becomes shorter when the transformation occurs at temperatures progressively further below the eutectoid temperature; the time reaches a minimum at about 550°C, and at lower temperatures diffusion is slow so that pearlite does not form at all. That is why the cooling rate is decisive until the temperature reaches about 550 °C.

2.4 Normalizing

The process of normalizing consists of heating the steel about 30 to 60 °C above the upper critical range and cooling it in still air, down to room temperature. This process is mainly used to relieve internal stresses, or to achieve desired results in physical properties. Most commercial steels are normalized after being rolled or cast.

2.5 Hardening

Hardening is the process of heating a piece of steel to a temperature within or above its critical range and then cooling it rapidly. In any heat-treating operation, the rate of heating is important. Heat flows from the exterior to the interior of steel at a definite rate. If the steel is heated too fast, the outside becomes hotter than the interior, and uniform structures cannot be obtained. If a piece is irregular in shape, a slow rate is all the more essential to eliminate warping and cracking. The heavier the section, the longer must be the heating time to achieve uniform results. Even after the correct temperature has been reached, the piece should be held at the temperature for a sufficient period of time to permit its thickest section to attain a uniform temperature.

The hardness obtained from a given treatment depends on the quenching rate, the carbon content, and the work size. In alloy steels the kind and amount of alloying elements influences only the hardenability of the steel but it does not affect the hardness except in unhardened or partially hardened steels.

Water, oil and air are the universal quenching media. For low and medium plain-carbon steels, quenching in a water bath is a common method of rapid cooling. Brine or water spray is most effective for extreme cooling. For high carbon and alloy steel, oil is generally used as the quenching medium, because its action is not as severe as that of water. Certain alloys can be hardened by air cooling, but for ordinary steels, such a cooling rate is too slow to give an appreciable hardening effect.

An overview over the different cooling rates and resulting microstructures, depending on the carbon content of steel, is given in the following table:

Quenching Medium	Cooling Rate $^{\circ}C/sec$	Eutectoid	Hypo-eutectoid	Hyper-eutectoid
Water	165	M	M	M
Oil	16.5	P	P+α	P+θ
Air	0.6	P	P+α	P+θ
Furnance	0.006	P	P+α	P+θ

M-martensite; P-pearlite; α-ferrite; θ-cementite

Reference to the time-temperature-transformation diagram indicates that a very rapid quench is necessary to avoid intersecting the nose of the curve and to obtain a martensitic structure. Because of the rapid cooling rate,

which may reach 3000 °C per second at times, quenching is the most critical operation encountered in heat treating. Particulary in water quenching the part must come into contact with fresh fluid all around during cooling, since a static area will soon lose its cooling power, and with still water may even contain an insulating steam layer.

2.6 Tempering

Steel that has been hardened by rapid quenching is brittle and not suitable for most uses. By tempering or "drawing", the hardness and brittleness may be reduced to the desired point for service conditions. As these properties are reduced, there is also a decrease in tensile strength and an increase in the ductility and toughness of the steel. The operation consists of the reheating of quench-hardened steel to some temperature below the critical range, followed by any cooling rate.

In the process of tempering, some consideration should be given to time as well as to temperature. Although most of the softening action occurs in the first few minutes after the temperature is reached, there is some additional reduction in hardness, if the temperature is maintained for a prolonged time. Usual practice is to heat the steel to the desired temperature and hold it there only long enough to have it uniformly heated.

Tempering is possible because of the instability of martensite. Low temperature draws, from 170 to 220 °C, do not cause much decrease in hardness and are used principally to relieve internal strains. As the tempering temperatures are increased, the breakdown of the martensite takes place at a faster rate and at about 300 °C the change to the structure of *tempered martensite* is very quick.

Tempered martensite structures can be produced with a wide range of strength and ductility that makes them very useful engineering materials.

2.7 Relation of Design to Heat Treatment

A metal has a certain strength depending upon its composition, quality and the heat treatment to which it has been subjected. When subjected to a combination of forces beyond its ultimate strength, it cracks or fails, owing to the combined action of the internal stresses set up during fabrication and

heat treatment of the parts, and the external forces of service.

Sometimes the internal stresses alone exceed the strength of the metal and the parts crack during and after the hardening treatment. Or the internal stresses may tax a high percentage of the total strength, and failure will occur in service under relatively light loads. The useful strength of a part therefore decreases in proportion as the internal stresses increase.

These internal stresses arise from many causes, but the most serious, by far, are those developed during quenching, as a result of differential cooling or *temperature gradient*. The temperature gradient is the rate of variation in temperature over a given unit distance. This gradient is largely a function of the size and shape of the piece being quenched. The basic principle of successful design is to plan shapes that will keep the temperature gradient throughout a piece at a minimum during quenching.

When a piece of metal is removed from the hardening furnace preparatory to quenching, it is presumably at a uniform temperature. As soon as quenching begins, the temperature is different in almost every part of the section. The reasons for this difference in temperature are twofold:

First, the heat capacity may be greater in one part than another, because there is more metal in one part than in another. And second, the rate of cooling is also affected by the shape of the surface.

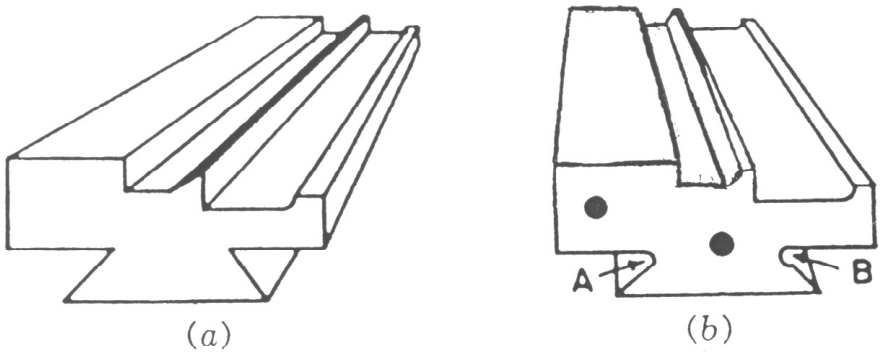

Figure 2.3: Form tool with dovetail (a)Unequal masses and sharp coners promote susceptibility to hardening cracks. (b) Holes balance sections, and radii at A or B reduce quencing strains

The cross section of the tool in *Figure 2.3a* consists of heavy and light sections, joined together with sharp re-entrant angles. It is impossible to get

uniform cooling during the quench in the immediate neighbourhood of such a sharp angle because the corner is inaccessible to the coolant, and vapour pockets may form.

A tool of this shape would be hazardous to harden in a water. A correct design is illustrated in *Figure 2.3b*. Holes have been drilled through the two heaviest sections, and thus the weight of the metal has been well balanced throughout the cross section of the tool. The sharp angles on the cutting end cannot be eliminated because they are a part of the form of the tool. Two suggested treatments are shown for the angle at the base of the dovetail. The best treatment is shown at A, where a generous fillet is provided. An alternative is shown at B, where the corner has been undercut to provide a radius and still give the effect of a sharp corner on the dovetail.

Success in preventing warpage and other forms of internal strain will be directly proportional to success in balancing the weight of the sections and producing uniform cooling conditions. Large dies or parts of intricate design are sometimes made in sections, which often simplifies the problems of the heat treatment.

2.8 Heat Treatment Process of *Metalogenia*

Metalogenia produces excavator teeth of plain Martensite. To be able to produce parts with a massive cross section of up to 7 cm, they use a certain alloy which is treated in three steps to optimize the product. The applied heat treatments are normalizing, hardening and tempering; a detailed description of these treatments is given above.

After casting the teeth in a sand mould, it is cooled down in the mould. To normalize the steel, the part is taken out of the mould, heated to a temperature of 1036 °C, six degrees above the upper critical range. It is kept at this temperature for at least one hour and then cooled in still air for two hours.

The next step is the hardening of the steel. For that the part is heated up to 930 °C within three hours, kept at this temperature for one hour and quenched in circulating water at 30 °C for two to three minutes.

Within and after quenching many of the teeth break. The reason for this effect is examined with the finite numerical program COMET. The following chapters deal with the first steps of the application.

Chapter 3

Theoretical Background

In this work the thermo-elastic simulation of a heat treatment process is focused. To say in advance, the program COMET obtains much further going calculation possibilities. It is based on a constitutive model which is defined by a thermo-visco-elasto-visco-plastic model.

It is not the aim of this work to explain the various application possibilities of the program with all its functions. Therefore only the part of the program which is relevant for the following simulations is mentioned.

3.1 Thermomechanical Interactions

The heat treatment process can be divided into different subproblems, depending on each other. A possible decomposition is:

- thermal problem
- metallurgical problem and
- mechanical problem

The thermal problem consists of the evaluation of the *thermal history* of the heat treated material. This evaluation can be realized by using the equation of the balance of energy, which is produced for the volume of the material. The fundamental variable of this problem is the temperature. The method of considering the problem is framed into the *phenomenological theory*, which means in this context that it is based on a macroscopic measurement.

The metallurgical problem deals with the different microstructures, which develop inside the material during the heat treatment processes. It is clear that this problem has to be examined from the microscopical point of view.

Finally, for the mechanical problem the conditions of equilibrium must be defined. They have to satisfy the stresses which develop during the process of cooling with one or more phase changes. Besides, these stresses are obtained with an appropriate constitutive model for the heat treated material.

The interaction between these three problems can be visualized with the help of a scheme:

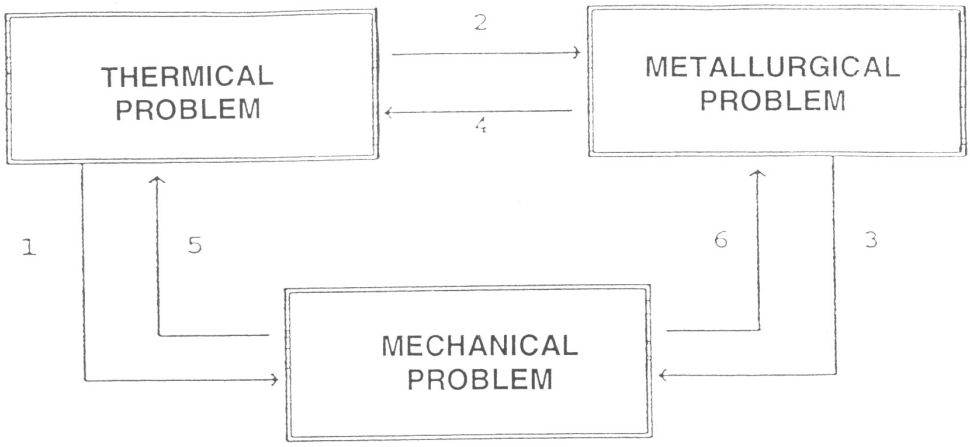

Figure 3.1: Thermomechanical Interactions

Interaction 1 (thermal problem → mechanical problem) refers to the *thermal deformations* and consequently to the *thermally induced stresses* within the constitutive model which depend on the temperature.

Interaction 2 (thermal problem → metallurgical problem) conditions the metallurgical transformations of the problem. Therefore all the microscopic phenomena which are involved in the heat treatment process depend, together with other variables, on the temperature at which they develop.

Interaction 3 (metallurgical problem → mechanical problem) is important as well, because the phase transformations generate macroscopic volumetrical deformations.

Interaction 4 (metallurgical problem → thermal problem) governs the energy changes derived from the phase change phenomenon. This heat release or absorption modifies the local thermal history of the material.

Interaction 5 (mechanical problem → metallurgical problem) has to be considered, if the thermal energy, associated to the change of volume and/or the plastic work, becomes important to the total energy balance.

Interaction 6 (mechanical problem → metallurgical problem) has influence on some of the microscopic phenomena.

In the frame of a global phenomenological theory applied to a heat treatment problem, the influence of the microscopic behaviour can be extrapolated to the macroscopic level. Therefore it is possible to take into account the interactions 3 and 4 in the phenomenological analysis.

Another simplification consists in analysing the metallurgical problem through a *Time-temperature-transformation diagram (Fig.:2.2).* Such a diagram allows for the real metallurgical characterisation of the material to be obtained, consequently defining clearly the interactions 4 and 6. These interactions basically include macroscopic variables which result from microscopic effects.

3.2 Local Governing Equations

The local system of partial differential equations governing the coupled thermomechanical initial boundary value problem is defined by the momentum and energy balance equations, restricted by the inequalities arising from the second law of the thermodynamics. The local form of the momentum and energy balance equations can be written as

$$\mathbf{0} = \boldsymbol{\nabla} \cdot \boldsymbol{\sigma} + \mathbf{B} \tag{3.1}$$

$$C\dot{\Theta} = R - \boldsymbol{\nabla} \cdot \mathbf{Q} \tag{3.2}$$

where $\mathbf{B}$ are the (prescribed) body forces, $\boldsymbol{\nabla}\cdot\,(\cdot)$ is the divergence operator, $\boldsymbol{\sigma}$ is the Cauchy stress tensor, Θ is the absolute temperature, C is the heat capacity, $\mathbf{Q}$ is the heat flux and R is the prescribed heat source.

As a next step the boundary conditions and the initial conditions are described

Boundary conditions

Thermal Problem

$$\Theta = \bar{\Theta} \text{ in } \Gamma_T \times \Upsilon \tag{3.3}$$

$$\mathbf{Q} \cdot \mathbf{n} = -\bar{Q} - q^* = \bar{q} \text{ in } \Gamma_q \times \Upsilon \tag{3.4}$$

with $q^* = h(\Theta - \Theta_{ext})$

Mechanical Problem

$$\mathbf{u} = \bar{\mathbf{u}} \text{ in } \Gamma_u \times \Upsilon \tag{3.5}$$

$$\boldsymbol{\sigma} \cdot \mathbf{n} = \bar{\mathbf{t}} \text{ in } \Gamma_\sigma \times \Upsilon \tag{3.6}$$

Initial Conditions

Thermal Problem

$$\Theta(t = 0) = \Theta_0 \text{ in } \Omega \tag{3.7}$$

Mechanical Problem

$$\mathbf{u}(t = 0) = \mathbf{u}_0 \text{ in } \Omega \tag{3.8}$$

where Ω is a open domain and $\Upsilon \in R^+$ is the time interval of the analysis ($t \in \Upsilon$).

With the Dirichlet and Newman conditions it is assumed that the temperature field and the heat flow are prescribed within Γ_T and Γ_q. $\bar{\Theta}$ is the prescribed boundary temperature, $\bar{Q}$ is the normal prescribed heat flux and $q^* = h(\Theta - \Theta_{ext})$ is the normal heat flux, which is dependent on the convection-radiation phenomenon, where h is the convection-radiation coefficient.

In the same way the displacement field $\mathbf{u}$ and the stress tensor $\boldsymbol{\sigma}$ are described by the parts Γ_u and Γ_σ, respectively, where $\mathbf{n}$ is the normal vector, $\bar{\mathbf{u}}$ is the displacement field of the prescribed boundary and $\bar{\mathbf{t}}$ is the vector of tensions of the prescribed boundary.

3.3 Weak Form of the Governing Equations

In this section the weak form of both the balance of momentum 3.1 and balance of energy equations 3.2 are presented.

3.3.1 Weak Form of the Balance of Energy Equation

The solution of the thermal part of the system of equations 3.1 and 3.2 have to satisfy the boundary conditions which are defined in 3.3 to 3.6. The Dirichlet conditions are not considered for the integration equation of the field. This way, the integral of the thermal equilibrium equation over the whole volume Ω has to be zero as well as the integral of the Newman conditions over Γ_q. Applying the weighted residual method it results

$$\int_\Omega WC\dot{\Theta}d\Omega - \int_\Omega WR_{ext}d\Omega + \int W\nabla\cdot\mathbf{Q}d\Omega + \int_{\Gamma_q} W(\bar{\mathbf{q}} - \mathbf{Q}\cdot\mathbf{n})d\Gamma_q = 0 \quad (3.9)$$

where W are the test functions which are associated with the temperature field and which satisfy the Dirichlet boundary conditions in Γ_q. Applying the Gauss theorem to the conductivity term of 3.9 it results

$$\begin{aligned}\int_\Omega W\nabla\cdot\mathbf{Q}d\Omega &= \int_{\Gamma_q} W\bar{\mathbf{q}}d\Gamma_q - \int_\Omega \nabla W\mathbf{Q}d\Omega \\ &= \int_{\Gamma_q} W\bar{\mathbf{q}}d\Gamma_q + \int_\Omega \nabla W k_\Theta\nabla\Theta d\Omega \qquad (3.10)\end{aligned}$$

in which the Fourier law ($\mathbf{Q} = -k_\Theta\nabla\Theta$) was used. Inserting equation 3.9 in equation 3.10 the weak form of the balance of energy equation is obtained:

$$\int_\Omega WC\dot{T}d\Omega - \int_\Omega WR_{ex\Theta}d\Omega + \int_{\Gamma_q} W\bar{\mathbf{q}}d\Gamma_q + \int_\Omega \nabla W k_\Theta\nabla\Theta d\Omega + \int_{\Gamma_q} W(\bar{\mathbf{q}} - \mathbf{Q}\cdot\mathbf{n})d\Gamma_q = 0 \quad (3.11)$$

3.3.2 Weak Form of the Balance of Momentum Equation

The solution of the mechanical part of the differential equation system 3.1 has to satisfy the imposed boundary conditions. The integral of the balance of momentum equation over the volume Ω has to be zero as well as the Newman conditions over Γ_σ. Applying the weighted residual method it results

$$\int_\Omega W\boldsymbol{\nabla}\cdot\boldsymbol{\sigma}d\Omega + \int_\Omega W\mathbf{B}d\Omega + \int_{\Gamma_\sigma} W\cdot(\bar{\mathbf{t}} - \boldsymbol{\sigma}\cdot\mathbf{n})d\Gamma_\sigma = 0 \quad (3.12)$$

where W are the test functions which are asociated with the displacement field. Note that $W = 0$ in Γ_σ.

Applying the divergence theorem to the first term of equation 3.12 one obtains

$$\int_\Omega W\boldsymbol{\nabla}\cdot\boldsymbol{\sigma}d\Omega = \int_{\Gamma_\sigma} W\boldsymbol{\sigma}\cdot\mathbf{n}d\Gamma_\sigma - \int_\Omega \boldsymbol{\nabla}W\boldsymbol{\sigma}d\Omega \tag{3.13}$$

Inserting equation 3.12 in 3.13 the weak form of the balance of momentum equation is obtained

$$\int_\Omega \nabla W\boldsymbol{\sigma}d\Omega = \int_\Omega W\mathbf{B}d\Omega + \int_{\Gamma_\sigma} W\bar{\mathbf{t}}d\Gamma_\sigma \tag{3.14}$$

3.4 Thermo-Mechanical Constitutive Model

In order to define a thermo-elasto-plastic constitutive model let us introduce the free energy ($\Psi = \Theta S$), with the functional form

$$\Psi = \Psi(\boldsymbol{\epsilon}, \Theta) = W(\boldsymbol{\epsilon}, \Theta) + T(\Theta) \tag{3.15}$$

In this expression $W = W(\epsilon, \Theta)$ is the mechanical contribution and $T = T(\Theta)$ is the thermal contribution.

The total strain tensor $\boldsymbol{\varepsilon}$ can be split into its *elastic* and *inelastic* parts $\boldsymbol{\varepsilon}^E$ and $\boldsymbol{\varepsilon}^I$:

$$\boldsymbol{\varepsilon} = \boldsymbol{\varepsilon}^E + \boldsymbol{\varepsilon}^I \tag{3.16}$$

where the elastic strain tensor $\boldsymbol{\varepsilon}^E$ is given by the sum of the effective elastic deformation plus the thermal deformation, $\boldsymbol{\varepsilon}^e$and $\boldsymbol{\varepsilon}^\theta$, respectively, so that

$$\boldsymbol{\varepsilon}^E = \boldsymbol{\varepsilon}^e + \boldsymbol{\varepsilon}^\theta \tag{3.17}$$

while the inelastic strain tensor in our case is equal to the viscoplastic deformation

$$\boldsymbol{\varepsilon}^I = \boldsymbol{\varepsilon}^{vp} \tag{3.18}$$

with

$$\boldsymbol{\varepsilon}^{vp} = \gamma^{vp}\cdot\frac{d\phi}{d\mathbf{s}} = \gamma^{vp}\cdot\mathbf{n} \tag{3.19}$$

where $\mathbf{n}$ is the unit normal to the yield surface and γ^{vp} is the viscoplastic parameter. The Von Mises yield surface is assumed in the form

$$\Phi(\mathbf{s}, \mathbf{q}, q, \Theta) = \| \mathbf{s} - \mathbf{q} \| - R(q, \Theta) \leq 0 \tag{3.20}$$

where $\mathbf{s} = dev(\boldsymbol{\sigma})$ is the deviatoric part of the stress tensor, $\mathbf{q}$ and q are state variables which are defined as the derivatives of the free energy function and $R(q, \Theta)$ is the radius of the yield surface given by

$$R(q, \Theta) = \sqrt{\frac{2}{3}}[\sigma_0(\Theta) - q] \tag{3.21}$$

with σ_0 being the flow stress.

Therefore the total strain tensor can be split as follows

$$\boldsymbol{\varepsilon} = \boldsymbol{\varepsilon}^e + \boldsymbol{\varepsilon}^\theta + \boldsymbol{\varepsilon}^{vp} \tag{3.22}$$

Straining during phase change

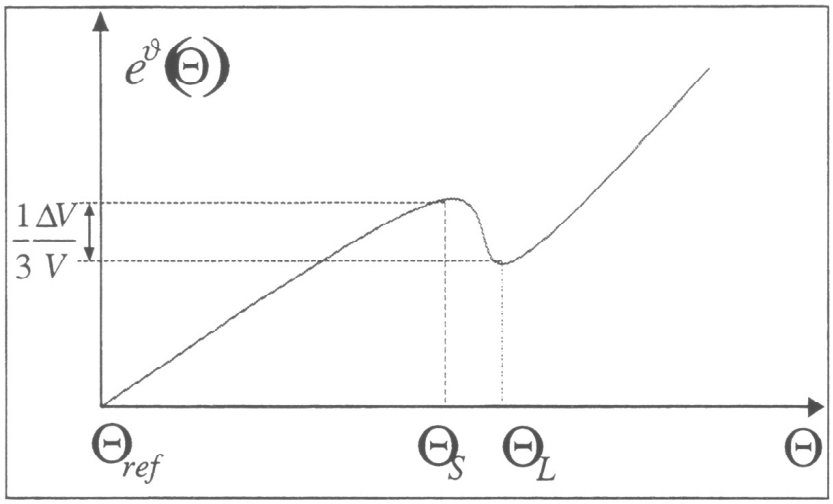

Figure 3.2: Thermal deformation including straining contribution

The straining during phase change is a particular volumetric contraction or dilatation that occurs when the material is changing its internal structure (see *figure 3.2*). Θ_L and Θ_S stand for the liquid and the solid phase change, respectively. But this scheme can also be used to explain a solid-solid phase change, which is relevant for this work. The direct consequence of the

straining during phase change is the modification of the volumetric thermal deformation $\boldsymbol{\varepsilon}^{\theta}(\boldsymbol{\Theta})$

$$\boldsymbol{\epsilon}_{\Theta} = [\alpha(\Theta)(\Theta - \Theta_{ref}) - \alpha(\Theta_0)(\Theta_0 - \Theta_{ref})]\mathbf{1} \tag{3.23}$$

where $\alpha = \alpha(\Theta)$ is the thermal volumetric change coefficient, Θ_0 is the initial temperature, Θ_{ref} is the reference temperature for the experimental determination of α and $\mathbf{1}$ is a unit tensor.

With these definitions, the elastic mechanical part of the free energy can be expressed as

$$W = W(\boldsymbol{\epsilon}^e, \Theta) = \frac{1}{2}K(\Theta)(\mathbf{e}^e)^2 + G(\Theta)dev^2[\mathbf{e}^e] \tag{3.24}$$

where $K = K(\Theta)$ is the bulk modulus, $G = G(\Theta)$ is the shear modulus, $e^e = tr\boldsymbol{\epsilon}^e$ is the volumetric strain and $dev[\cdot]$ means deviatoric part.

The thermal term of the free energy can be formally expressed as

$$T = T(\Theta) = \int_{\Theta_0}^{\Theta} T_{\Theta}(\bar{\Theta})d\bar{\Theta} = -\int_{\Theta_0}^{\Theta}\int_{\Theta_0}^{\Theta} c_0(\bar{\Theta})\frac{d\bar{\Theta}}{\bar{\Theta}} \tag{3.25}$$

where $c_0 = c_0(\Theta)$ is the specific heat of the material.

The constitutive equation is obtained from the definition of the free energy using Coleman's method as:

$$\sigma = \frac{d\Psi}{d\boldsymbol{\epsilon}^e} = K(\Theta)e^e\mathbf{1} + 2G(\Theta)dev[\boldsymbol{\epsilon}^e] \tag{3.26}$$

3.5 Time Integration of the Coupled Problem

The numerical solution of the coupled thermomechanical problem involves the transformation of an infinite dimensional transient system, governed by a system of linear partial differential equations into a sequence of discrete algebraic problems by means of a Galerkin finite element projection and a

time marching scheme for the advancement of the primary nodal variables, displacements and temperatures.

The following scheme illustrates the transformation from the continuum transient problem into the discrete algebraic system of equations:

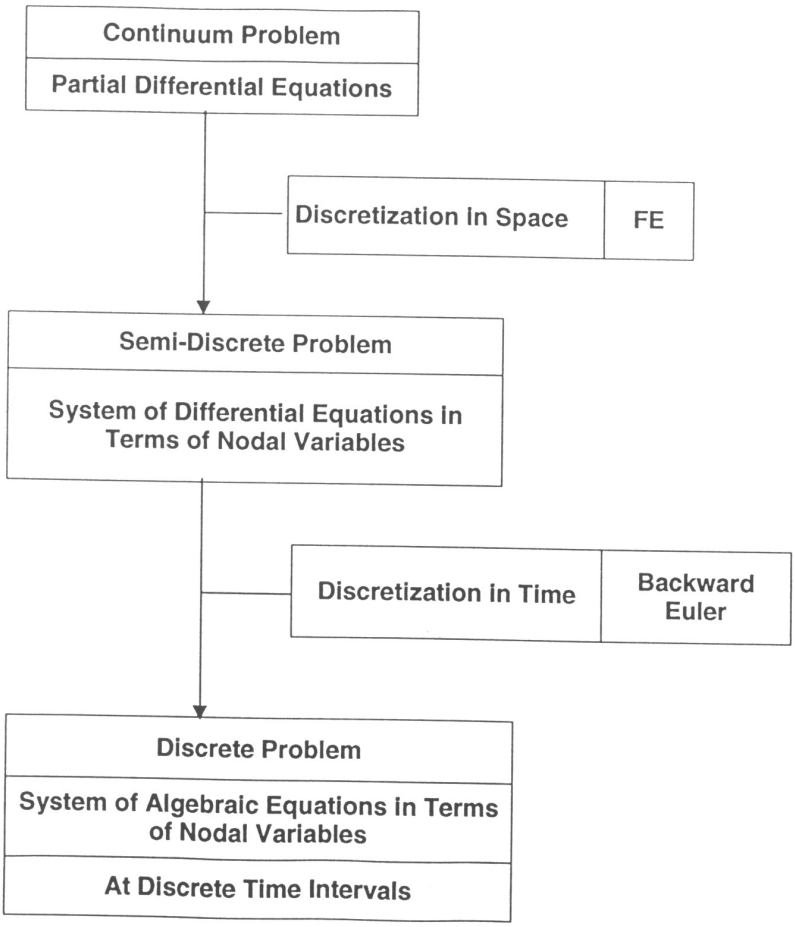

Figure 3.2: Scheme for the numerical solution of the transient problem

With regard to the time marching scheme different strategies are possible to perform this transformation, but they can be grouped in two categories: *simultaneous* time-stepping algorithms and *staggered* time-stepping algorithms.

Simultaneous time-stepping algorithms solve both the mechanical and the thermal equilibrium equations together, thus advancing all the primary nodal variables of the problem, displacements and temperatures, simultaneously. This invariably leads to large and unsymmetric systems of equations, usually prohibitively expensive to solve. Furthermore, the use of different standard time-stepping algorithms developed for the single uncoupled problems is not straightforward, and it is not possible to take advantage of the different time scales possibly involved in the problem for the mechanical and thermal parts. On the other hand, it is relatively simple to devise unconditionally stable schemes using this approach.

A variant of this approach is to attempt the solution of the resulting equations using a block-iterative solution. This leads to smaller and usually symmetric systems of equations to be solved, but then the study of the stability of the algorithms is complicated, as it depends on the tolerances used to assess convergence. The problem of stability in time is the linked to that of convergence within the time step.

Staggered time-stepping algorithms are based on the use of an operator split, applied to the coupled system of differential equations, and a product formula algorithm, which leads to a scheme in which each one of the subproblems defined by the partitions is solved sequentially, within the framework of classical *fractional step methods*. This leads to the partition of the original problem into smaller and typically symmetric (physical) subproblems. Furthermore, the use of different standard time-stepping algorithms developed for the uncoupled subproblems is now straightforward, and it is possible to take advantage of the different time scales involved. Additionally, it is now possible to obtain unconditionally stable schemes using this approach, providing that the operator split preserves the underlying dissipative structure of the original problem.In view of these motivations, in COMET the staggered scheme has been preferred.

In the classic *isothermal split* the coupled system of equations is partitioned into a mechanical phase at constant temperature, followed by a thermal phase at fixed configuration, leading to a conditionally stable staggered scheme.

In the alternative *isentropic split* the coupled problem is partitioned into a mechanical phase at constant entropy, followed by a thermal phase at fixed configuration, leading to an unconditionally stable staggered scheme.

However, if the mechanical terms appearing in the time derivative of the entropy are negligible, which is the case for the following simulations, then

both splits are identical. In particular, under these conditions, the standard isothermal split preserves the dissipative structure of the original coupled problem, and it can be shown to be unconditionally stable. As this is the case in most industrial heat treatment problems, only this split will be used here.

Also, for the simulation of heat treatment processes and other thermally driven coupled problems (that is, situations where the variation of temperature activates the mechanical part of the problem), it is advantageous to consider a scheme where the thermal phase of the operator split is performed before the mechanical phase.

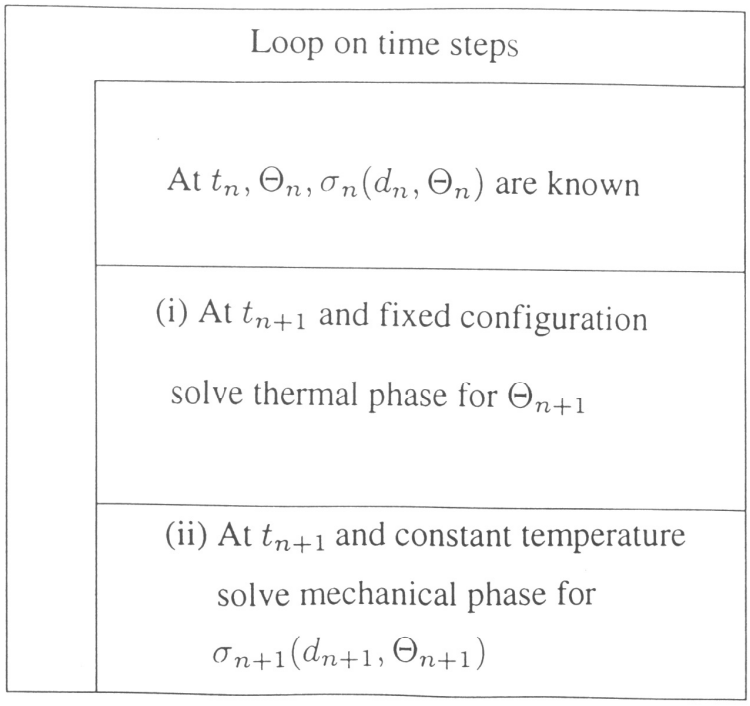

Figure 3.3: Scheme for Advancing in Time

For each time step two phases must be solved: the thermal and the mechanical partition.

At time t_n, the configuration, defined by the nodal displacements d_n, and the temperature field, defined by the temperature Θ_n, are known. Therefore,

advancing in time from t_n to t_{n+1} involves the following two phases (see *Figure 3.3*):

(i) Thermal Phase: At fixed configuration the thermal phase is solved to obtain the temperature field Θ_{n+1} at time t_{n+1}.

(ii) Mechanical Phase: At fixed temperature the mechanical phase is solved to obtain the final configuration d_{n+1} at time t_{n+1}.

Chapter 4

Cylinder - Elastic Case

As explained before, the most critical process of the production of martensite is the quenching of steel. This process will be simulated by the numerical program.

To assess the applications of the program to the problem, the geometry of a cylinder was chosen. First a slice of the cylinder is examined. The next step is to look at results for different cooling rates and to draw conclusions about the material behaviour and the program. Then at the whole cylinder variations on the application are considered. Finally, conclusions can be drawn about the possibilities of application of the program.

4.1 Mechanical Properties

Microstructural changes which are taking place during the heat treatment are not directly considered in COMET. Instead, mechanical properties can be assumed temperature dependent and the change of phase properties defined.

In this case the results of one phase change will be examined without taking temperature dependent property changes into account.

The *thermoelastic steel* is defined by the following material properties:

Density	DENSI	7850	kg/m^3
Specific Capacity	SHEAT	552.6	mm^2/s^2K
Conductivity	CONDU	45.64	N/sK
Elastic Modulus	YOUNG	1.96E+11	N/mm^2
Poisson Ratio	POISS	0.33	-
Thermal Expansion Coeff.	ALPHA	1.2E-5	$°C^{-1}$

Cooling the observed alloy steel, it passes the liquid - solid phase change between 1515 and 1495 °C. As explained in *chapter 2*, during the quenching of the material from 930°C, it directly changes from Austenite to Martensite: there is only one solid - solid phase change taking place within the process. The observed material passes the phase change between 270 and 180 °*C*.

The latent heat released is set to zero. The straining due to the phase change is assumed -0.03 during the second phase change, which means that the material is expanding during cooling within this temperature interval.

4.2 Cylinder of Infinite Height

4.2.1 Quenching Process

The first example analysed is a one centimeter thick slice of an infinitely long cylinder of radius 5 cm (*Fig.: 4.1*). The axisymmetrical mesh consists of 25 elements with a length of 1 cm in y-direction and 0.2 cm in x-direction. To simulate the real conditions in an infinitely long cylinder, the axisymmetrical piece is fixed in y-direction at the top (*Fig.:4.1.*, axis BB) and bottom surfaces (axis CC) and along the x-axis (axis AA).

The mechanical properties are those defined above. Quenching is implemented by defining the boundary conditions. The temperature development of the slice is like the one in the middle of an infinitely long cylinder as the cooling of the top and of the bottom of the cylinder have no influence on the cooling rate within the slice. The fixed boundary conditions in vertical direction represent the obstruction of deformation of the slice within the whole, infinitely long cylinder.

The results are plotted at three stations along the radius and at the symmetry axis of the sample: *node / element 1* in the core, *node / element 3* at the surface of the cylinder and *node / element 2* in the middle between both of them.

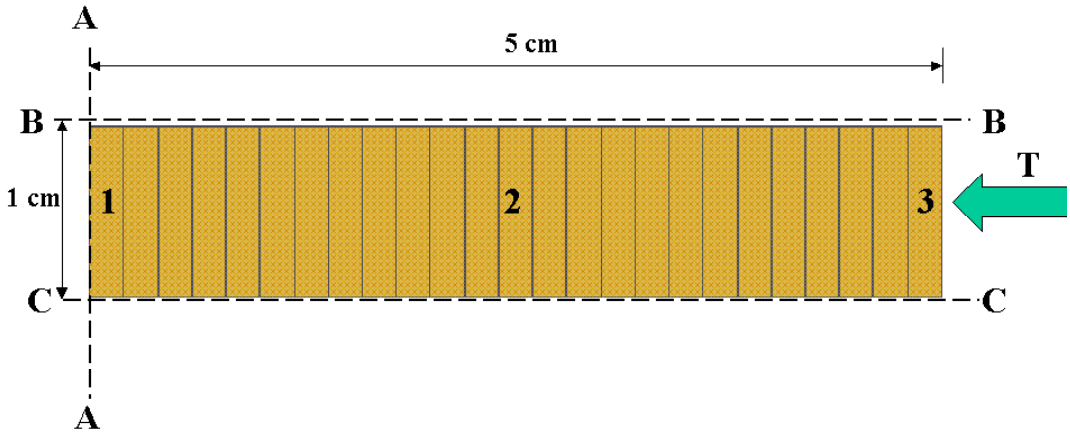

Figure 4.1.: Slice of an infinitely long cylinder

Run Conditions To get a martensitic structure for the whole body, it is important that a sufficient cooling rate is secured inside of the part as it is yet remarkably slower than at its boundaries. According to the given informations, the cooling rate at the surface has to be 180 °C/s for the geometry of the industrial parts of interest.

The drop of temperature is imposed as a forced *Dirichlet* boundary condition on the surface. The cylinder, initially at 930 °C, is cooled down to a temperature of 30°C at the surface. It is then kept at this temperature until a martensitic state has been reached throughout the structure. Expecting the simulation to last six to seven minutes, a time step of 0.4 seconds was selected resulting in a total of approximately 500 steps.

Results:

Time - Temperature - Curves

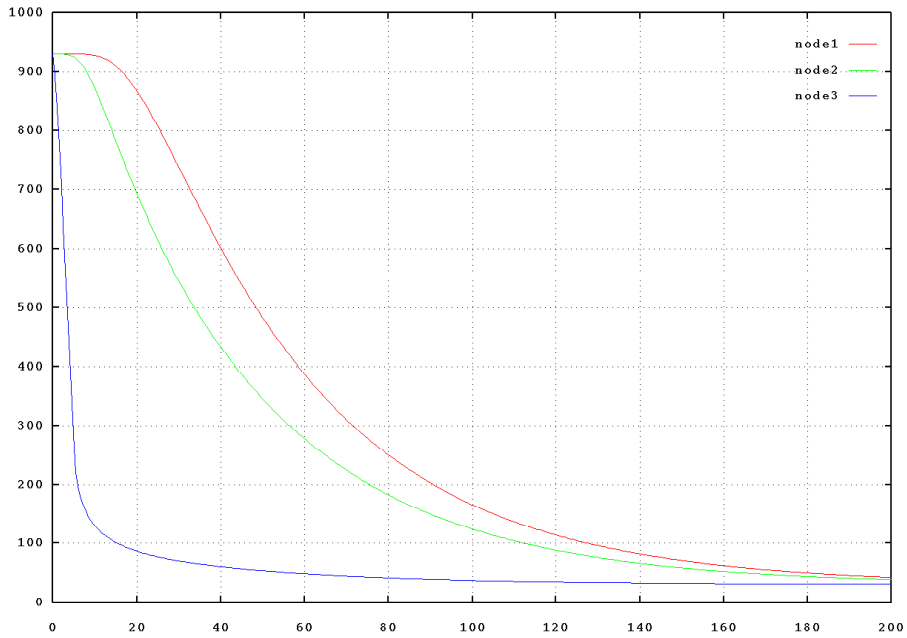

Figure 4.2: Temperatures for Quenching

The temperature curves present the cooling rates of the different parts of the cylinder. The cooling curve of *node 1* is of special interest as it represents the slowest cooling rate. As mentioned in the second chapter, at temperatures which are lower than 550 °C the diffusion is so slow that pearlite does not form. Therefore the decisive cooling rate of *node 1* is the value between 930 and 550 °C.

The temperature progression of *node 2* represents a realistic cooling rate for inside area of the industrial parts of interest. The area in which the node is situated, is cooling down from 930 to 550 °C within 30 seconds. This results in a cooling rate of less than 13 °C/s. To achieve a elementary conversion of plain carbon steel to pure Martensite, at least a ten times higher cooling rate would be necessary. Obviously the special alloy has the function of a strong catalyst.

Other important informations that can be extracted from the temperature curves are the times at which transition through the solid-solid phase change occurs at the defined stations. It is interesting, how displacement and stress

curves behave during this time, as the temperature development throughout the part is not uniform and the oposite deformation tendencies of contraction and expansion are expected to cause high stresses.

Time - Displacement - Curves

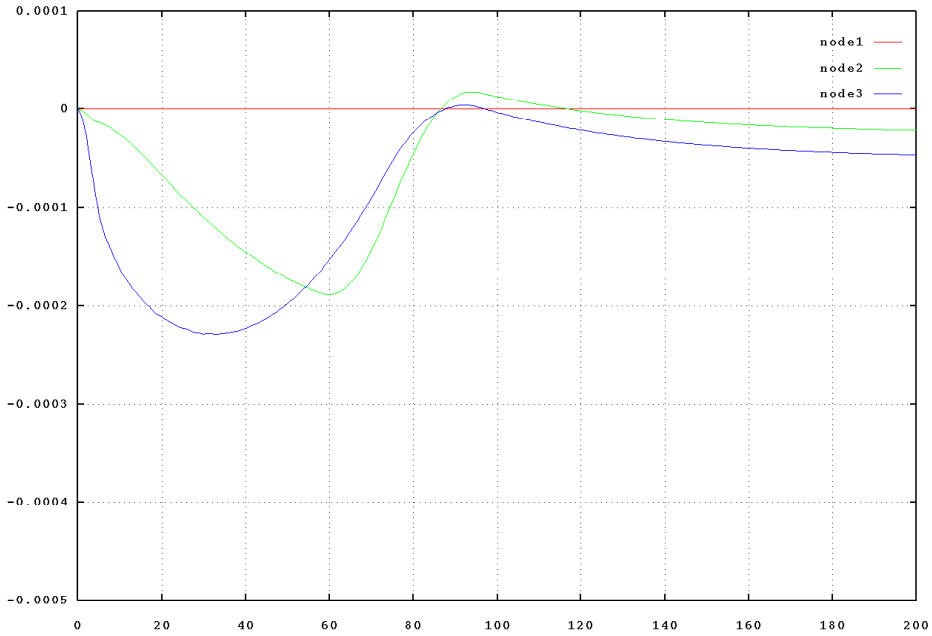

Figure 4.3: Displacements for Quenching

The constant thermal expansion coefficient ALPHA defines a contraction which is directly proportional to the temperature drop.

Looking at *node 3* at the surface of the cylinder, the curve slope declines, passing through the beginning of the phase change, but the cylinder is still shrinking. However, the slope is flattening out. Later on the curve reaches its minimum and the examined point of the slice shows an expansive movement. If temperature and the displacement curves are compared, this course can be explained. At the surface, where the cooling rate is very high, only a small volume fraction is passing the phase change at the same time. This tendency of contraction therefore has a small effect on the behaviour of the part: the contraction slope is diminishing.

In the inside of the part the cooling rate is smaller, a larger proportion of the volume is undergoing the phase change simultaneously and is forcing the surface to expand as well.

The final deformations are shown at *nodes 2* and *3*. It can be observed that they are not equal to zero at the bound. This means, the defined contraction during cooling has a higher influence on the whole process than the defined expansion during the phase change.

As *node 1* in the inside of the cylinder is fixed in x-direction, there is no displacement in this direction.

Time - Stress - Curves

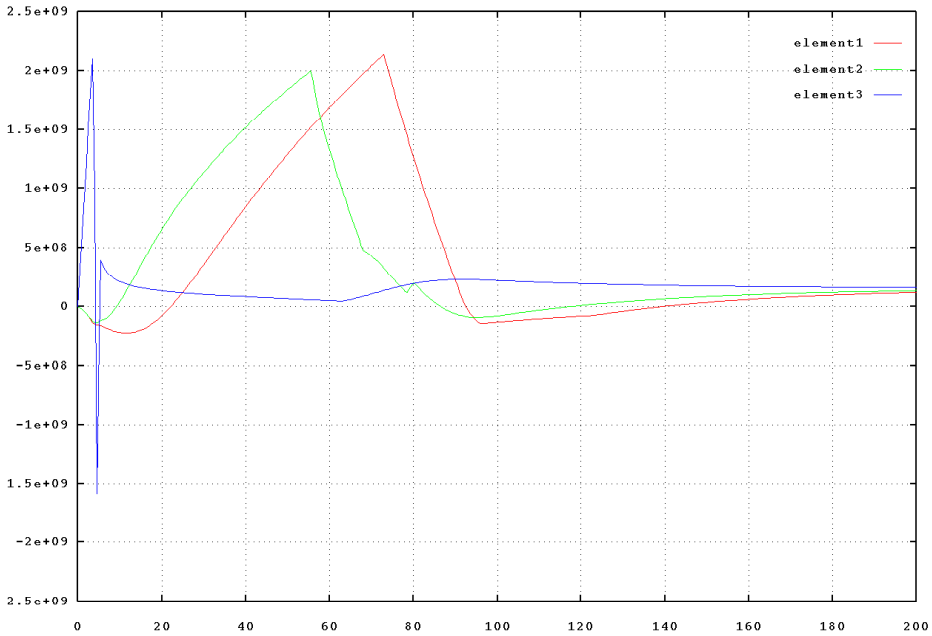

Figure 4.4: Vertical Stresses for Quenching

Vertical, radial and circumferencial stress curves show qualitatively very similar courses for the quenching process, therefore it is enough to look at vertical stresses, which reach the highest values.

Cooling is much quicker at the surface of the specimen than inside. Due to this cooling, the contraction at the outside is higher. Inside the contraction is not so fast and it opposes the outer surface contraction. This leads to tensile stresses at the outside and compression at the inside. The extreme swing of the stress curve into the compressive side is physically improbable. It is true that the stress may change its sign while passing through the phase change: If the tensile stresses are totally released and the expansion lasts

on while the inside is contracting, the result is compression at the surface. But this situation only lasts for a short period of time. When the phase change is completely passed, the surface is expanding again until it reaches the prescribed temperature.

Once the outside has reached the goal temperature of 30 °C, it does not deform any more. On the other hand the inside is still cooling and contracting. Growing tensile stresses at the inside are the result. These stress curves reach a similar amplitude like the curve of the surface. At each point of the body this tensile stress is released as soon as the temperature reaches the critical range. The slope of the stress curve changes its sign as explained above. Looking at *element 1* and *2* it is obvious that only small compressive stresses result out of the phase change. So why do we receive such a big overshoot at the surface?

As the quenching is a rapid process, the phase change affects the outer parts of the cylinder like a shock wave. The results of the calculation with the *Finite Element Method* are related to a finite part at a finite time. Therefore this method of calculation may overestimate the results in the area in which the reactions are very rapid.

To interpret these results the problem will be illustrated in two steps: In the first case the cylinder is cooled down with a clearly slower cooling rate than for the quenching. This way the reactions are taking place slower and the finite steps are small enough to result in a steady curve. The material behaviour can be examined.

In the second case the mesh for the quenched part is improved. Assuming that the deformation development of the part is converging to the true value, a finer mesh will give a better approximation of reality.

4.2.2 Slow cooling

The surface is cooled down from 930 to 30 °C within 1500 seconds. This is synonymous with a cooling rate of 0.6 °C/s, comparable to the one provided by air. The whole time interval is 1600 s, split into 400 time steps of a size of 4 seconds.

Results:

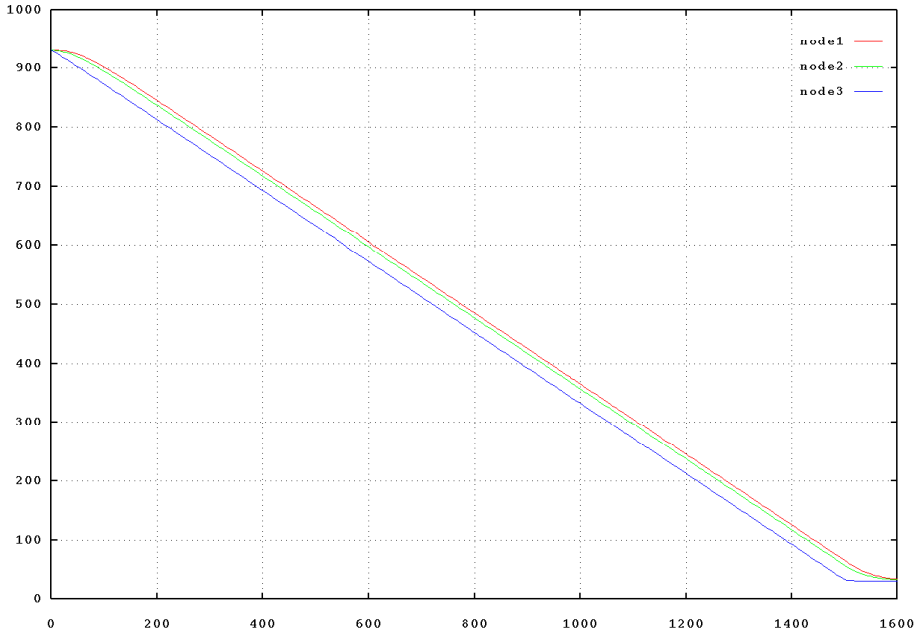

Figure 4.5: Temperatures for Slow Cooling

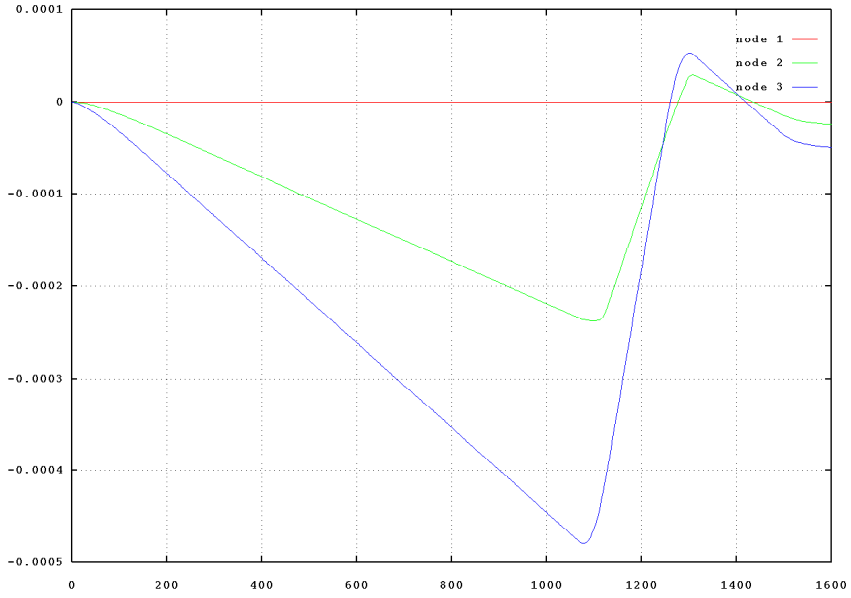

Figure 4.6: Displacements for Slow Cooling

Looking at the temperature curves it is noteable that all parts of the cross-

section have a similar cooling rate. Compared to the deformation curve of the quenching process, at a smaller cooling rate the different points of the part are expanding within a similar time. The volume fraction at the surface, which passes the phase change at the same time, is much bigger and the temperature gradient is smaller.

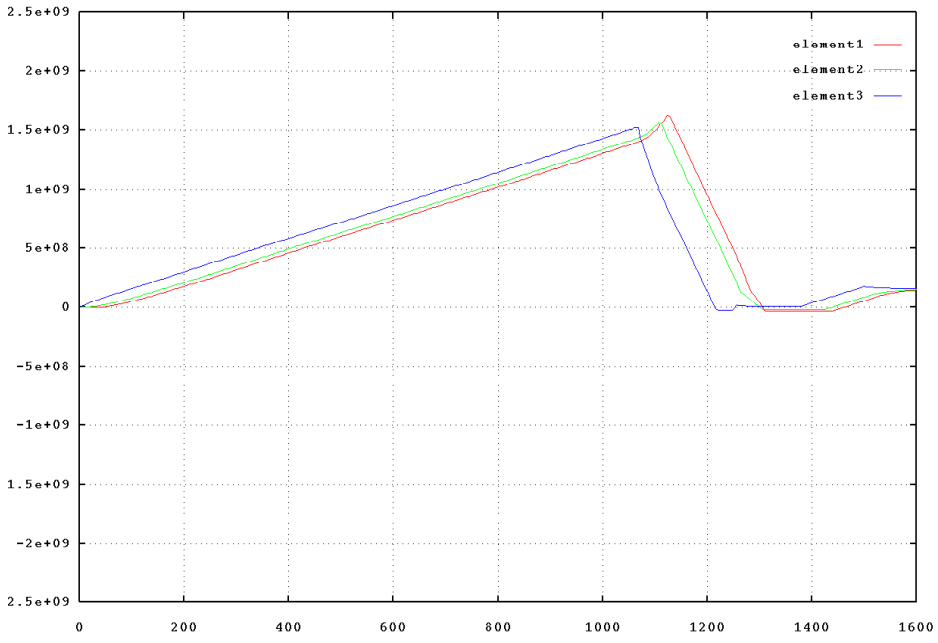

Figure 4.7: Vertical Stresses for Slow Cooling

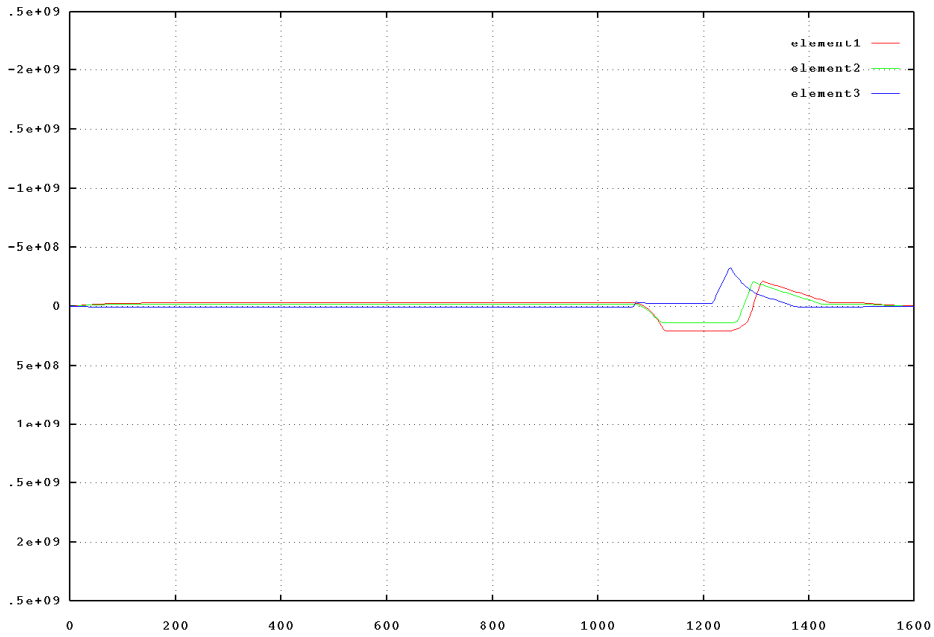

Figure 4.8: Radial Stresses for Slow Cooling

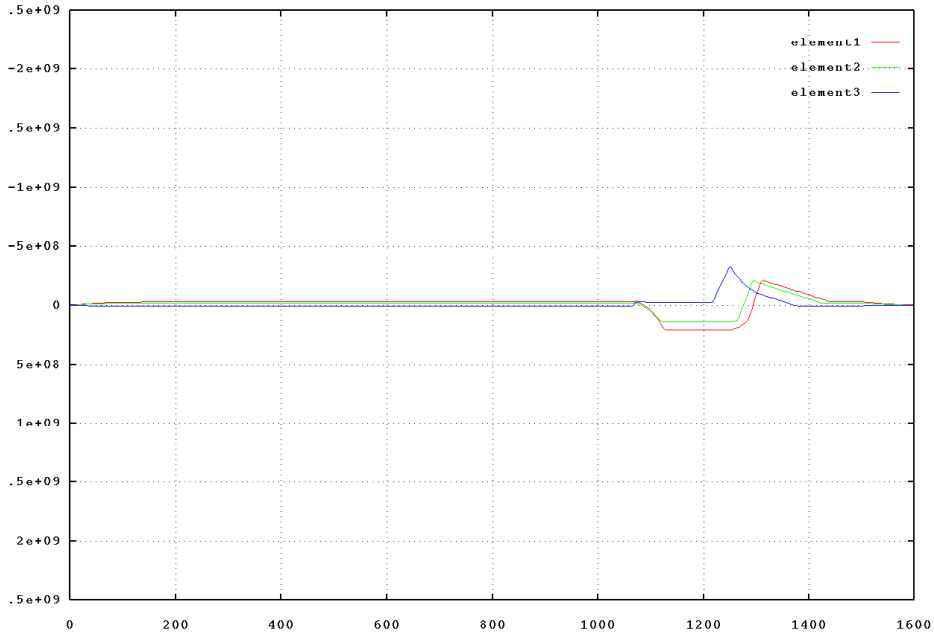

Figure 4.9: Circumferencial Stresses for Slow Cooling

Therefore the developing stresses are considerably smaller. However,

the vertical stress reaches a high value, which is due to the clamping in y-direction.The radial and circumferencial stress curves show some small stress development during the period of the phase change. It can be considered that the uniform, slow cooling of the part produces neglectable in-plane stresses.

4.2.3 Fine mesh

The mesh is quadrupled, each element of the old mesh is replaced by four elements of the new. To compare the results of the finer mesh with the old results, each of the three examined elements has to be compared with the corresponding four elements of the finer mesh. To get a clear idea of the changes, the elements are compared separately.

Results:

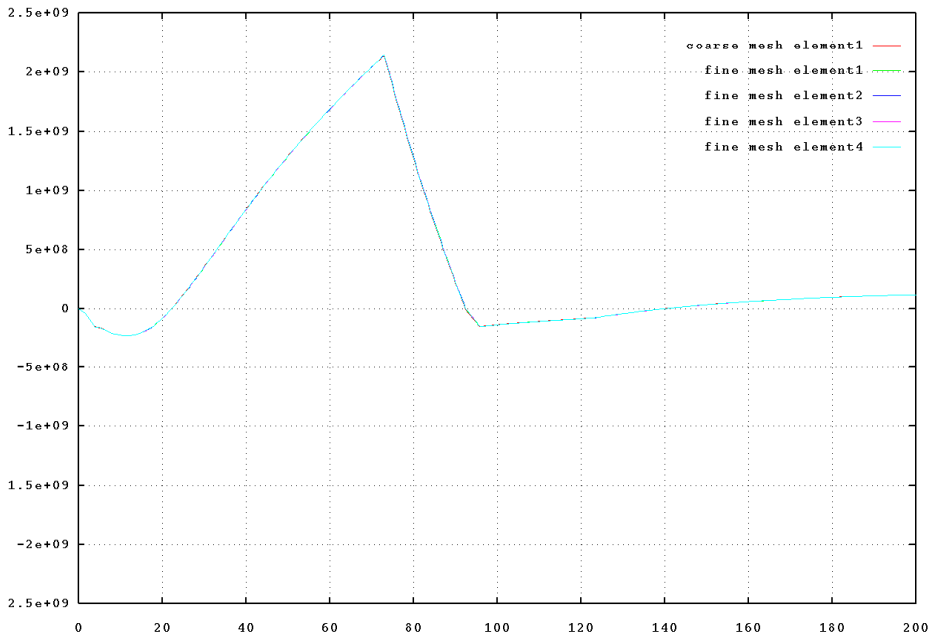

Figure 4.10: Vertical Stress for Quenching, Element 1

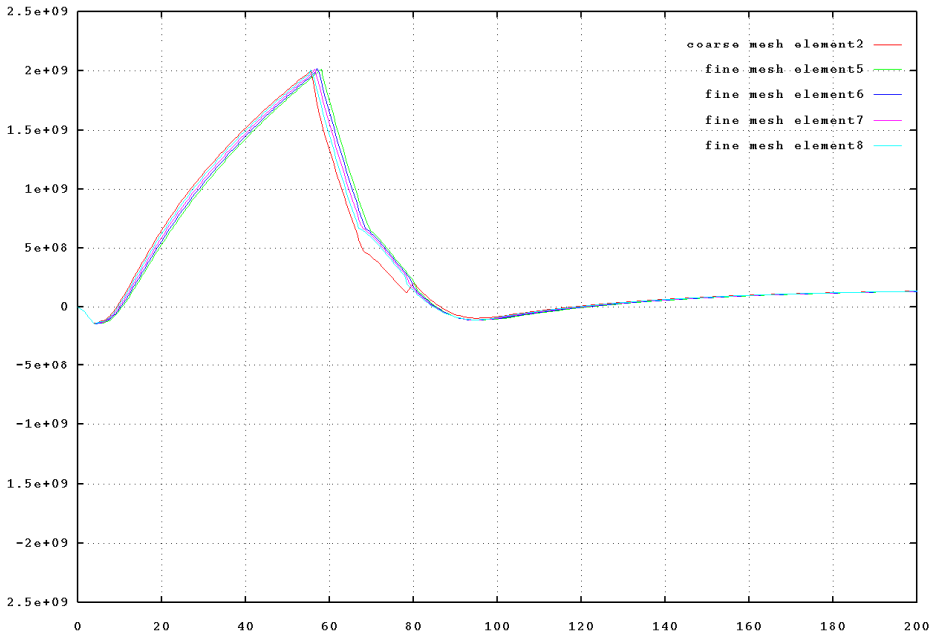

Figure 4.11: Vertical Stresses for Quenching, Element 2

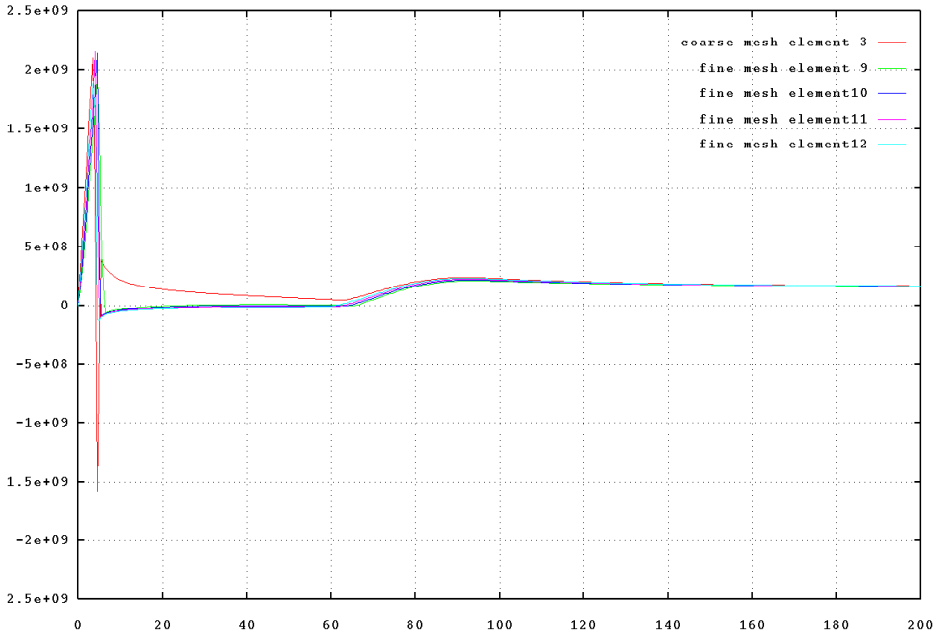

Figure 4.12: Vertical Stresses for Quenching, Element 3

For *element one*, there are no visible changes. At this part of the cylinder

- in the inside - the cooling rate has its minimal value. The results of the old mesh seem to be precise enough for the speed of the process.

The curve of *element 2* shows small differences to the four new curves, all together the curves of the finer mesh have more continuity.

Important changes of the results are caused by the finer mesh at the surface of the cylinder. The assumption is confirmed that the high compressive stress of *element 3* is the result of a too coarse mesh.

4.3 Cylinder of Finite Height

In the further analyses, the cylinder is now of finite height (200 mm). The axial symmetry of the problem allows for only a section to be modelled. The boundary conditions that must therefore be applied are as follows:

No radial displacements are allowed along the vertical axis of the section of the cylinder (*Fig.:4.13b*, Axis AA); no vertical displacements are permitted on the symmetry plane of the sample mid cross section (*Fig.:4.13b*, Axis BB).

The applied conditions are defined in order to have isostatic support of the sample. The sample is discretized into a structured grid, with 100 elements along the height and 25 along the radius (*Fig.:4.13b*). Note that this discretization results in elements of the same width as for the infinite span cylinder (*section 4.2*).

The objective of this section is to analyse the behaviour of the sample with varying the thermal expansion/contraction parameter (ALPHA) and straining due to the phase change (PSTRA).

Three cases will be further discussed, taking into account the changes in material properties.

The first run will be performed under the same conditions as for the infinite height cylinder and will be used as reference case; the next run without thermal dilatancy and the last one without straining due to the phase change. In the results further presented, four stations have been observed in the sample and the curves plotted for each one of them. The stations are distributed as can be seen in *Figure 4.13c*.

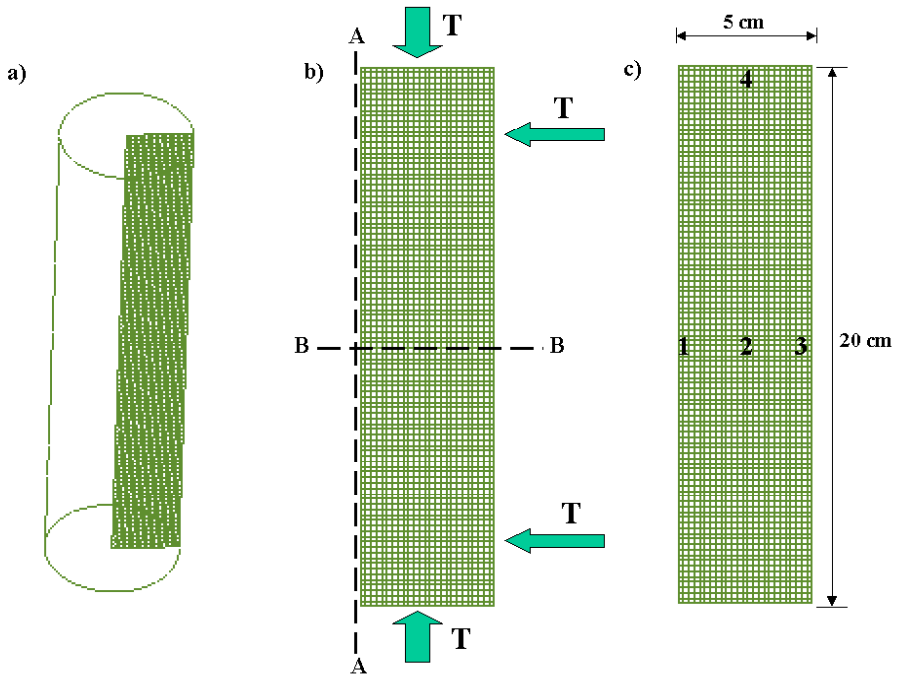

Figure 4.13: Cylinder of finite height: a) visualization of the axisymmetric model in 3D; b) boundary conditions; c) lokalisation of the observed stations

Note that *stations 1, 2*, and *3* are located similarly to the ones used in the previous example and they will be compared later. *Station 4* is situated at the top of the cylinder. The changes in vertical direction can be observed comparing the progression of the *stations 2* and *4*.

In order to grasp the effects of quenching, a visualization tool will be used to postprocess temperature and stress distribution in the sample at several time steps, besides the traditional time dependent diagrams.

4.3.1 Reference Properties

Run Conditions

The surface is cooled down from 930 to 30 °C within 5 seconds, while the whole process has a duration of 200 seconds. In this new examples for the first 20 seconds a time step of 0.1 seconds is selected, while a time step of 1 second is used for the remaining 180 seconds. This is done to anticipate

possible overshoots in the simulation due to the complexity of the physical phenomena.

The initial stage of the process that implies the cooling of the outer surface of the sample is characterized by a strong local temperature gradient. The physical problem of a very high gradient could also be numerically overcome by increasing drastically the number of elements, but this would result in a strong increase of the computational costs of the simulations.

TIME [s]	NSTEPS	NTIME [s]
20	200	0.1
180	180	1.0

Results:

Time - Temperature Curves

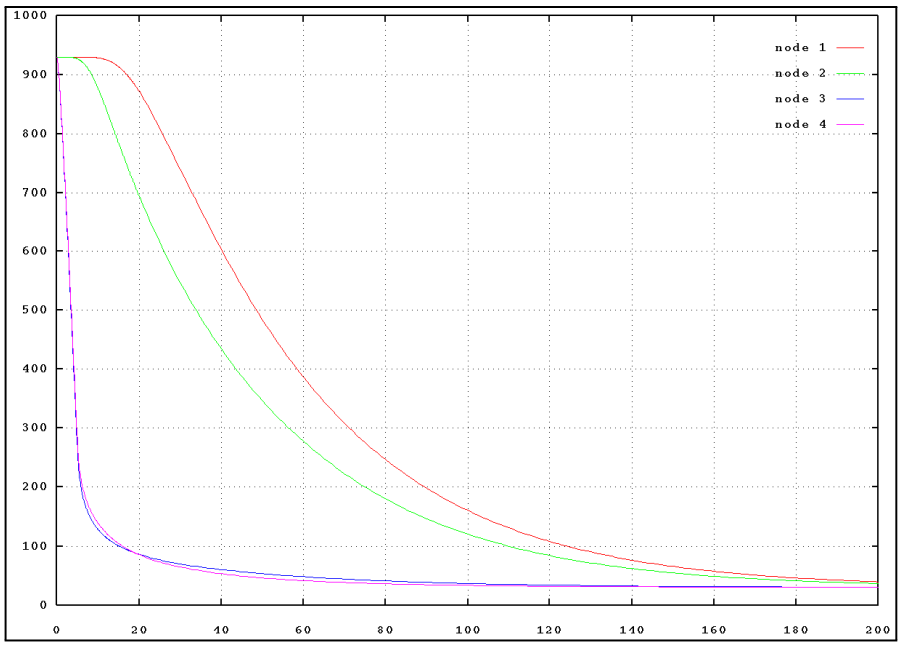

Figure 4.14: Temperatures at Quenching

The characteristics of the curves obtained in this run are very similar to the ones described in *section 4.2.1.* The observed cooling rate at *station 1*, besides having the same appearance as previously, also shows comparable values in the time - temperature - diagram. This means that for such a

cylinder (aspect ratio 4 : 1) the cooling of the top and bottom surfaces has virtually no influence on the temperature at the center of the specimen.

Time - Displacement Curves

Radial Displacements

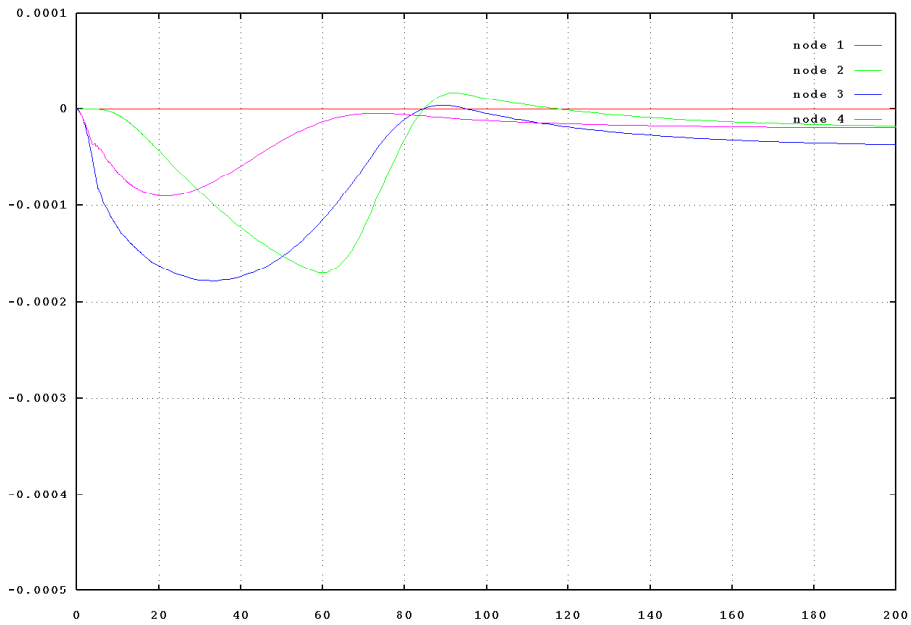

Figure 4.15: Radial Displacements

The radial displacements are smaller in the case of the short cylinder than for the slice of the indefinitely long cylinder. This is due to the fact that now the deformation during the process takes place both vertically and radially. This phenomenon was expected, as deformation is now allowed in all directions, as opposed to the fully vertically constrained infinite cylinder.

Stations 3 and *4* respond faster to the temperature changes as they lay close to the outer surface of the cylinder. Comparing with the previous simulation where for the same reason the response first occured at *station 3*, it can be observed that the radial displacements are smaller now to what was previously obtained. Towards the end of the simulation, the radial displacements at *station 2* and *4* tend to the same value.

Time - Stress Curves Vertical, radial and circumferencial stresses show some variances in behaviour, compared to the results of the infinite long cylinder. Here vertical stresses are plotted to obtain comparable results to previous examples.

Vertical Stresses

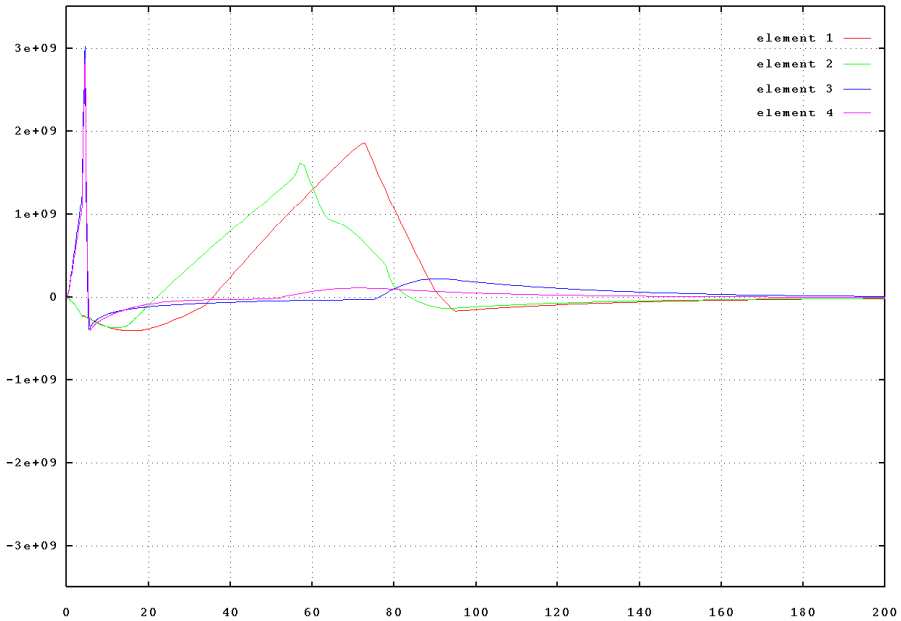

Figure 4.16: Vertical Stresses for Quenching

The results obtained for the coarser mesh of the cylinder slice showed overshoots in compression. They have disappeared in the finite height sample with a similar mesh. The fact that deformations are allowed in all directions has lead to a more flexible system with stress reductions throughout the piece during the whole of the cooling process. The higher flexibility counteracts to the initial rapid rise of stresses, the initial formation of stresses slows down. The process of stress evolution being slower, a better behaviour of the numerical code is observed.

Comparing to the vertical stress curves of the coarsely meshed infinitely long cylinder, the peaks yield lower values. This has an abating effect on the vertical stresses: the elements have more liberty of action.

After the whole cylinder has passed the phase change, it reaches a new equilibrium state where all stresses tend to zero. This is due to the elastic behaviour and the final uniform thermal distribution.

Circumferencial Stresses The program derives the vertical and radial stresses from the circumferencial stresses and therefore represent a curve of interest. They will later be used for comparison purposes.

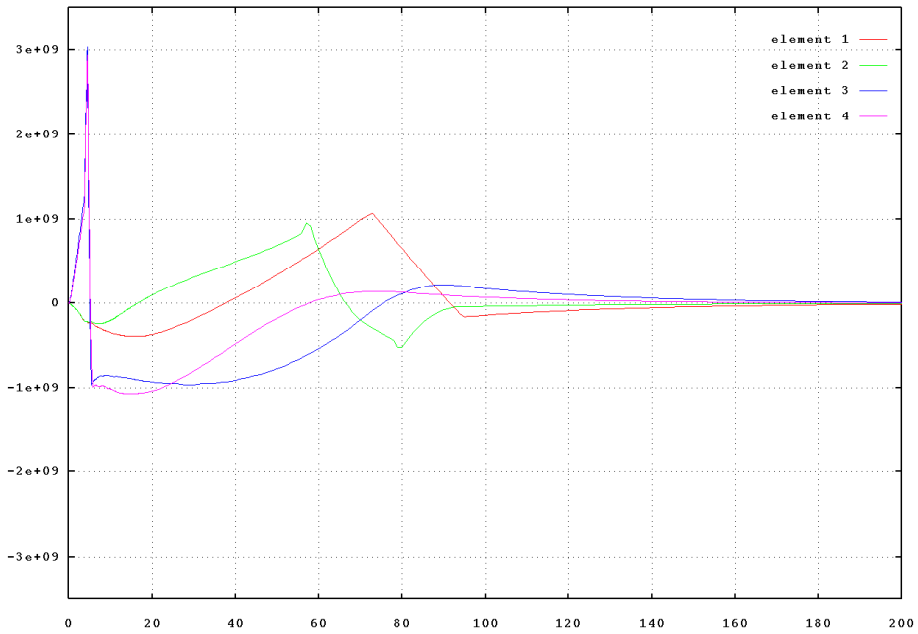

Figure 4.17: Circumferencial Stresses for Quenching

Here it is becoming obvious that the compressive stresses at *station 4* are decreasing more rapidly than at *station 3*, which is also situated close to the surface.

4.3.2 Parametric Studies

What effects do the contraction during cooling and the expansion during phase change exactly have on the whole process?

To take a closer look at the influence of the two parameters, they are examined separately.

- Firstly, the expansion coefficient of the material during the phase change, is set to zero. Only contraction due to cooling is allowed.
- Secondly, the contraction coefficient within the whole cooling process is set to zero. In this case, only the expansion of the cylinder during the phase change is observed.

- Both variations are compared with the original curves to provide more detailed information about their effect on the resulting curves.

Pure Contraction

The time - temperature prescriptions are the same as before. Displacement- and stress evolution curves are analysed.

Time - Displacement Curves It is sufficient to take a look at the radial displacements. Vertical displacements qualitatively behave in the same way.

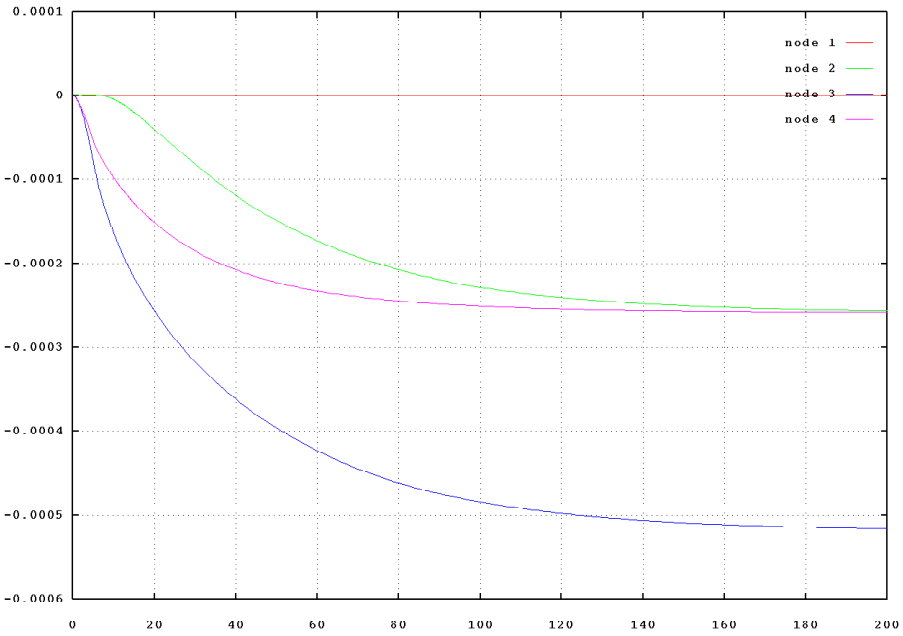

Figure 4.18: Radial Displacements for Pure Contraction

Point 2 and *point 4* , situated at the same radial coordinates, show a similar behaviour. Final deformations are larger without the influence of the phase change.

Time - Stress - Curves

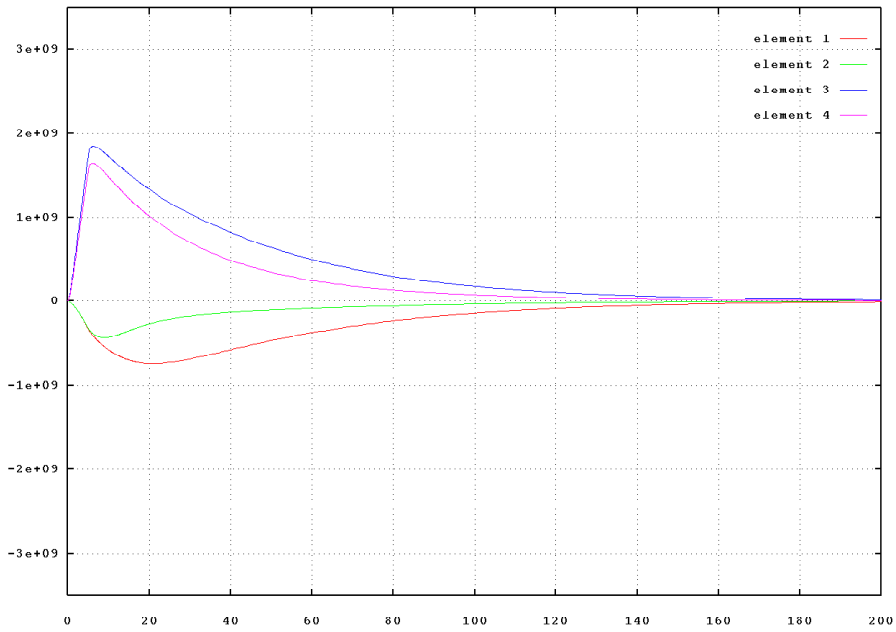

Figure 4.19: Circumferencial Stresses for Pure Contraction

Looking at the circumferencial stresses, the progression is quite uniform: The surface of the cylinder is cooling quicker than the inside, the outside tends to undergo heavier contraction loads than the inside. Tensile stresses develop on the surface. This behaviour reproduces itself in the curves obtained at the *surface stations 3* and *4*. *Element 3* reaches higher stress values than *element 4*, it is situated at half the height of the cylinder and therefore is hindered to contract in the vertical direction. At the same time, the inside is set under compression by the quickly shrinking surface. When the cooling curve of the surface elements starts to flatten, a regression of tensile stresses occurs, hence reducing the compressive forces inside the cylinder.

Pure Expansion

The temperature evolution is the same as before. Now the only defined deformation will be the expansion of the material while undergoing the phase change.

Time - Displacement - Curves

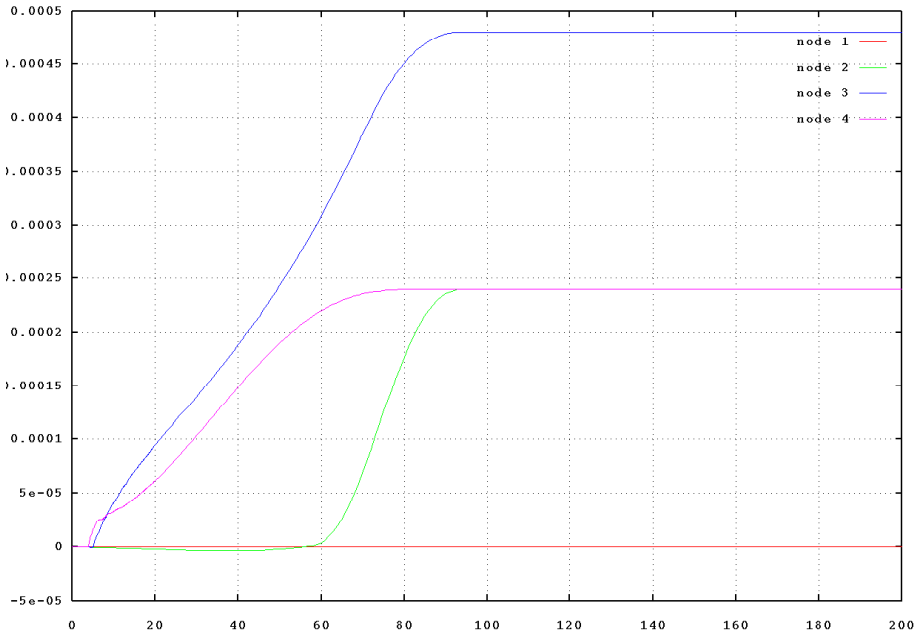

Figure 4.20: Radial Displacement for Pure Expansion

In contrast to the previous examples, here changes in deformation are only visible in a fixed time interval: from the moment the surface goes into the phase change until it is over throughout the sample. Looking at the radial displacements, *stations 2* and *4* reach the same final expansions but slightly out of phase. Compared to the previous example, the deformation curves reach a similar value, but within a much shorter time: the slopes are steeper. The quicker the element size is passing the phase change, the higher is the corresponding deformation slope.

Time - Stress - Curves

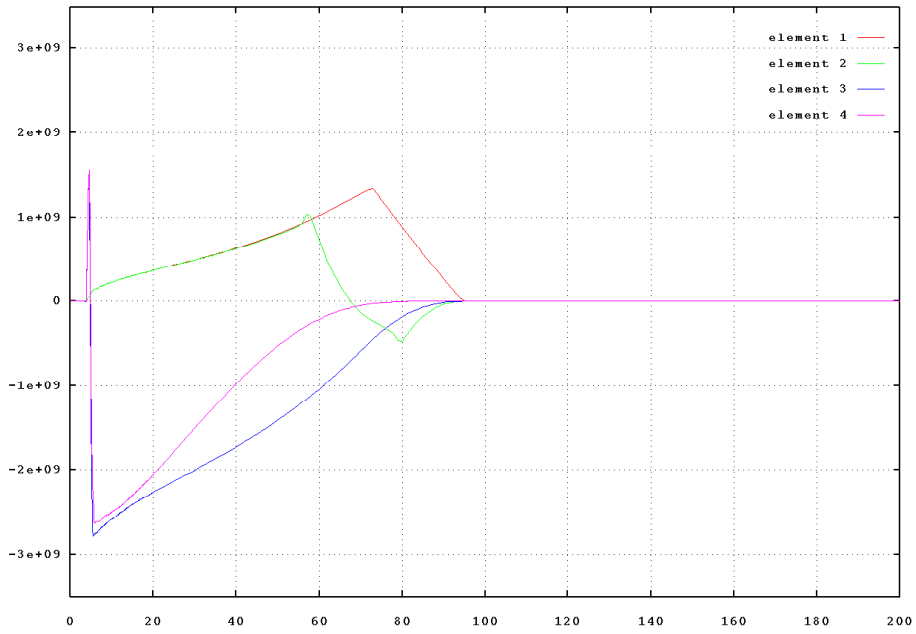

Figure 4.21: Circumferencial Stresses for Pure Expansion

The strong tendency of the surface to expand, while the inside value is not yet altered, obviously leeds to compressive stresses on the surface. As tensile stresses are concerned, the peaks which are visible on the plots (*stations 3* and *4*) must be interpreted as overshoots.This phenomenon refers to the speed of the process, as explained before. Apart from that, the general behaviour is inverse to the previous example: the inside of the cylinder is set under tension, due to the tendancy of the surface to expand.

4.3.3 Postprocessing

To illustrate the results, the postprocessor GiD is used. With its help one can get an impression of the development of various parameters over the whole cylinder throughout the process. The output limits are set from -200 to 200 MPascal, representing realistic breaking stresses of steel. Each of the first five seconds, in which the surface completes its cooling, are observed, then the plots are chosen in bigger time intervals. The process is only observed until the whole cylinder has passed the phase change. Looking at the pure expansional curves (*Fig.:4.21*), this is the case after about 87 seconds.

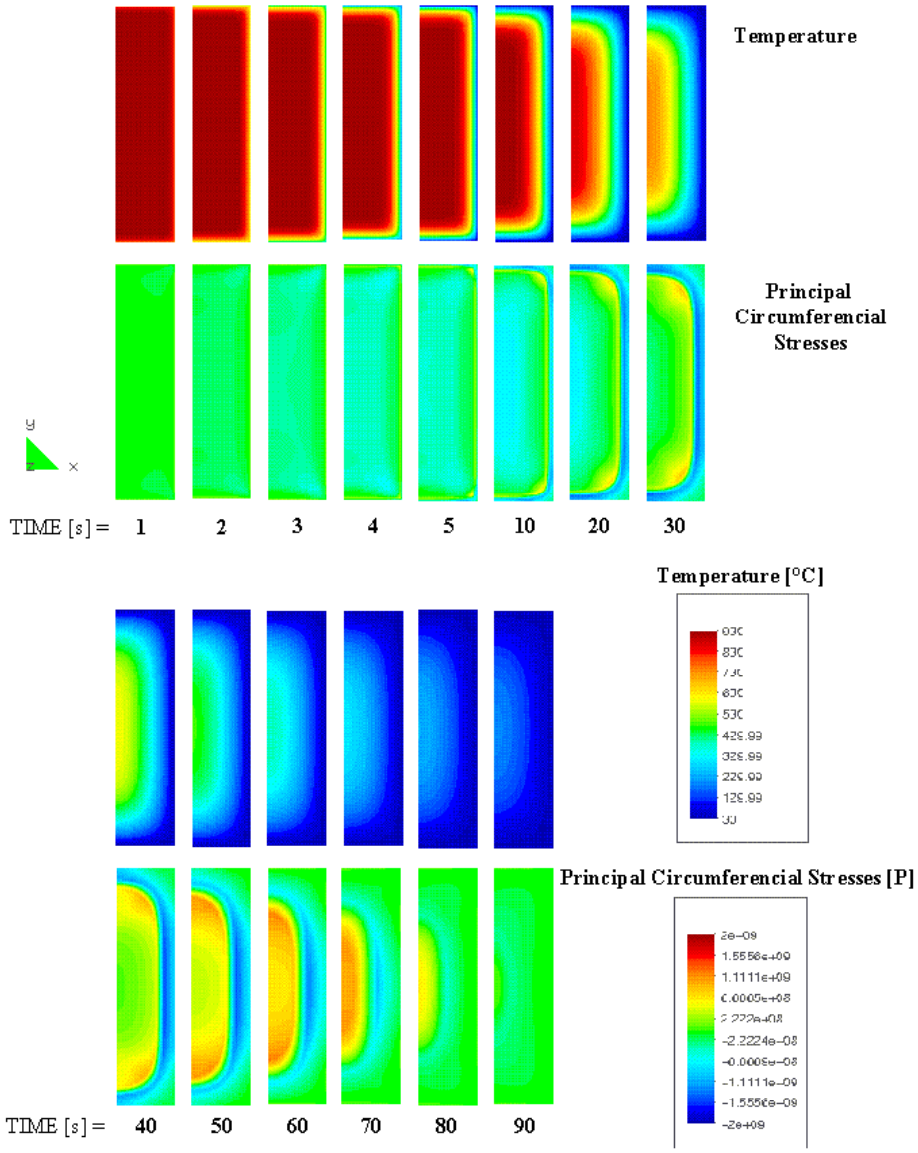

Figure 4.22: Original Material Properties

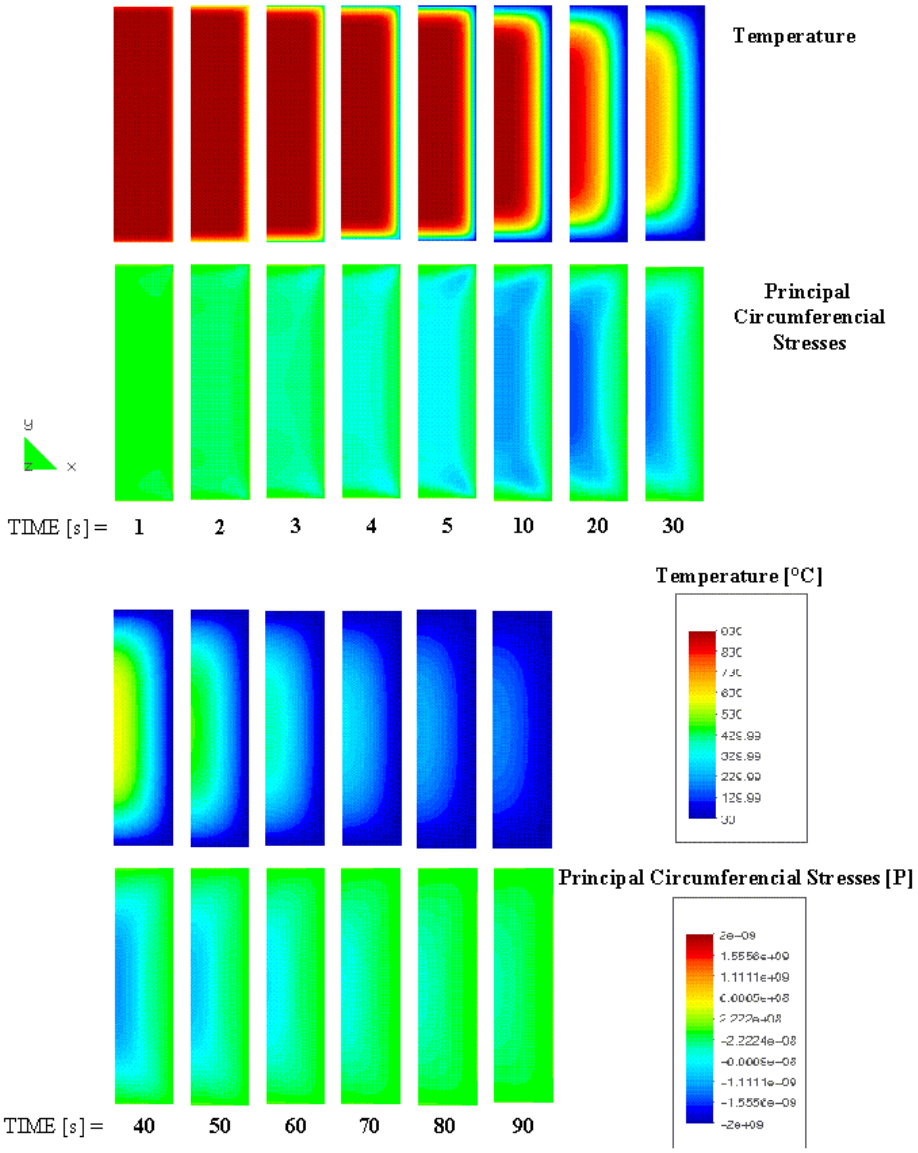

Figure 4.23: Pure Contraction

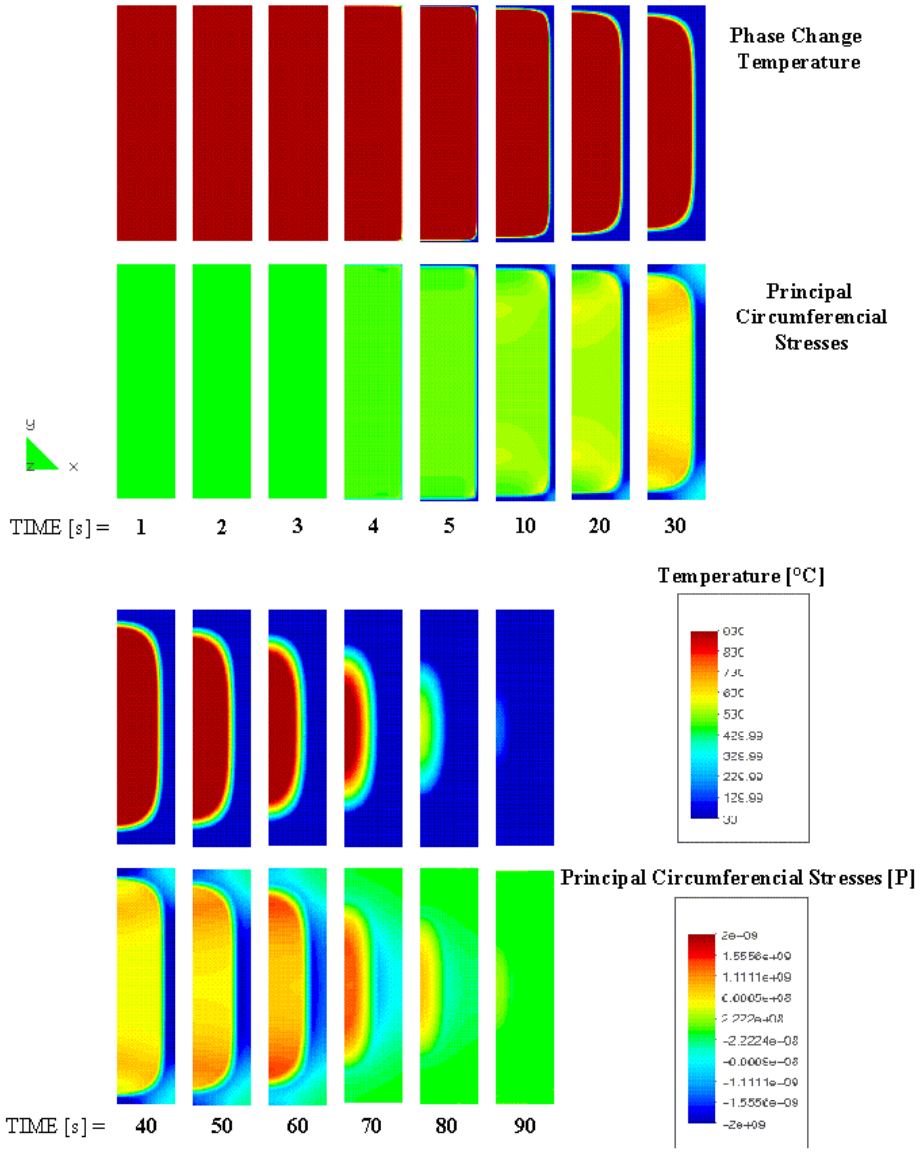

Figure 4.24: Pure Phase Change Straining

The three cases, previously discussed in this section, are plotted: The quenching of the cylinder with reference material properties, then without

the phase change straining coefficient (PSTRA=0) and at last without the thermal expansion coefficient (ALPHA=0).

For each case and for each of the time steps of interest the circumferencial stresses and the temperature are plotted:

Figure 4.22: Original Material Properties Comparing these pictures to the curves (*Fig.:4.17*), the GiD - plots show more homogenous results: Note that the first overshoot of the surface stations is not visible here. The surface does not reach as high tensile stresses as the inside. This variation of results may be due to the fact that the result pictures of the cross sections show the state at certain time steps. Unlike the curves, the results are plotted continously in plane but not in time. It is probable that at a different time step, the overshoot appears. For this example, the illustration gives a good impression on the process progression.

Figure 4.23: Pure Contraction The stresses only reach low values. Keeping the same scale as for the other examples, only the compressive stresses are visible.

Figure 4.24: Pure Phase change Straining In this case the process is compared to the progression of the phase change region throughout the piece: The upper and lower phase change rate are the limits of the temperature plot. It is conspicuous that the stresses and phase change temperatures progress simultaneously. Like in *Figure 4.22*, the first overshoot does not appear in the plot. Looking at the progression of the phase change area it is clearly observable how the cooling rate diminishes to the inside of the cylinder. The width of the area which passes the phase change at the same time, grows.

4.4 Conclusion

The high temperature gradients induced by the rapid cooling of the analysed specimen (*sections 4.2.1* and *4.3.1*) generate stresses which are many times higher than the ones created through slow cooling (*section 4.2.2*). Above a certain cooling speed, overshoots occur in the resulting curves. Due to the convergence of the program to the true value there are two possibilities to improve the results:

- increasing the number of elements (*section 4.2.3*)
- application of a smaller time step for the critical initial phase of the process (*section 4.3*)

Compared to the infinitely long cylinder, the process speed of the cylinder of finite height is abated due to increased flexibilty of the system. This fact and the effect of using a smaller time step leeds to a better approximation to the true material behaviour.

As a next step the two parts, in which the process can be divided - expansion and contraction - were analysed separately. The results for the complete quenching process have to be understood as the superpositions of the two parts. In *Figure 4.17* the first peak of the circumferencial stress curve for the *stations 3* and *4* obviously is reaching a value which cannot be explained by the real material behaviour. The peak of the pure compressive behaviour (*Fig.:4.19*) shows the maximum value which only can be reached by the material, if not already before the surface temperature drops down to the upper phase change limit. Therefore the peak is a calculation overshoot, initiated by the rapid process. This becomes obvious with the process part of pure expansion (*Fig.:4.21*).

When the surface temperature drops down to phase change temperature, the expansion of the material evokes compression at the surface. The compressive stresses of the whole process do not reach as high values as the pure expansional process: expansion due to the phase change and contraction due to the cooling are counteracting, the stress peak is diminished.

Chapter 5

Cylinder - Plastic Case

A big goal for industrial design is to determine the regions in which the produced steel part is most likely to break during the heat treatment. To make realistic predictions about the rupture behaviour more aspects of the physical problem have to be taken into account: Strong temperature dependency of the properties, plastic- and damage effects can not be neglected.

This chapter examines the influence of the added calculation aspects. The program enables a split of the resulting strains into its single components. This possibility can be used to get an insight about the interactions of elastic, plastic, thermal and viscous influences on the results.

The same geometry like for the thermoelastic calculation - cylinder of finite length (see *chapter 4.3*) - under the same run conditions (*chapter 4.3.1*) is examined.

5.1 Mechanical Properties

Most of the material properties of *chapter 4.1* remain the same, just the *elastic modulus* now is determined to be temperature dependent. Additive to that, three new material properties, also temperature dependent, are defined: the *initial yield stress,* the *tensile strength* and the *maximum plastic deformation (figure 5.2).*

Density	DENSI	7850	kg/m^3
Specific Capacity	SHEAT	552.6	mm^2/s^2K
Conductivity	CONDU	45.64	N/sK
Poisson Ratio	POISS	0.33	-
Thermal Expansion Coeff.	ALPHA	1.2E-5	$°C^{-1}$

Figure 5.1: Temperature-Independent Data

Temperature	Elastic Modulus (YOUNG) [N/mm^2]
20	200E+9
180	100E+9
270	50E+9
Temperature	Initial Yield Stress (YEINI) [N/mm^2]
20	300 E+6
180	800 E+6
270	1300 E+6
Temperature	Tensile Strength (YEFIN) [N/mm^2]
20	1E+9
180	1.5E+9
270	2E+9
Temperature	Maximum Plastic Deformation (EPFIN) []
20	4E-2
180	20E-2
270	40E-2

Figure 5.2: Temperature-Dependent Data

As explained in *chapter 2* and *4.1*, the examined steel passes the phase change between 270 and 180 $°C$. The temperature dependent data are defined in three steps: before, during and after the phase change. Converting from Austenite to Martensite, the material becomes more and more hard and brittle. The rising hardness is expressed by the increasing *elastic modulus*, the brittleness through the lower *tensile strength* and *maximum plastic deformation*. The *initial yield stress* is set lower for lower temperatures in this example, although to define a higher brittleness it should have been chosen the other way round. This has been done to better see the plastification differences for the different geometries (see *chapter8*).

5.2 Results

The resulting graphs have to be compared with those of the elastic example (see *figures 4.14 - 4.17*). The situation of the observed nodes and elements remain as defined in *figure 4.13*. The temperature development obviously remains equal, as the run conditions are not changed. In addition to the elastic deformations in this example the equivalent plastic deformations and the thermal deformations have to be observed.

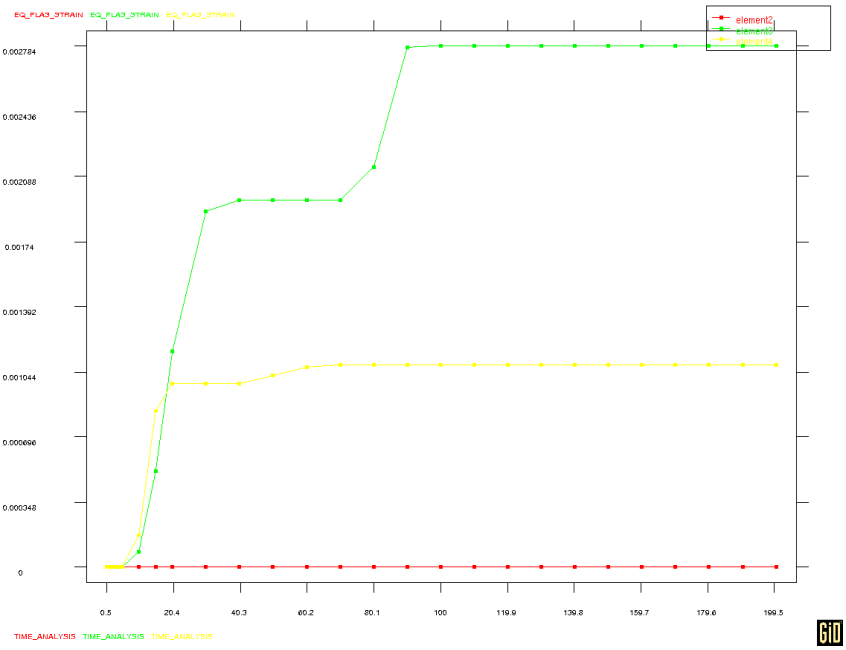

Figure 5.3: Equivalent Plastic Strains

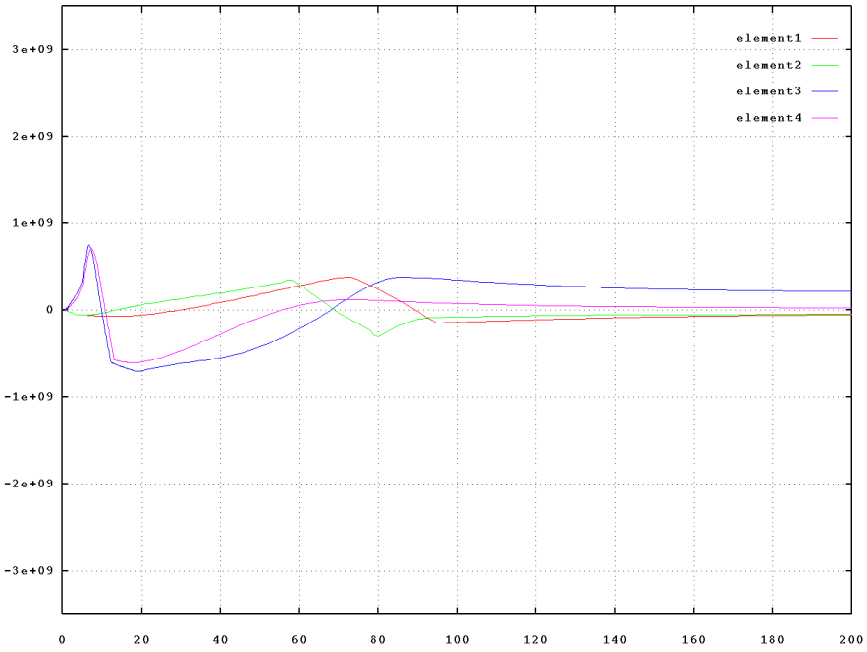

Figure 5.4: Circumferencial Stresses

The circumferencial stresses (*figure 5.4*) only reach values which are less than half as big as the ones of the elastic example. To understand the course of the stresses, they have to be compared to the graph of the equivalent plastic strain (*figure 5.3*) and to the temperature dependent values of the initial yield stress (*figure 5.2*). Looking at the development of the equivalent plastic strain of the point near the surface at half hight of the cylinder (*element 3, figure 4.13*) there can be five time-sections distinguished: The first from zero to about five seconds, in which the plastic strain is zero. Then a continous rise until second 20 of the cooling, afterwards a flat course during 40 seconds, another rise for 20 seconds and finally another flat course.

This distribution can be explained in the following way: During the first seconds of the cooling, the stresses at the surface rise rapidly but do not yet reach the initial yield stress. Once the stresses reach the limit of the initial yield stress, the cylinder starts to plastify - the plastic strain rises. As the body plasticifies, the tensile stresses do not reach as high values as in the elastic case. Passing the phase change, the surface expands, the tensile stresses are released and compressive stresses develop at the surface. Once the phase change temperature has passed, the surface contracts again, the

compressive stresses are released. As soon as the stresses drop under the initial yield stress limit, the next time-section of the equivalent plastic strain is reaches: the plastic strain remains constant. When the outside has reached the goal temperature of 30 $^{\circ}C$, it does not contract any more. On the other hand, the inside is still cooling and contracting. Tensile stresses at the outside are resulting. These stresses again become higher than the limit of the initial yield stress, this produces the second plastification - the second rise of the equivalent plastic strains. Finally the temperature of the body becomes more and more homogeneous, the tensile stresses at the outside are released, the plastification stops and the equivalent plastic strain remains constant.

In a similar way the courses of the other elements can be explained: at *element 2*, situated in the inside of the cylinder, the stresses do not reach high enough values to cause plastification - the equivalent plastic strain remains zero. At *element 4* the cylinder undergoes the first plastification phase. Later on the stresses remain too small to reach plastification values.

5.2.1 Postprocessing

Like in the elastic case, the postprocessing gives a better impression of the result distribution throughout the body than the observation of single points. The behaviour of the different regions of the geometry and their relation to each other become clear. Each of the first five seconds, in which the surface completes its cooling, are observed, then the plots are chosen in bigger time intervals. The process is only observed until the whole cylinder has passed the phase change.

Figure 5.5: Deformations

The plot of the deformed mesh shows qualitatively how the geometry deformes with progressing cooling. The amplification factor was set to 40. Before entering the phase change, the cylinder contracts uniformly. It can be observed that the shape of the surface bounds becomes a convex curvature near the edge. This is because the edge cooles down from two sides and therefore shrinks quicker. As it cools quicker, it is the first part of the surface to enter the phase change. While the surface passes the phase change, it expands. At the edges now the inverse effect appears: Expansion is faster than for the rest of the surface, the curvature near the edge becomes concave. The most distinctive deformations appear at second 10, when the surface is

still cooling and contracting rapidly while the inside passes the phase change with the same effect as described above: the areas near the edges expand to a greater extension than the core. Later, the surface reaches the goal temperature while the inside still expands, passing the phase change. Now the core of the cylinder passes the phase change, the expansion is intense in the area of the core. This leads to a compensation of the curvatures at the surface and finally even to a slight convex shape.

Figure 5.6: Von Mises Stresses

The *Von Mises stresses* appear concentrated in the area of the cylinder in which the phase change just passed. This area cools down and contracts while the immediately following area passes the phase change and expands. High compression and therefore Von Mises stresses in the contact area are the result.

Figure 5.8: Equivalent Plastic Strains

The *equivalent plastic strains* already were explained in relation to the graph. Comparing to the graphs the post process plots show sometimes surprising results. Looking at the course of *element 4* (*figure 5.3*) one could draw the conclusion that at the top surface the equivalent plastic strains do not reach as high values as at the lateral surface. But it should not be forgotten that the curve only represents the results at a certain point and not always at the sorrounding neighbourhood. The GiD-plots show quite the reverse to the assumption drawn from the results of the graph: The equivalent plastic strains reach their maximum at the top surface, even though closer to the symmetry axis than *element 4*. The pattern of the strain-distributions reminds of the shape of the deformations and can be related to the same reasons: the areas which remain plastified - after the described deformation development - show the highest plastic strains. The steps in which the plastic strains appear and rise correspond to the steps explained from the graphs: The plastification appears in the area in which the highest stresses occured during the second part of the cooling - when the body already passed the phase change and the initial yield stress limit is lower in comparison to the cooling phase before the phase change.

Figure 5.7: Temperature Gradient

The temperature gradient is the rate of variation in temperature over a given unit distance. To understand the plots, it is helpful to compare them to the temperature graphs of *figure 4.14*. The temperature graph of the surface is very steep during the first ten seconds while the inside graphs run flat. The distance between the curves at the outside and the inside reaches its maximum at around second 5. The temperature gradient plots show a corresponding development. It is conspicious that the upper and lower edges of the cylinder show a much lower temperature gradient than the surfaces next to it. As the edges are cooled down from two sides they cool down more prfoundly then the neighbourhood, therefore in the area of the edges the temperature is more uniform than along the rest of the surface.

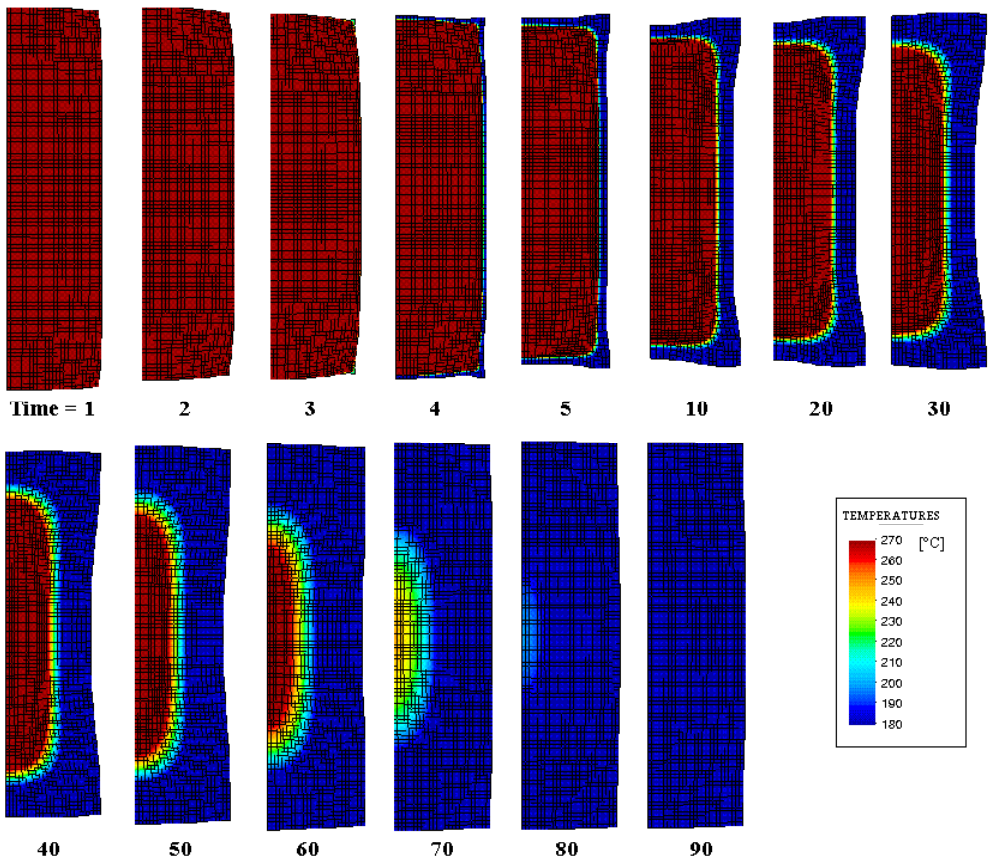

Figure 5.5: Deformations and Phase Change Temperatures

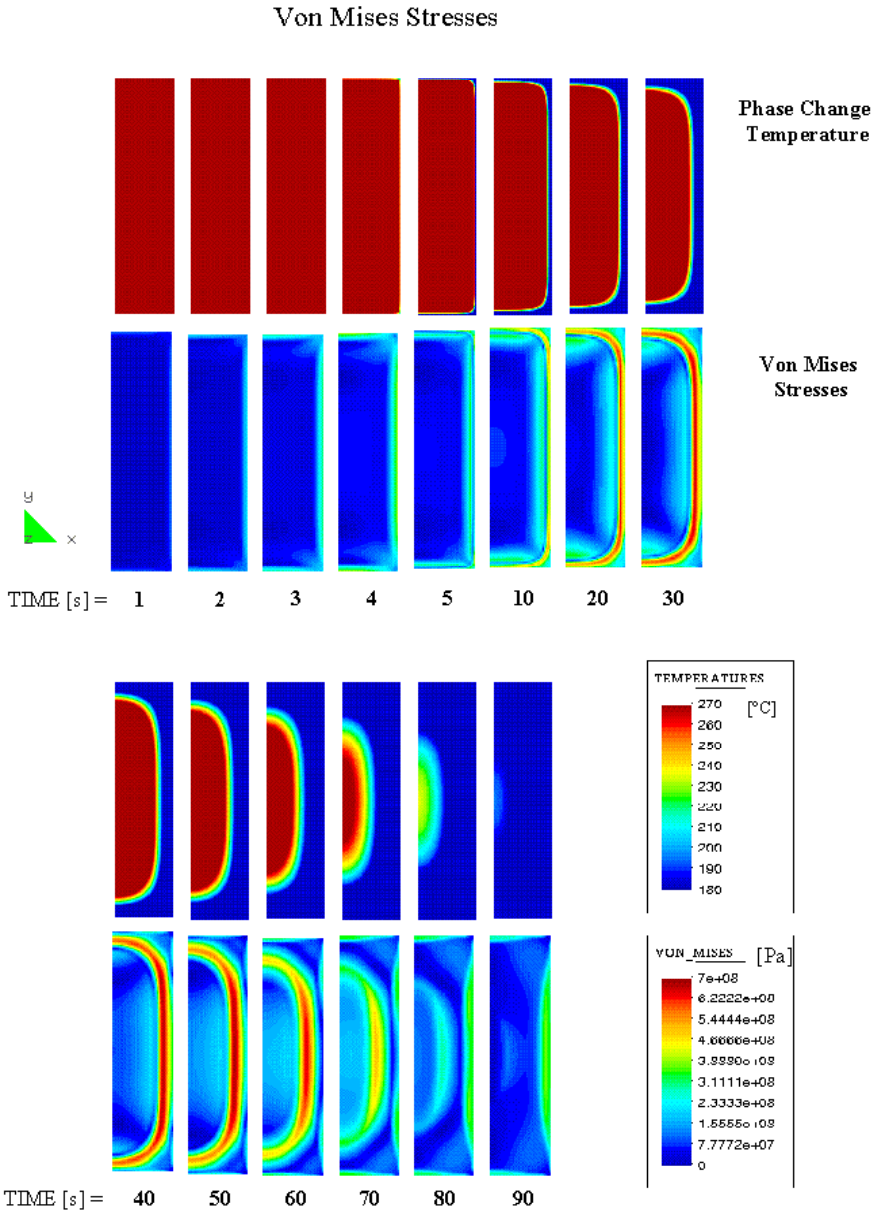

Figure 5.6: Von Mises Stresses

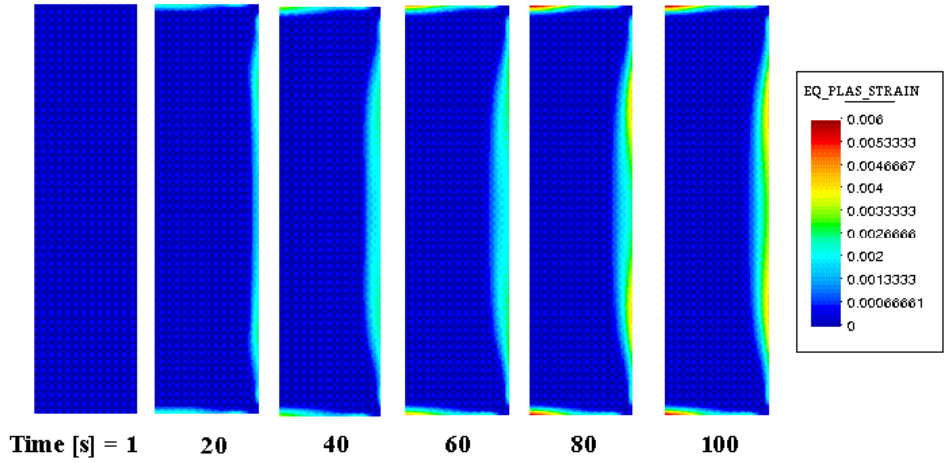

Figure 5.7 : Equivalent Plastic Strain

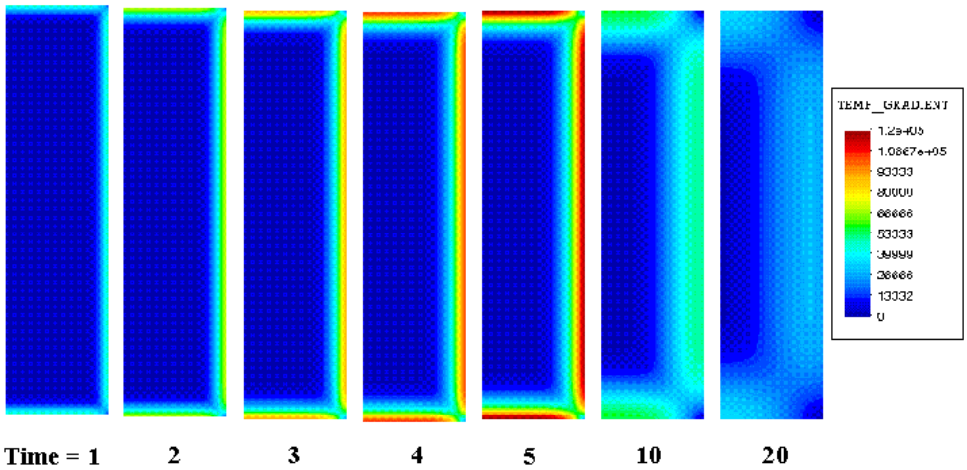

Figure 5.8: Temperature Gradient

Chapter 6

The Cube

The basic principle of successful design is to plan shapes that will keep the temperature gradient throughout a piece at a minimum during quenching. Examining different shapes it is possible to show how specific variations in design influence the stress development. The geometry of a cube (side length 10 cm) is chosen for a second thermo-plastic calculation, as this 3D-example shows clearly how the more unhomogeneous shape leads to a higher temperature gradient and therefore to a higher damage.

To examine the effect of the straining during phase change for the plastic case, the results of deformation and equivalent plastic straining are compared to the parameter variation without straining during phase change (pure contraction).

Figures 6.1 and 6.2: Deformed Mesh

Like for the cylinder, the amplification factor was set to 40. Looking at the results of the cube that is submitted to cooling without phase change expansion (*figure 6.1*), a quite uniform deformation can be observed. It is remarkable that the edges are rounded off in the first steps and later on become sharper again. This phenomenon was already explained from *figure 5.5*: The edges cool down from two sides and therefore shrink quicker. Once the surface has cooled down to the goal temperature and the massive core still continues shrinking, the surface center moves to the inside, the edges appear again and even a slightly concave curvature results.

The deformation of the calculation with phase change expansion does not show the rounding off before the surface entering the phase change as

observed for *figure 5.5* as the time steps are too big. But it shows clearly how the expansion of the surface-near area leads to protruding edges as they are forced to expand from two sides (time-step 30, *figure 6.2*). Later on, when the surface is already cooled down and the core passes the phase change, the area around the core expands, convex curvature can be noticed in the center of the surfaces while near the edges the rounding remains concave (time-step 60 and 80, *figure 6.2*).

Figures 6.3 and 6.4: Equivalent Plastic Strains

To examine the development of the equivalent plastic strains, a cut through the middle of the cube is observed. The results can be connected with the deformations of the cube (*figures 6.1 and 6.2*) and with the temperature development throughout the body: The edges, which are the fastest cooling regions of the surface, show the highest plastic strains. As they tend to deform stronger than the rest of the body, they are the places where plasticity appears. In the case of the pure contraction they do not reach as high plastic strains as in the case with phase change, where the deformation orientation changes direction and therefore leads to high stresses or plastic strains, respectively.

It strikes how the corners of the cube represent the critical areas of the geometry. Assuming that the material is brittle and the tensions reach high enough values, the corners would break off. As already explained in *chapter 2* sharp edges and corners should be avoided in the design.

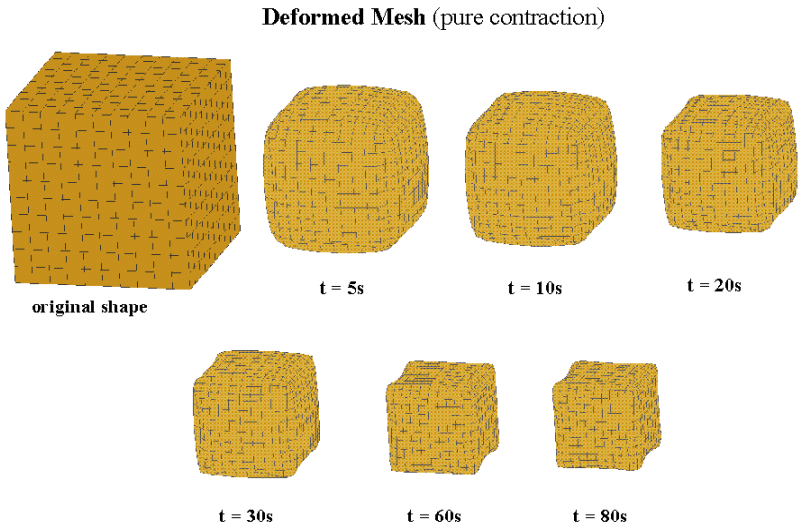

Figure 6.1: Deformed Mesh - pure contraction

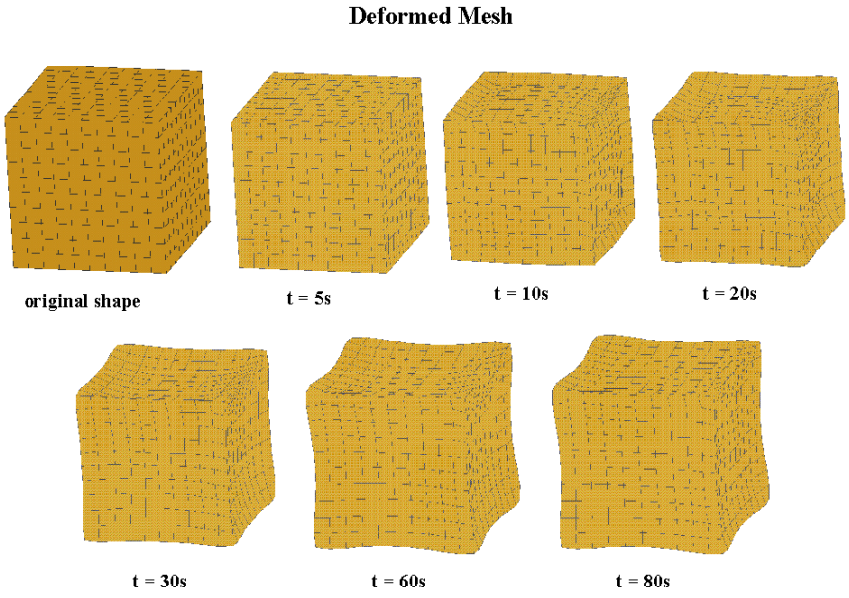

Figure 6.2: Deformed Mesh - with Phase Change

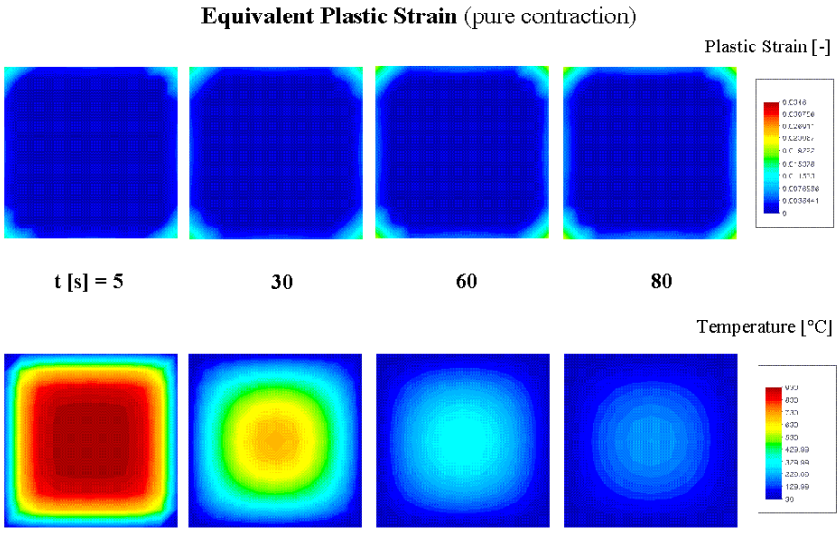

Figure 6.3: Equivalent Plastic Strain - Pure Contraction

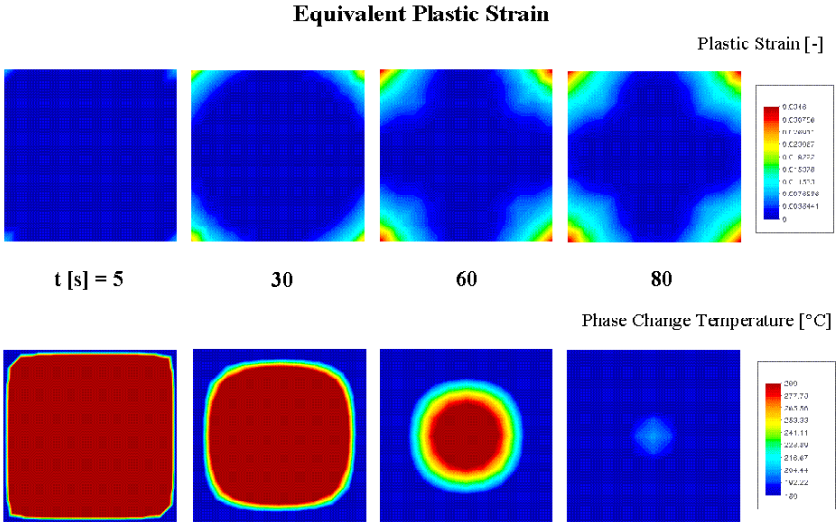

Figure 6.4: Equivalent Plastic Strain - with Phase Change

Chapter 7

The Excavator Tooth - Elastic Case

7.1 Introduction

In the previous chapters, different heat treatment processes have been theoretically explained (*chapter 2*) and the application of the quenching process to a numerical model executed and discussed (*chapters 3 to 6*). As mentioned before, the examined heat treatment process is related to a real industrial problem: the quenching of steel as part of the production of pure martensitic excavator teeth.

The previously defined mechanical properties of the elastic case (*chapter 4.1*) and cooling rate (*4.2.1*) can be used for the geometry of a tooth, the size of which is comparable to the one of the finitely long cylinder. The temperature-, deformation- and stress behaviour will roughly correspond to the descriptions of the previous chapter and will not be further discussed.

In this chapter the emphasis is put on the observation of the characteristics in design.

7.2 Geometry

The design of an excavator tooth has to be a compromise between the optimal manufacturing geometry and the optimal service geometry:

On one hand the manufacturing aspect demands a design which allows a uniform cooling. The temperature gradient throughout the piece has to be

kept at a minimum during cooling. (The optimal shape would be a sphere.)

On the other hand the teeth must be able to break hard materials like rocks. For such a purpose an edged body and a pointed end are the service requirements for the shape of the teeth.

Looking at the chosen design, many of those compromises become visible:

The back of the tooth is hollow, in this way the cross section becomes more uniform than it would have for the massive body of tapered shape.

The second aspect is the design of the surface: Sharp edges and re-entrant angles, providing dangerous stress concentrations and therefore a high damaging risk, are avoided and substituted by rounded edges. The effect of this aspect will be illustrated by further models (*section 4*)

Two variations in design are analysed and compared. As the geometry of the teeth is symmetric with respect to the longitudinal mid-plane, it is sufficient to analyze only one half of each body. This way the mesh can be chosen twice as fine for the same calculation time. The mesh of each body consists of nearly fifty thousand tedrahedral elements.

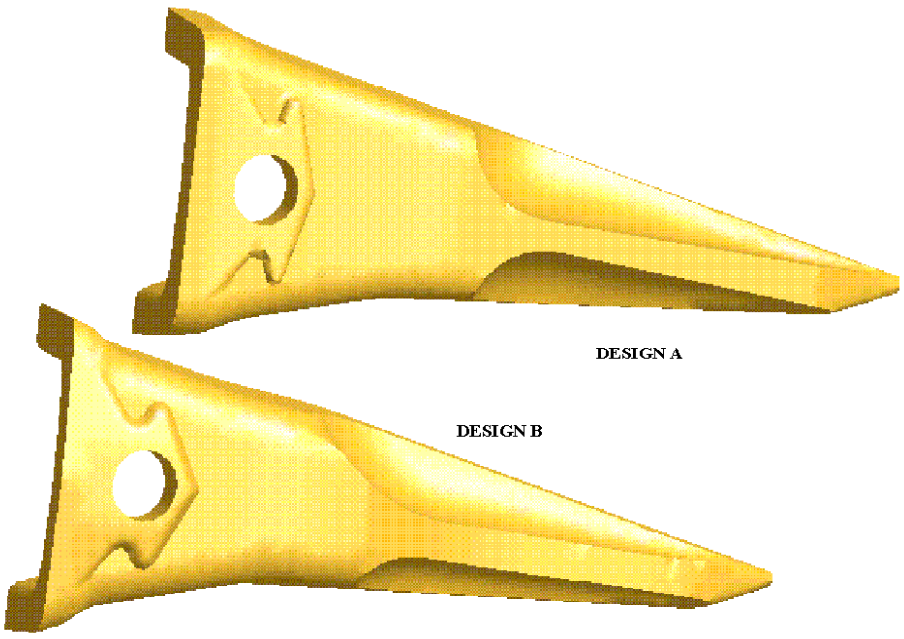

Figure 7.1: Models of the Teeth

It can be observed with *Figure 7.1* that Design B is of a more asymmetric

shape than Design B. Looking at the following cross-sections it also becomes visible that Design B is of reduced volume.

The results are examined by focussing on characteristic cuts through the bodies. Curves over time of single stations of the bodies, like plotted for the example of the cylinder, are not examined here. In the case of the cylinder, the chosen stations are representative for the clearly defined characteristics of the area where they are situated. The complexity of the body does not allow to draw conclusions valid for the whole body from the behaviour of single points. The different areas of the geometry influence each other in a way that can only be examined globally.

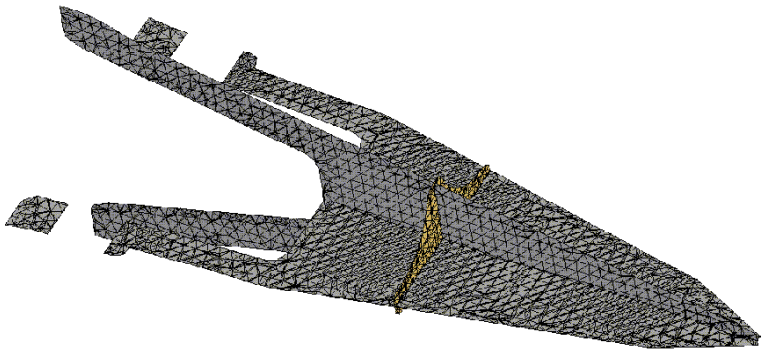

Figure 7.2: The Three Cuts through the Tooth

Cuts

The stress progression is observed at three cuts through the threedimensional body: along the xy-, the xz- and the yz-planes. The cuts are observed in the following order:

Firstly, the two longwise cuts are made. The crosswise cut is determined by the place at which the two initial cuts show the highest stress concentration in the inside. This cut is of special interest in the examination, because, according to the production experience, this is the cross section at which

the teeth have the highest probability of breaking due to the loads of the quenching process.

Like for the cylinder, the stress scale is set from -200 to 200 MPascal, representing realistic breaking stresses for steel.

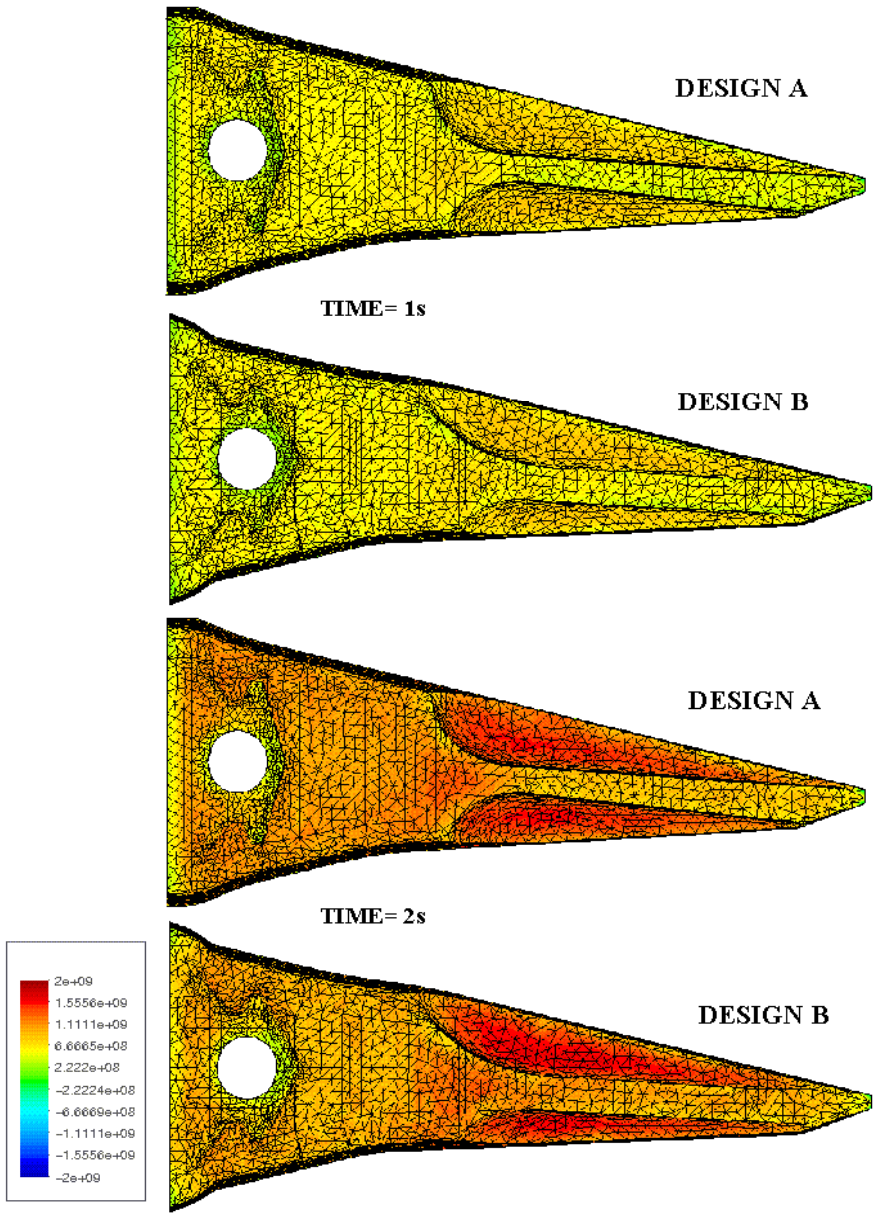

Figure 7.3a: 1.Principal Stresses [P] at the Surfaces of the Two Designs

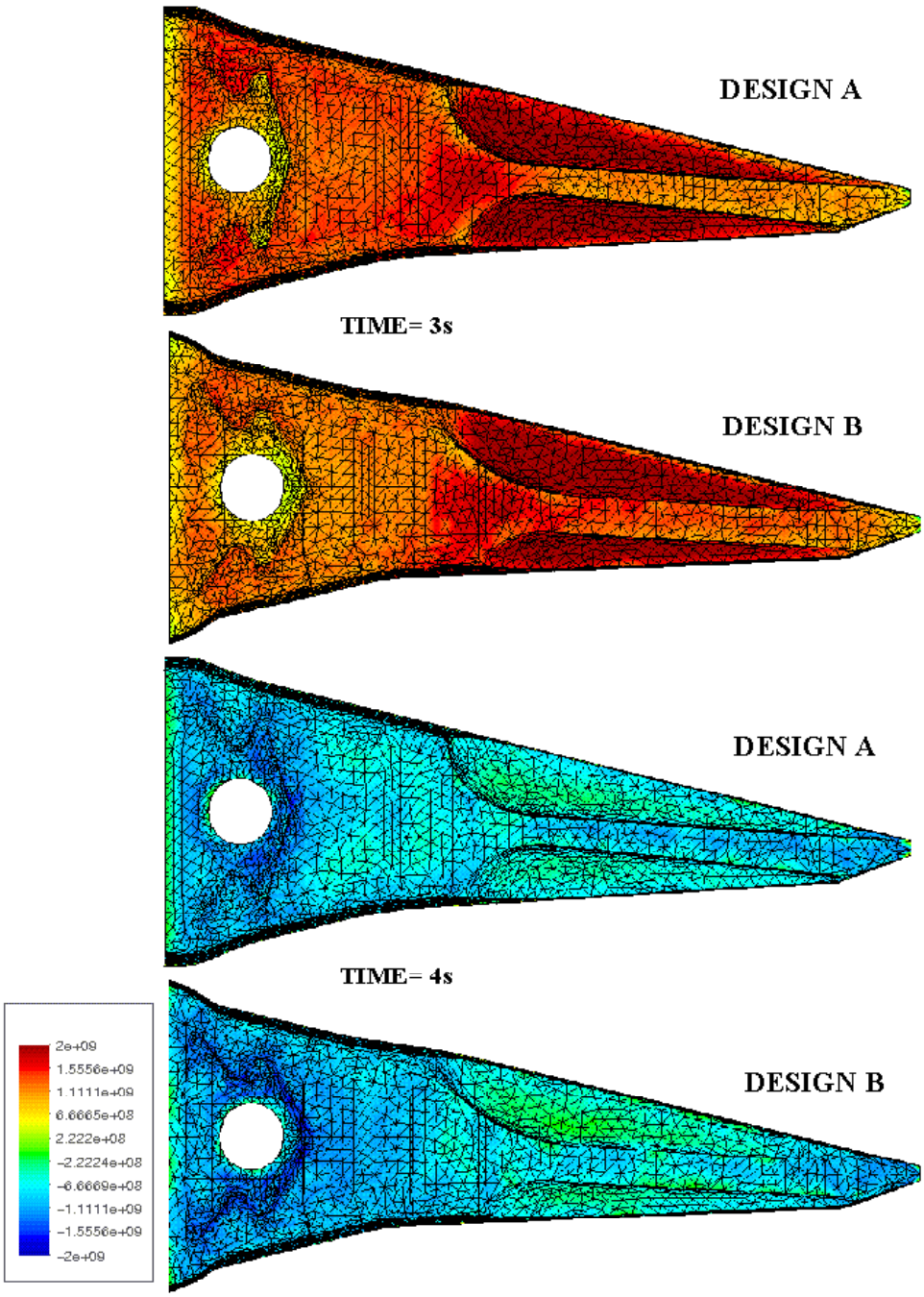

Figure 7.3b: 1.Principal Stresses [P] at the Surfaces of the Two Designs

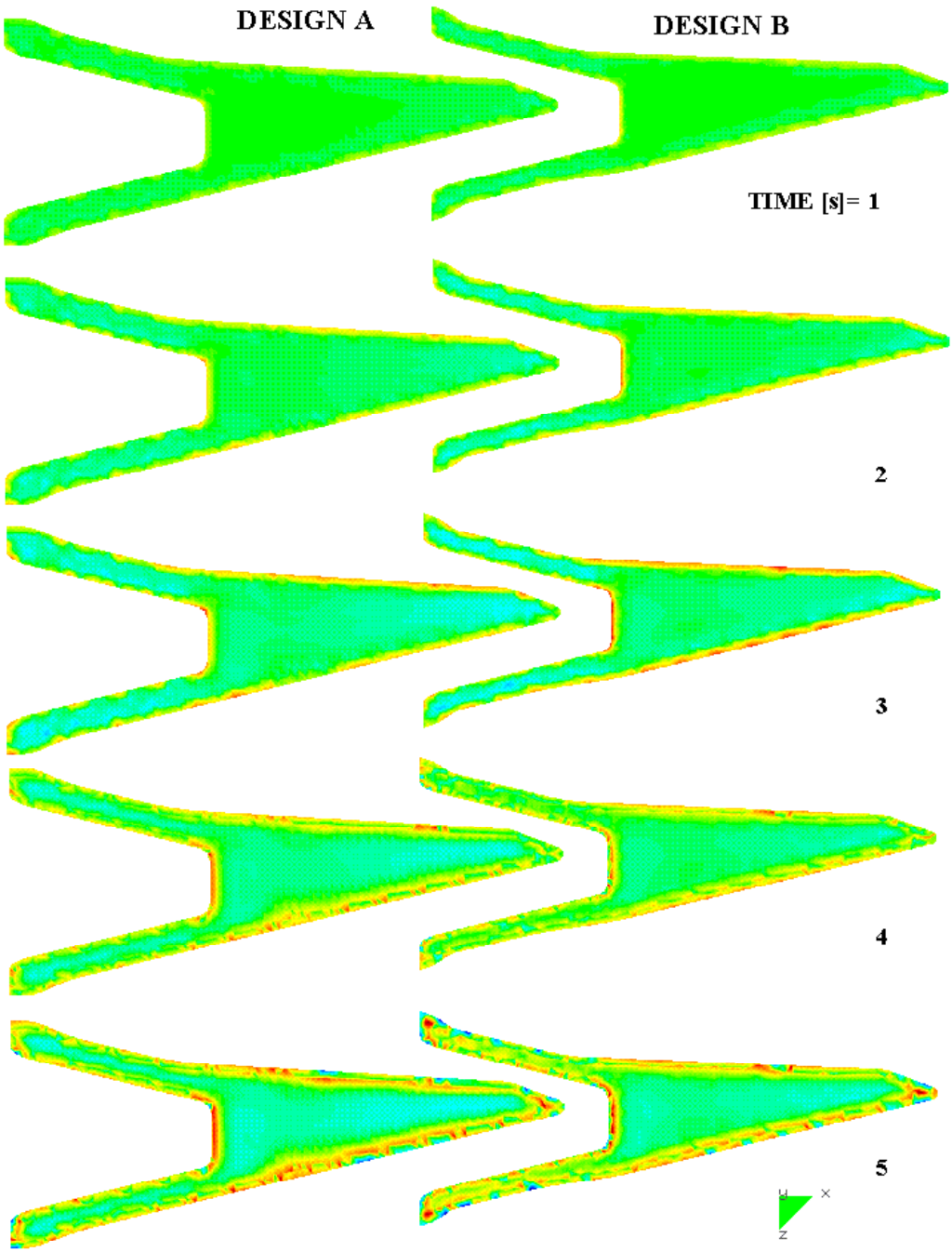

Figure 7.4a: 1.Principal Stresses [P] at the XY_Lengthwise Cut

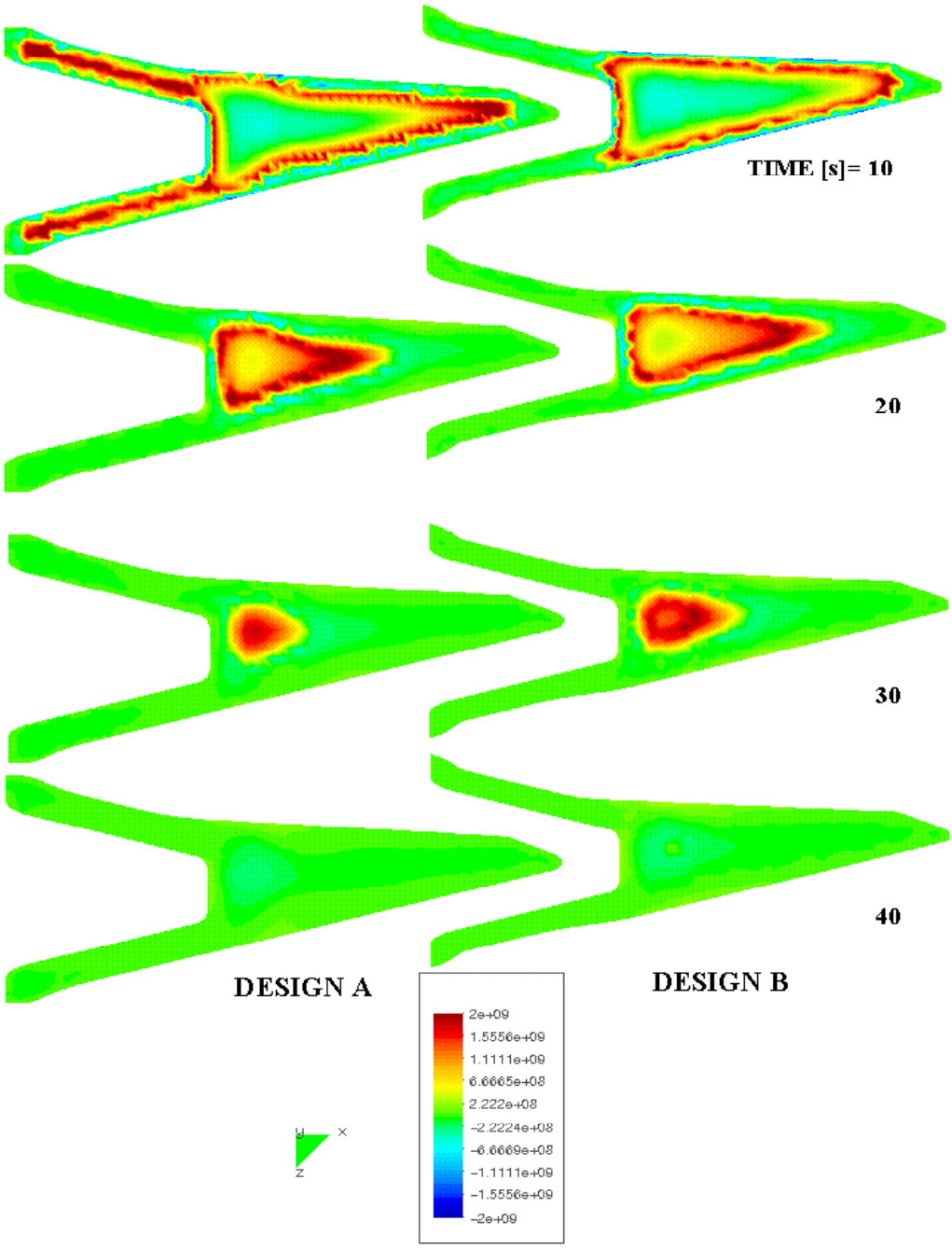

Figure 7.4b: 1.Principal Stresses [P] at the XZ_Lengthwise Cut

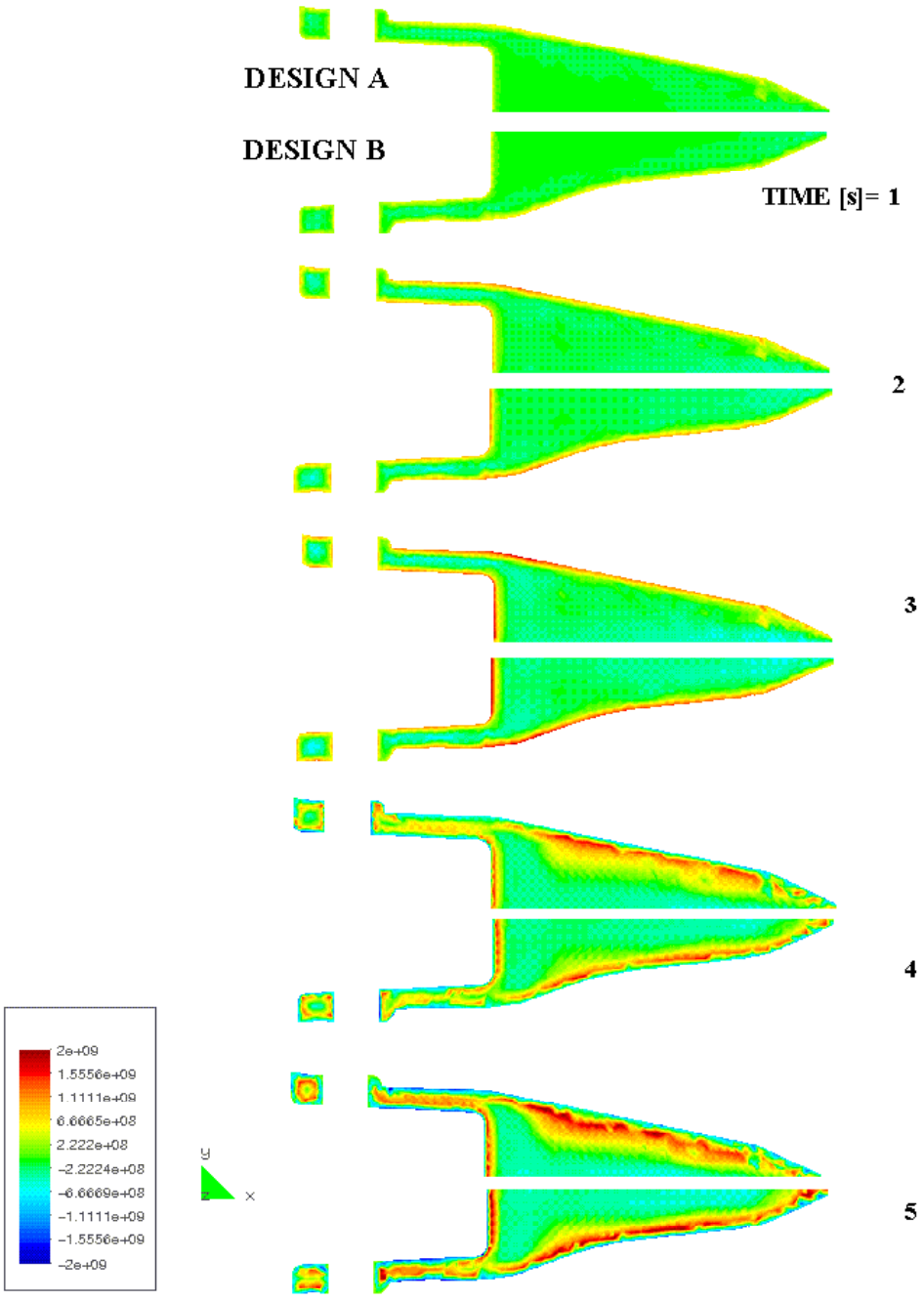

Figure 7.5a: 1.Principal Stresses [P] at the XY_Lengthwise Cut

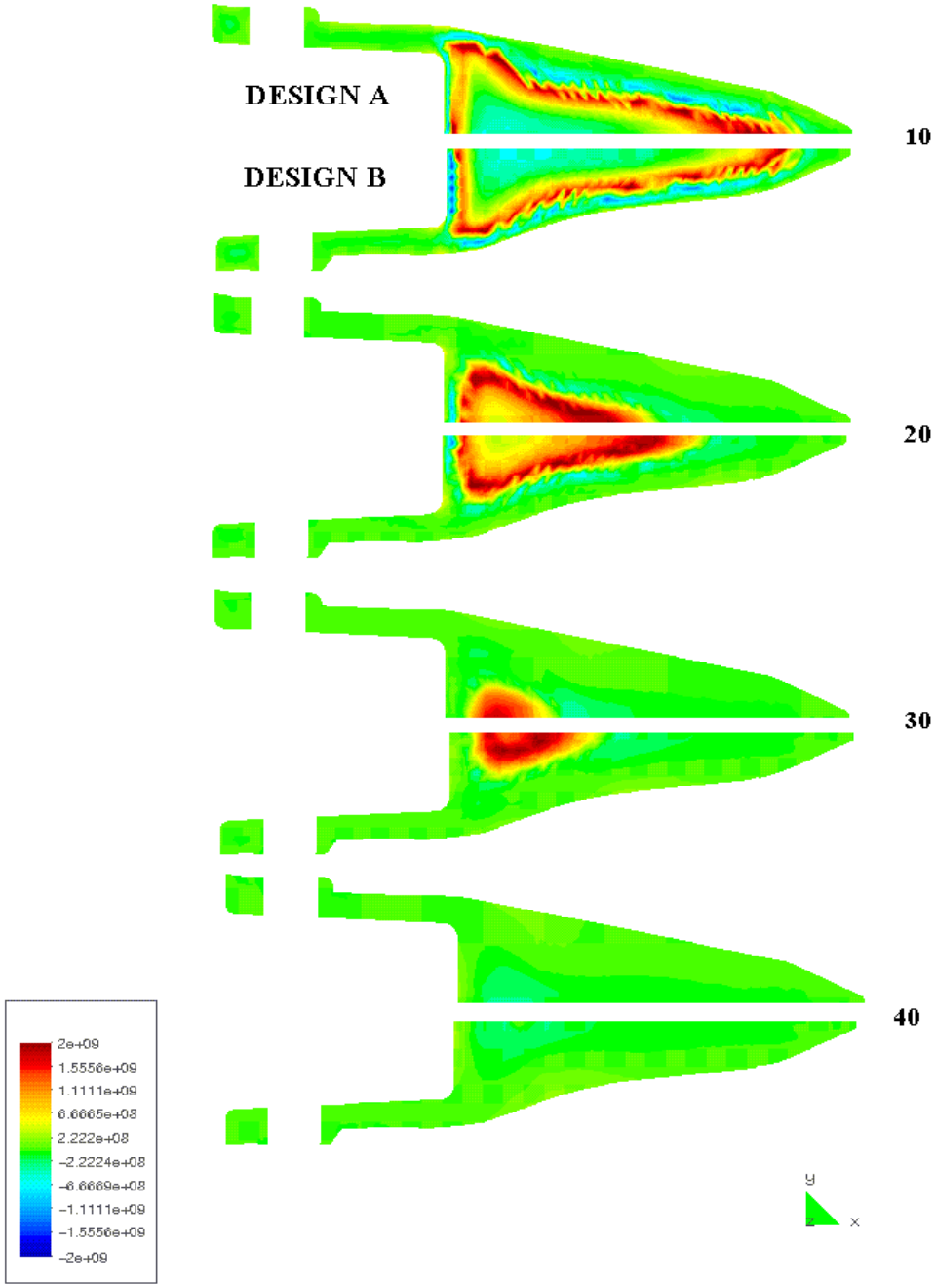

Figure 7.5b: 1.Principal Stresses at the XY_Lengthwise Cut

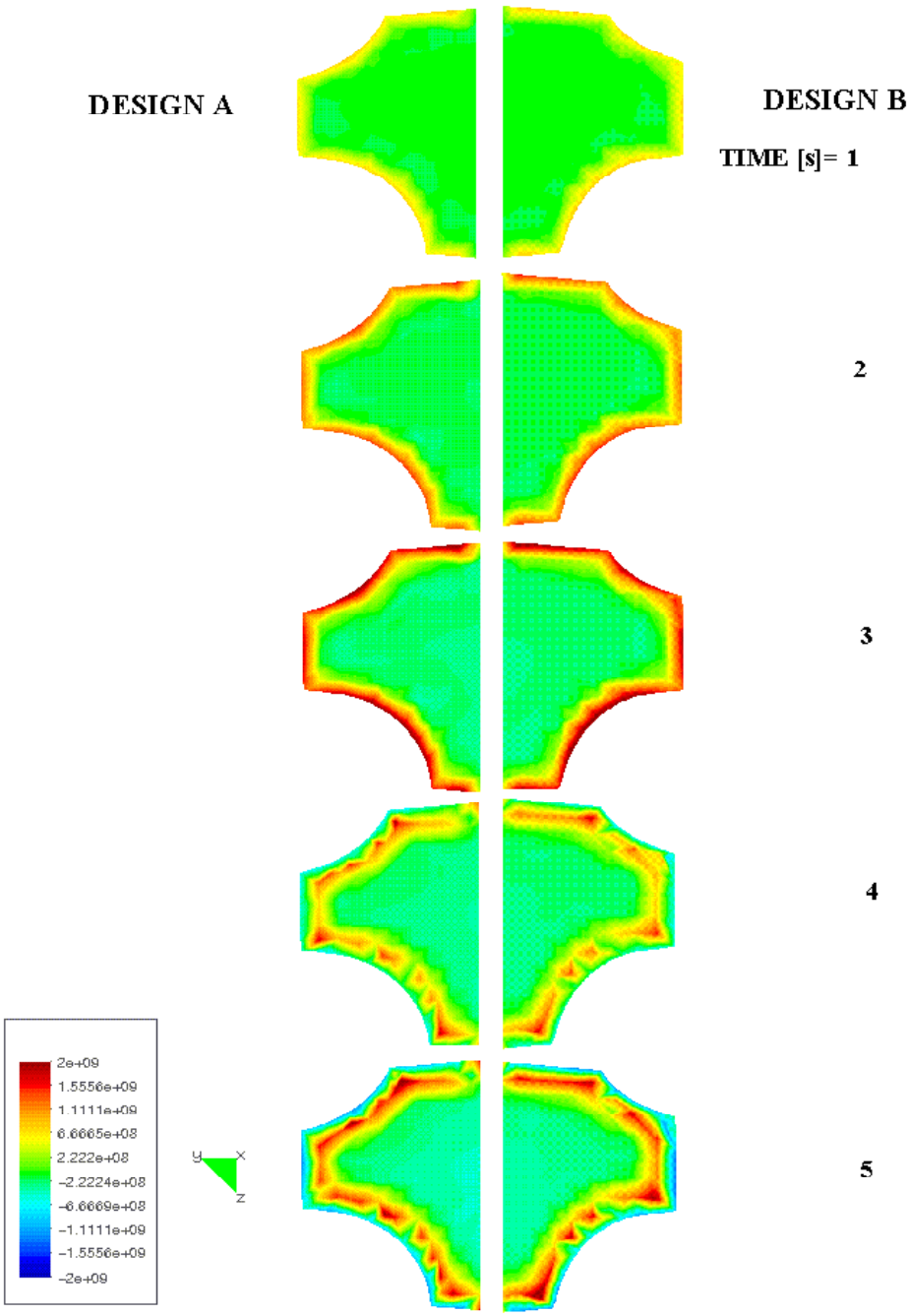

Figure 7.6a: 1.Principal Stresses [P] at the Crosswise Cut

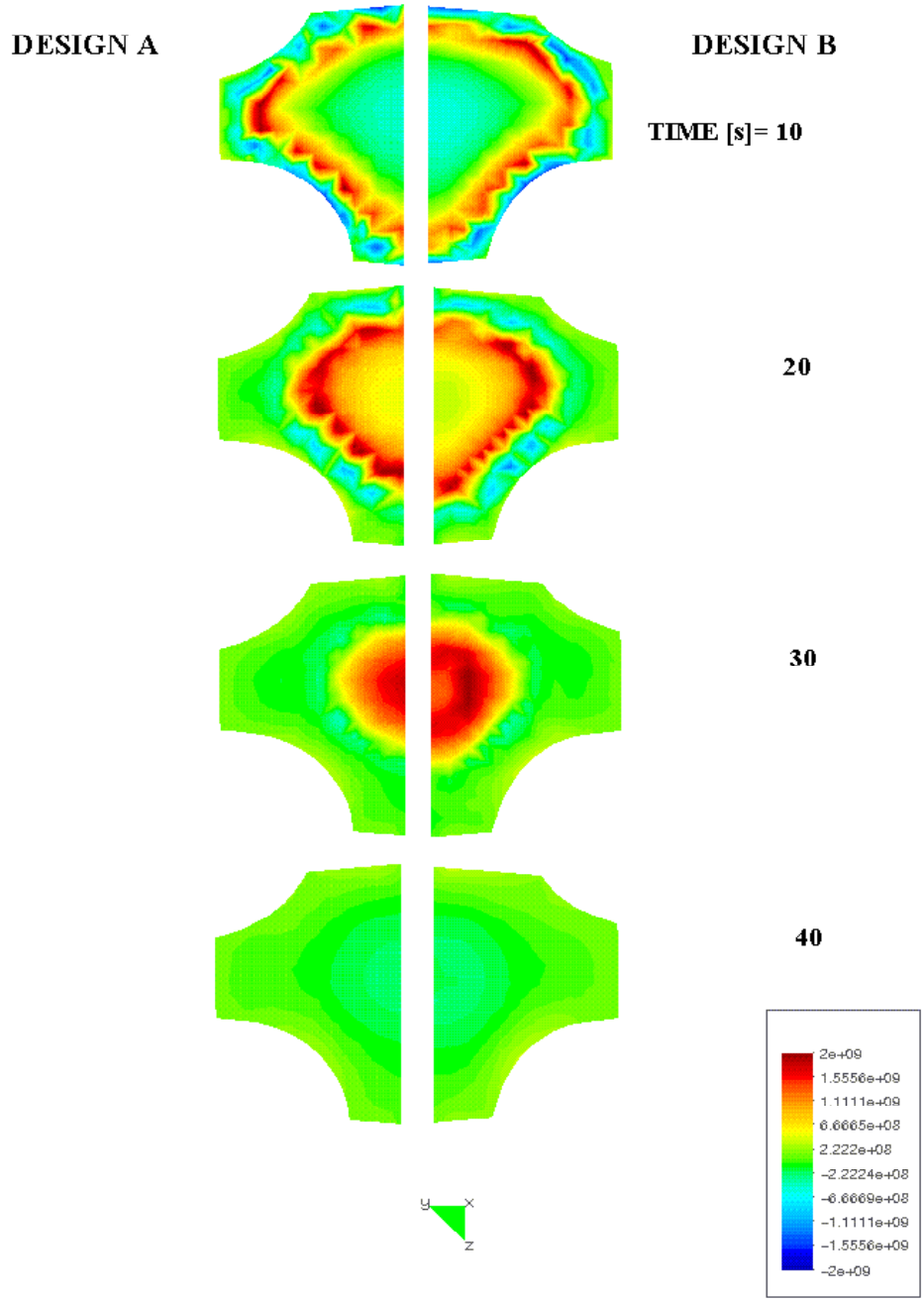

Figure 7.6b: 1.Principal Stresses at the Crosswise Cut

7.3 Results

The first principal stresses are plotted. The observed stress development corresponds approximately to the one described for the cylinder: The stress wave is passing the body from the surface to the center at the same time, in which the body undergoes the phase change.

The main difference between the results for the cylinder and the teeth is based in their differently distributed volume: While the cylinder has a completely uniform volume, whose stress wave approaches more and more the shape of a sphere (according to the distance to the cooled surface), the cooling of the teeth does not behave as uniformly: Thinner parts, like the pointed end or the hollow part, pass the cooling process clearly quicker than the massive core. This is because the thinner parts are cooled from more than one side at the same time. Looking at *Figures 7.4* and *7.5* it becomes clearly visible that the hollow parts are cooling first.

A further feature is that the surface does not cool down uniformly. As can be seen in *Figure 7.3*, the surface passes the critical phase within the first four seconds. It is also observable, that in some regions of the surface the stresses reach higher values than in others. This is due to the characteristics of the design. Especially the re-entrant parts of the surface show a stress concentration. These parts, to which heat is being supplied through a greater area as the one from which it is being dispelled, are naturally cooling slower than flat or protruding parts of the surface. In this context it means that at the moment, at which the rest of the surface already reaches the upper phase change temperature and starts to expand, the slower cooling parts are still contracting. This leads to the higher tensile stresses observed for second 3 in *Figure* 7.3.

Another difference, comparing the plots of the teeth to the ones of the cylinder, is the quality of the results. The cylinder with its much smaller elements shows a distribution of stresses which is obviously only dependent on the geometry of the body. However, in the stress distribution of the teeth the contours of the single tetrahedral elements become clearly apparent (*Fig.7.4*). This is especially true for the beginning of the cooling process, when the phase change range passes the outer part of the body and cooling front advances with a high speed, whereas the contours, the stress wave reaching the core of the body, become blurred.

The mesh is not distributed homogeneously over the volume, but it exists

a concentration of (smaller) elements along the region where the part changes from a massive to a hollow body. Along this line a more homogenous stress distribution can be observed. However, still the elements shapes are visible.

To attain better results, it would be useful to distribute the finer mesh along the whole surface, as the process speed is the highest at the outside.

Comparing the plots of the two designs of the tooth, it does not become apparent which one will have a better resistance against the loads of the quenching process. However, the geometric variations between the two design are clearly visible (*Fig.:7.4b and 7.6b*) and it can be observed that the cooling processes of the specimens vary in time. But the influence that those differences have on the manner in which they are examined here, are small. To get more information on the real material behaviour and the effect of those changes in design, other aspects have to be taken into account. Aspects like plasticity and time dependence of the mechanical properties have to be added to the calculation. But these steps are beyond the scope of this work.

Nonetheless the influence of variations in geometry are visualised in the following section.

7.4 Modified Cut

The chosen example refers to the crosswise cut (*Fig.:7.6*) The influence of the design of the re-entrant angle is focussed. Three cylinders, with cross-sections similar to the crosswise cuts of the teeth and the same cooling rate at the boundary, are calculated.

In the first example, the re-entrant angles are modelled as sharp edges. In the following examples these edges are rounded: For the first rounding a small radius is chosen, for the following one a three times bigger radius.

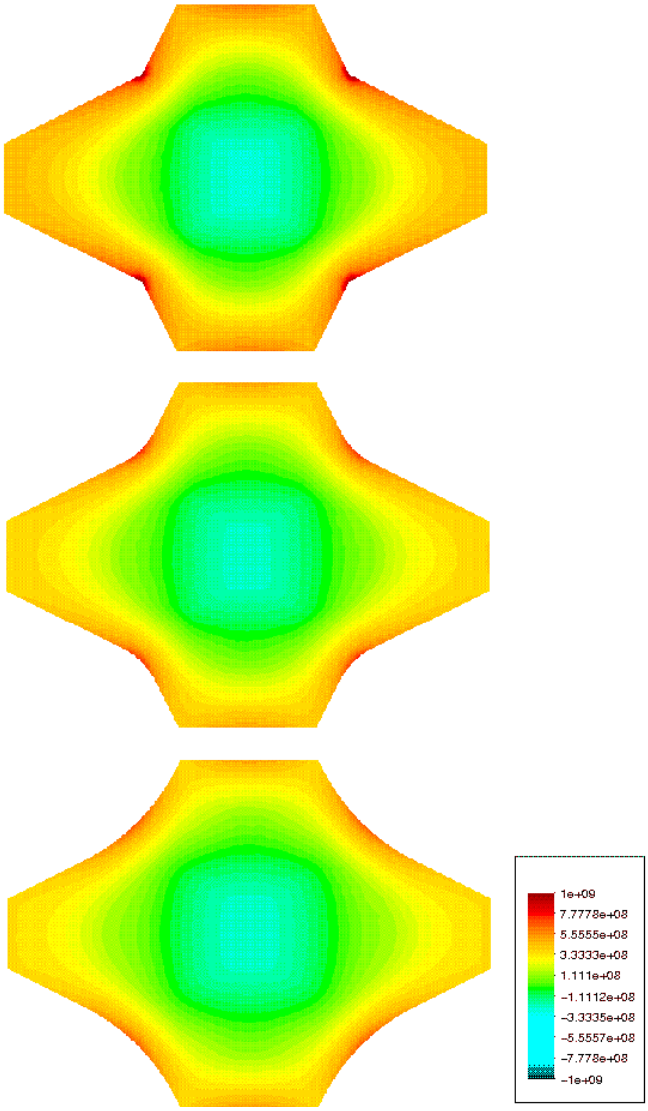

Figure 7.7: Qualitative Stress Distribution for Different Designs of the Re-Entrant Edges

Results

Results are shown for the time at which the core has just passed the phase change. In this situation the core is contracting while the surface has already cooled down to the prescribed ambient temperature and does not tend to

change its volume anymore. This leads to tensile stresses at the surface. Although these tensile stresses are much smaller than those obtained due to the phase change at the surface, they are not negligible. In the examinations up to now it has not been taken into account, that the material changes its properties after passing the phase change: It becomes brittle, while before reaching phase change temperatures it is more ductile. This means that at the observed moment, the brittle material is likely to break, especially at places where at an earlier stage some fissures due to high stresses might have appeared: the critical areas of the surface - the re-entrant regions.

Further examinations will give information about the influence of plasticity and time dependent properties, but already now the effect of relatively small variations in design on the straining at the critical stations gets qualitatively visible.

Chapter 8

Excavator Teeth - Plastic Case

Two new tooth designs were considered. These two teeth are designed for different usages - one for any kind of ground material, the other one for work at the sea ground. As the two geometries are very different and need different periods of time for the cooling, they were examined separately.

8.1 Standard Excavator Tooth

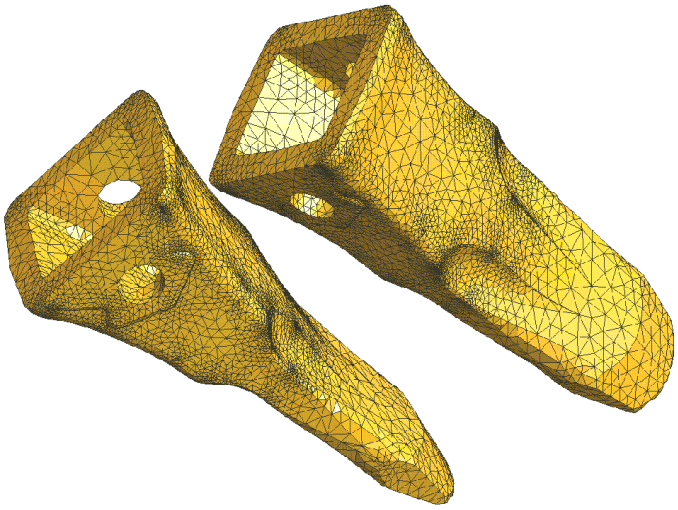

Figure 8.1: Standard Teeth

This type of tooth is produced in different sizes. In the examined case the tooth is about 32 cm long with a sidelength of 13 cm at the base and

it weights around 12 kg. This standard tooth is used for excavators which move different types of material.

8.1.1 Results

The results are observed in three cuts (*figure 8.2*), which are made with the same method as described in *chapter 7*.

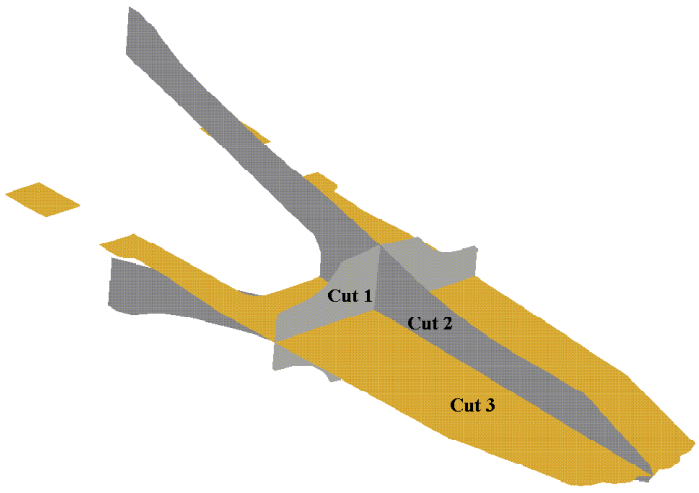

Figure 8.2: The Three Cuts Through the Tooth

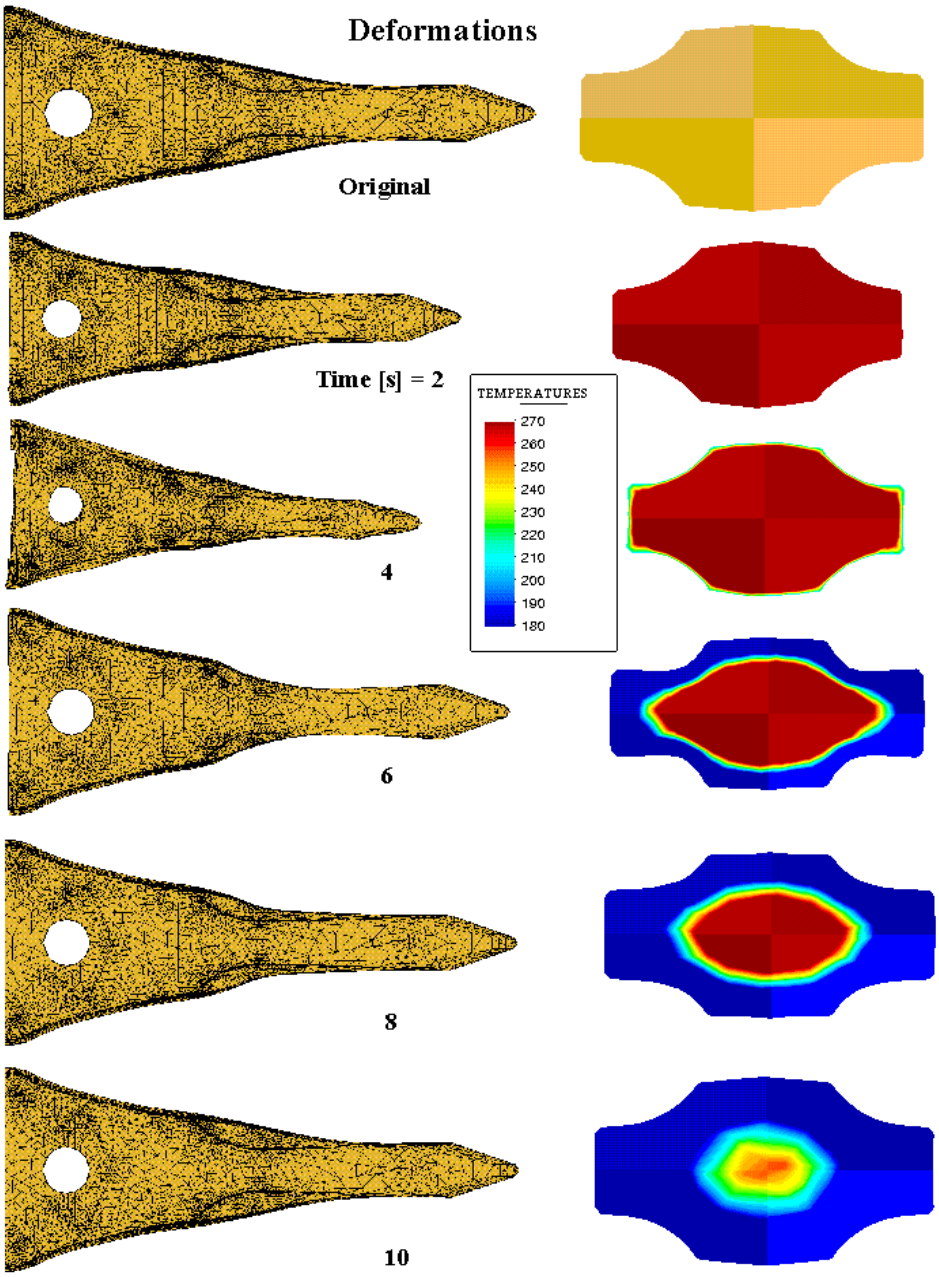

Figure 8.3: Deformations and Phase Change Temperature

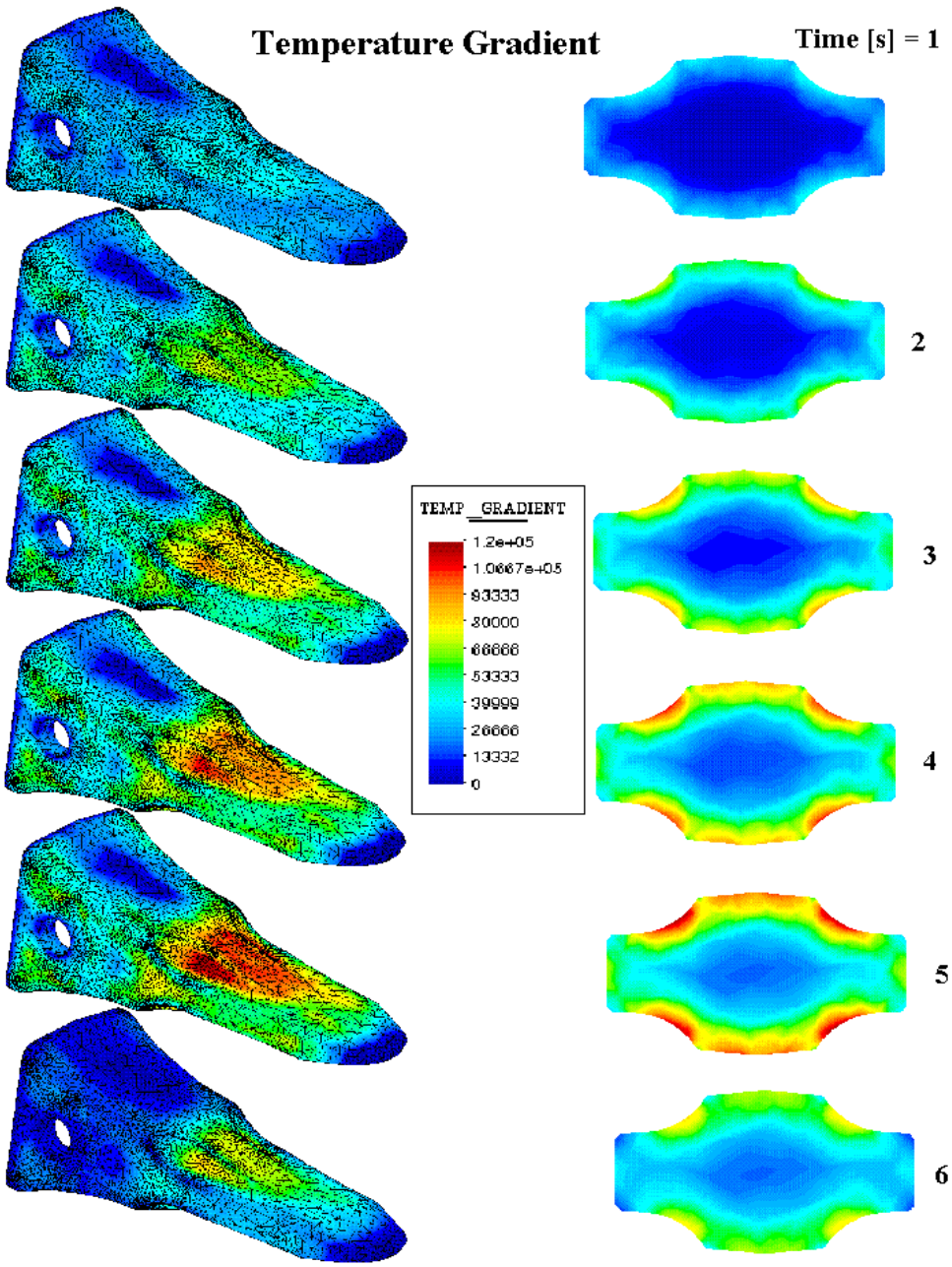

Figure 8.4: Temperature Gradient

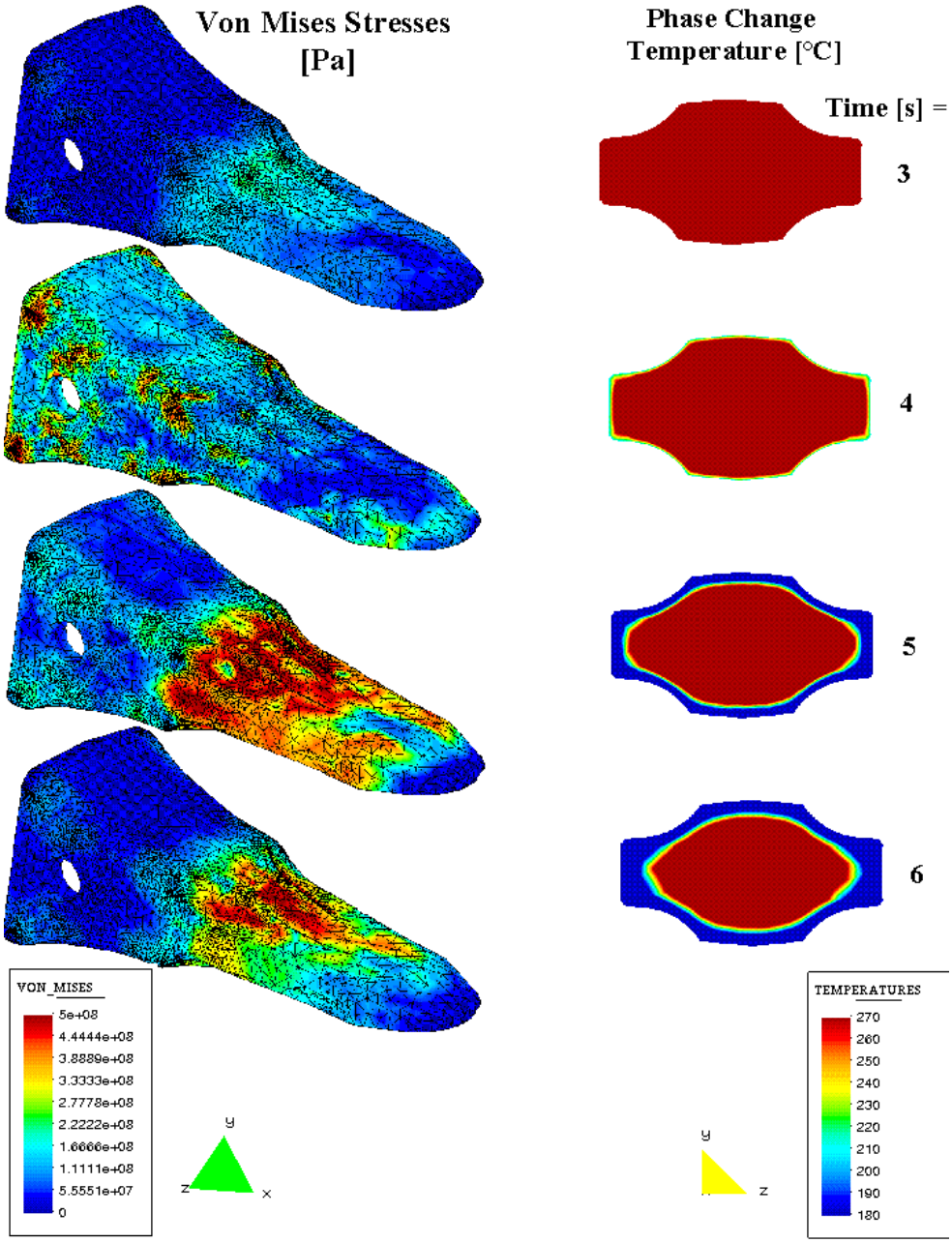

Figure 8.5: Von Mises Stresses (a)

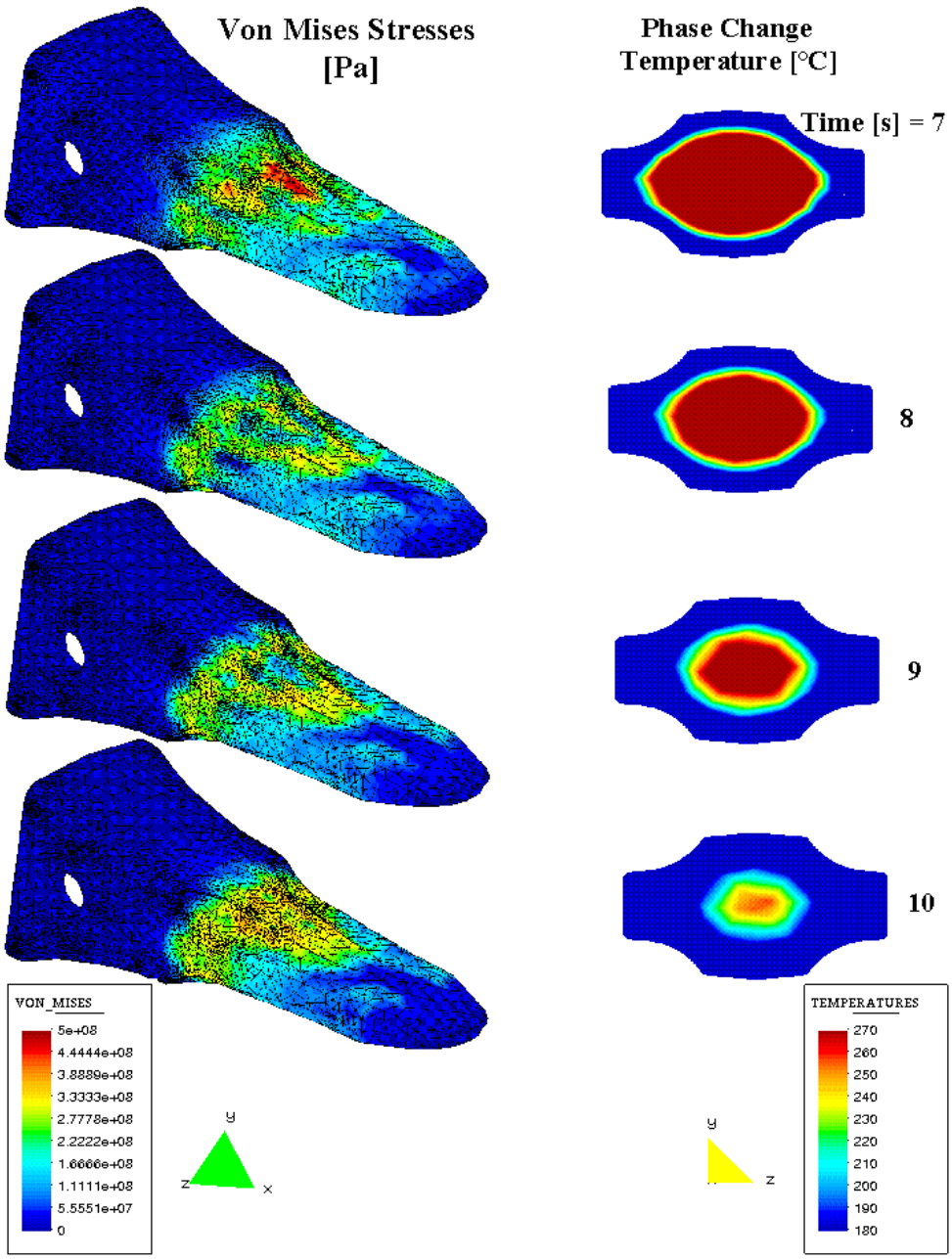

Figure 8.6: Von Mises Stresses (b)

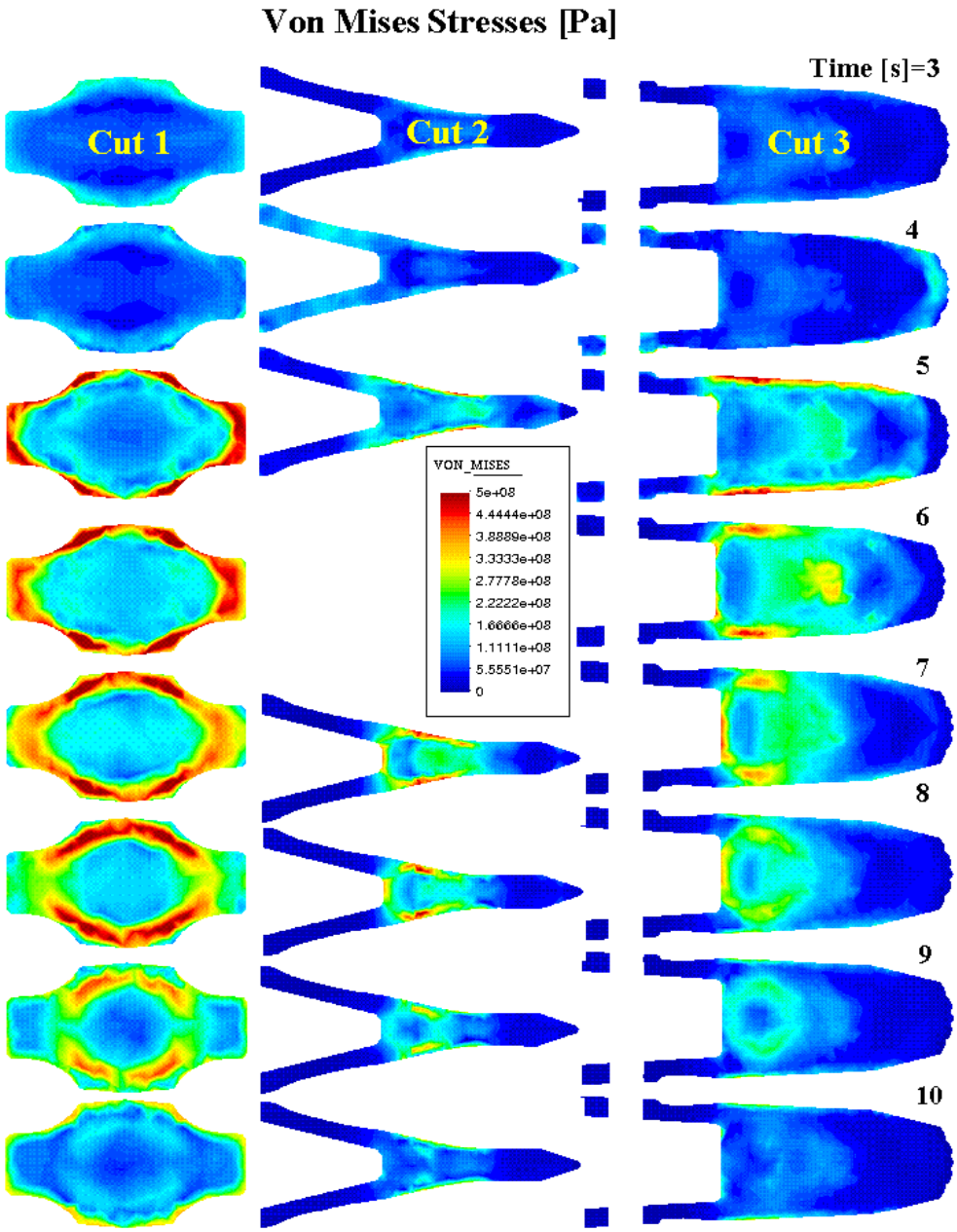

Figure 8.7: Von Mises Stresses (c)

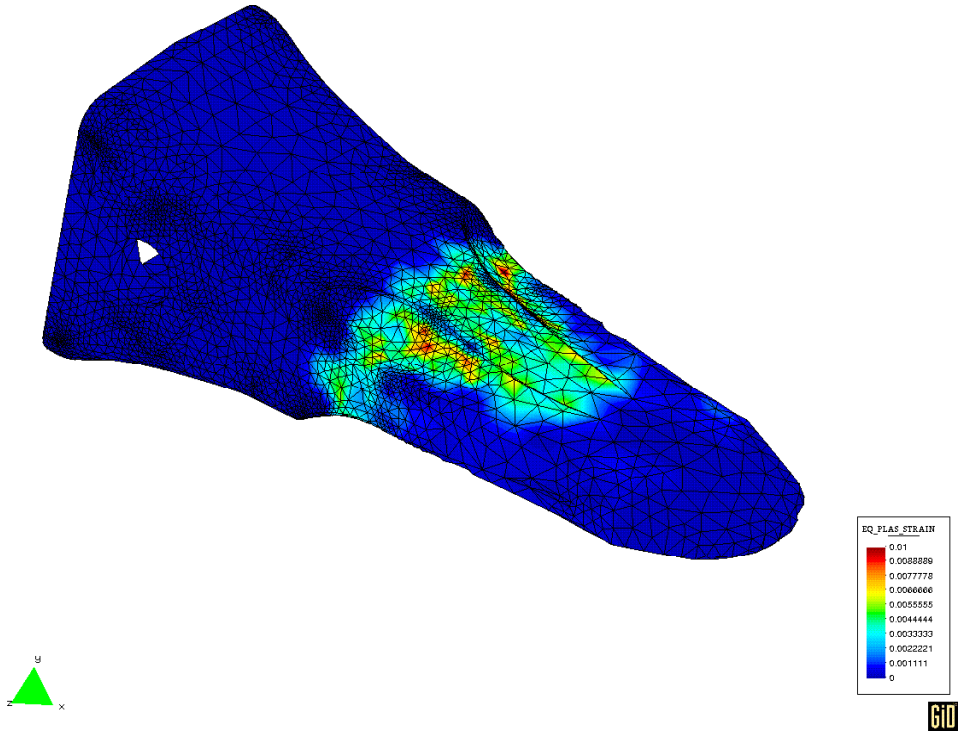

Figure 8.8: Equivalent Plastic Strain

Deformations (*Figure 8.3*):

The amplifying factor for the result plots is set to 40, like in the previous examples. The deformation plots of the entire body are compared to the phase change temperatures and the deformations of the cross section *cut 1*. The deformation of the tooth principally evolves according to the same scheme like for the cylinder. Before the surface enters the phase change, the tooth contracts. This contraction is not uniform throughout the body as the edges cool down from various sides and therefore contract quicker. Rounded shapes at time=2s are the result. The surface entering the phase change, the edges start to protrude again. The distorted geometry of the body at second 4 results from the fact that some parts of the surface have already passed the greater part of the phase change. Looking at the evolution of *cut 1* it can be noticed that the lateral parts of the piece expand quicker, as they cool down qicker than the upper and the lower surfaces. It comes to a momentary distortion of the cross section between seconds 6 and 8. When the core also

passes the phase change and expands, this distortion is mostly evened out.

Temperature Gradient (*Figure 8.4*):

Looking at the evolution of the temperature gradient, it strikes that in the center of the tooth near the re-entrant edges the highest temperature gradient developes. This phenomenon has already been explained for the elastic case: To these parts of the body heat is being supplied through a greater area - the inside of the part - as the one from which it is being dispelled - the surface. Therefore these areas of re-entrant edges are naturally cooling slower than flat or protruding parts of the surface. Looking at the temperature development of cut 1 (*figures 8.5 and 8.6*) it can be noticed that the lateral parts of the cut have already cooled down further while the center, especially the re-entrant edges still have a much higher temperature. High temperature gradients in this area are the result.

Von Mises Stresses (*Figures 8.5, 8.6 and 8.7*)

Figure 8.5 and 8.6 show the evolution of the *Von Mises stresses* over the surface in comparison to the phase change temperatures throughout *cut 1.* It is remarkable that the first stress peaks appear at the protruding parts of the tooth. These are the parts which are cooled down from various sides, therefore the expansion/contraction effects during cooling and phase change are intensified at these places as explained in *chapter 6.* The base part of the tooth, consisting of thin walls as the backpart of the tooth is hollow, cools quite uniformly and quickly. The stresses keep low while in the center, at the same places at which the highest temperature gradients appear, higher tensions develop. Inside the body passes the phase change and tries to expand while the outside contracts. Tensile stresses at the surface are the result. The higher the temperature gradient the higher values reach those stresses.

In *figure 8.7* the stress evolution of the three cuts can be observed. The highest stresses develop near the surface as the temperature gradients are much higher near the surface than in the more uniformly cooling inside of the tooth (compare temperature course, *figure 4.14*). Later on the stresses appear concentrated in the area of the body in which the phase change just passed. This area cools down and contracts while the immediately following area passes the phase change and expands, like already explained for the plastic case of the cylinder (*chapter 5.2.1, figure 5.9*) High compression in

the contact area is the result.

Equivalent Plastic Strains (*Figure 8.8*):

To get an impression of the plastified areas, it is sufficient to look at the plot of the last time step, which shows all the areas which plastify and the corresponding intensities. It is clear that the plastification appears in the area in which the highest stresses occured during the second part of the cooling - when the body already passed the phase change and the initial yield stress limit is lower in comparison to the cooling phase before the phase change.

8.2 Dredger Tooth

This type of tooth is used to work at the ground of the sea. It is installed at a cutterhead of a dredger. This cutterhead works as a mechanical tool which is rotated and pressed against the sea ground. This way it tears out material from the sea ground which is extracted to the surface by a pump system. You can see such a cutterhead in *figure 8.8*. The tooth (*figure 8.9*) is about 35 cm long and 20 cm high. Its weight is 21 kg. Compared to the standard tooth discussed above (12kg) it has a much bigger volume. Unlike the previous examples, this tooth has a unsymetrically placed hole to fix the tooth at the cutterhead.

Figure 8.9: View of a cutterhead

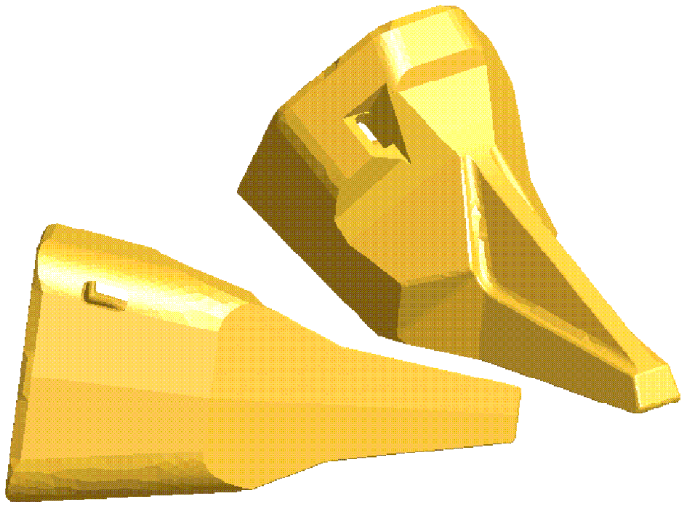

Figure 8.10: Dredger Teeth

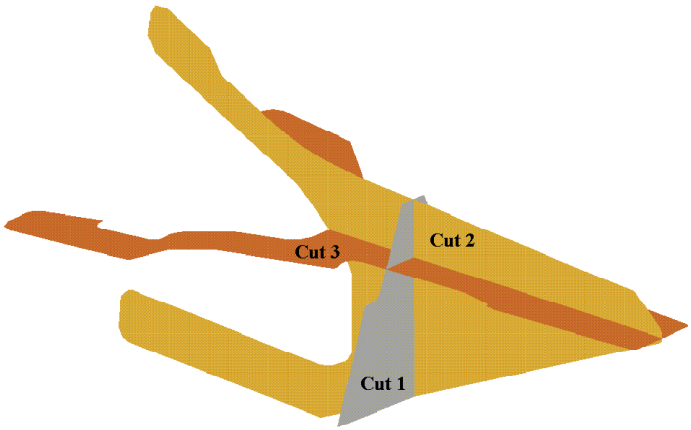

Figure 8.11: Three Cuts through the Tooth

Examining these three cuts (*figure 8.11*) one can get a good impression of the result progression throughout the different parts of the tooth. *Cut 1, 2* and *3* give information about the upper part of the tooth, where the cross section is very narrow, *cut 1* and *2* about the lower, much broader cross section, *cut 2* and *3* about the front and the back part of the body.

8.2.1 Results

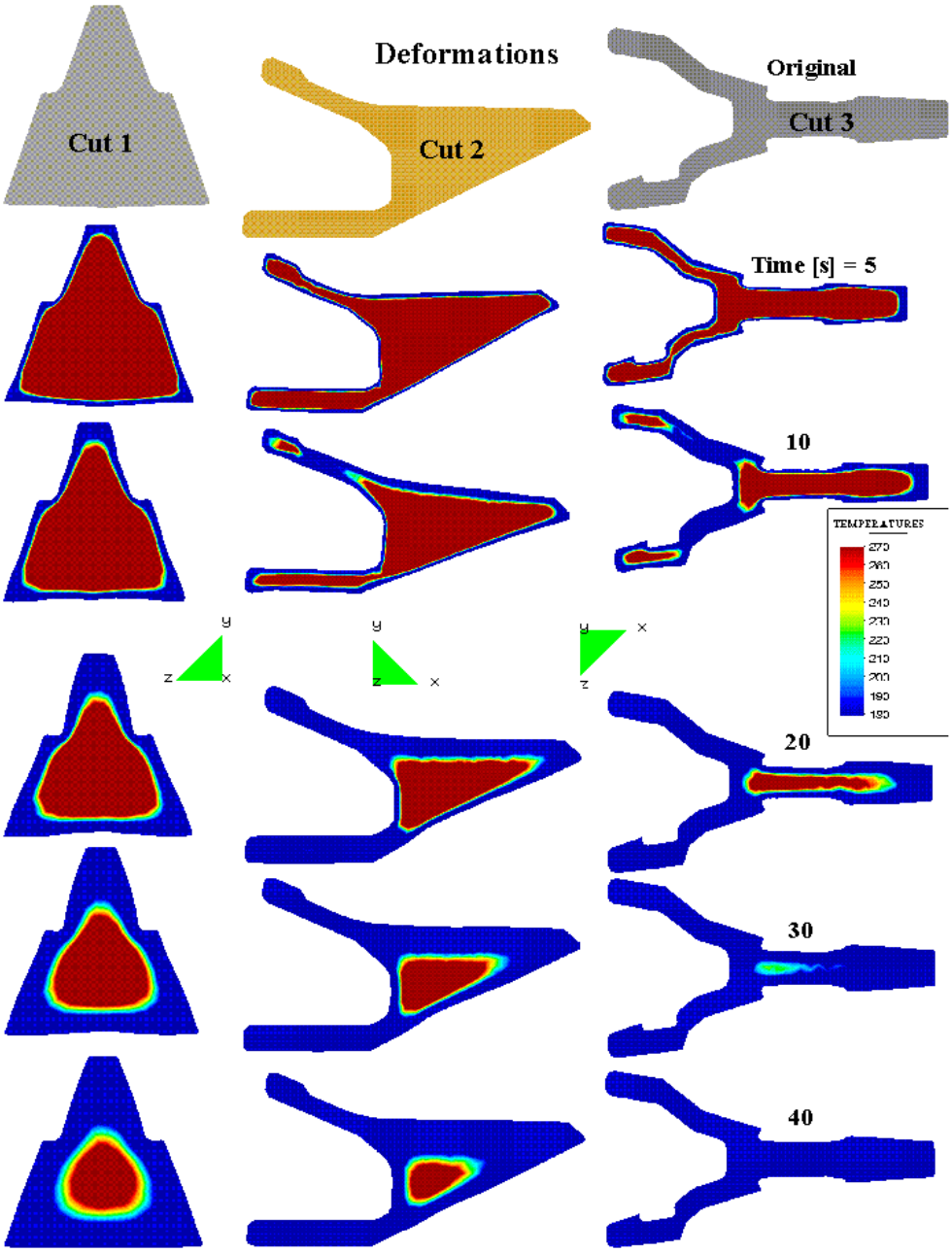

Figure 8.12: Deformations and Phase Change Temperature

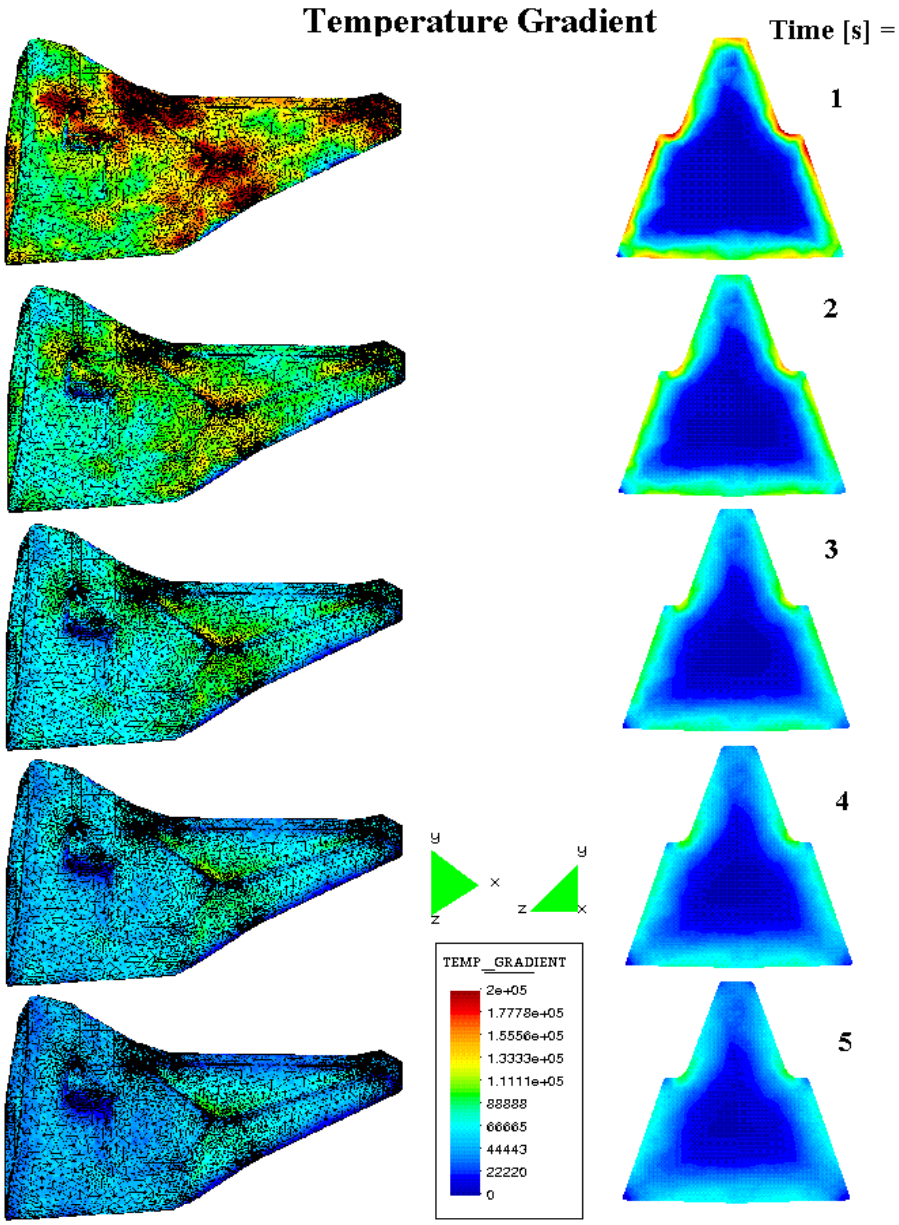

Figure 8.13: Temperature Gradient

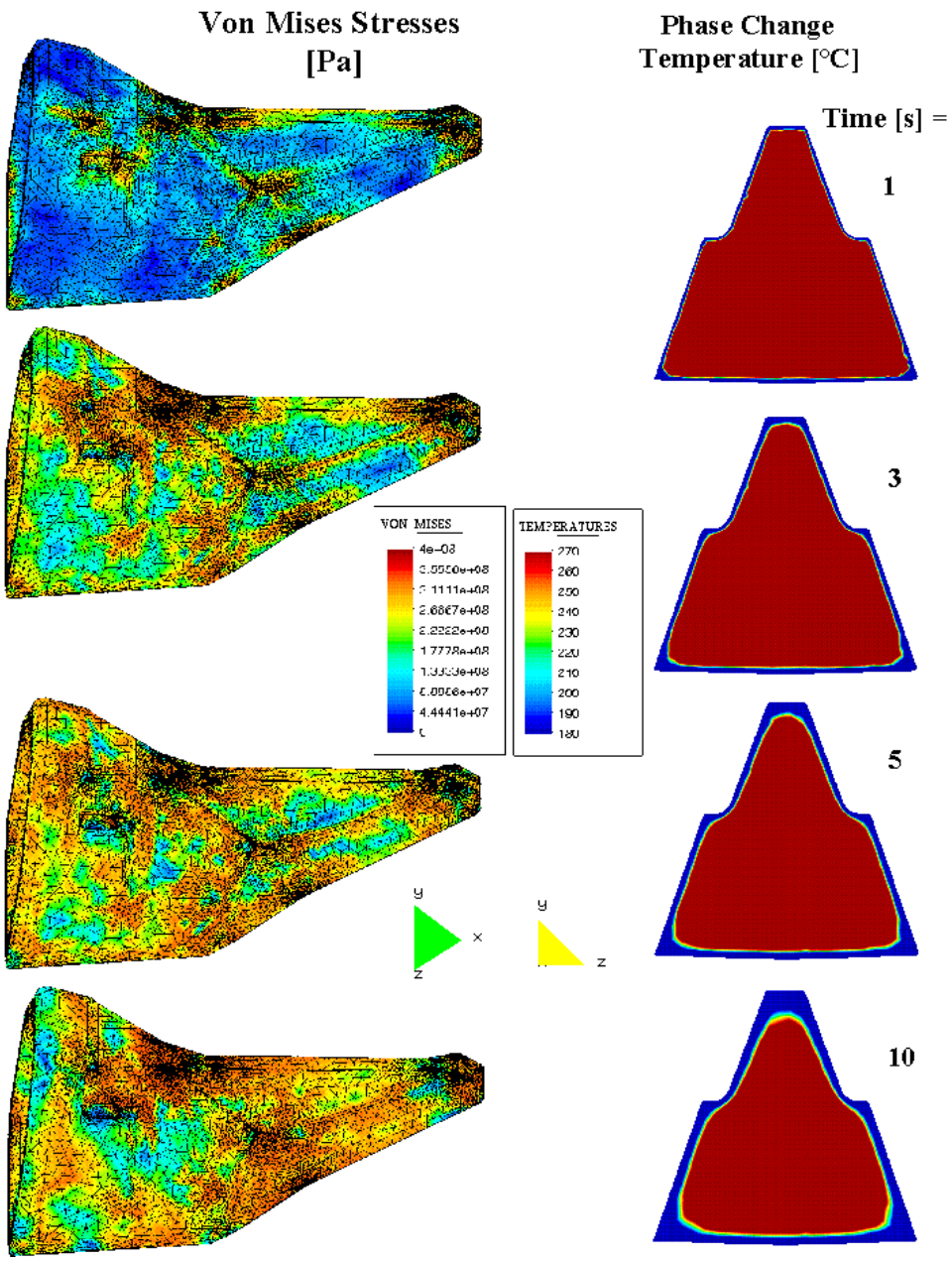

Figure 8.14: Von Mises Stresses (a)

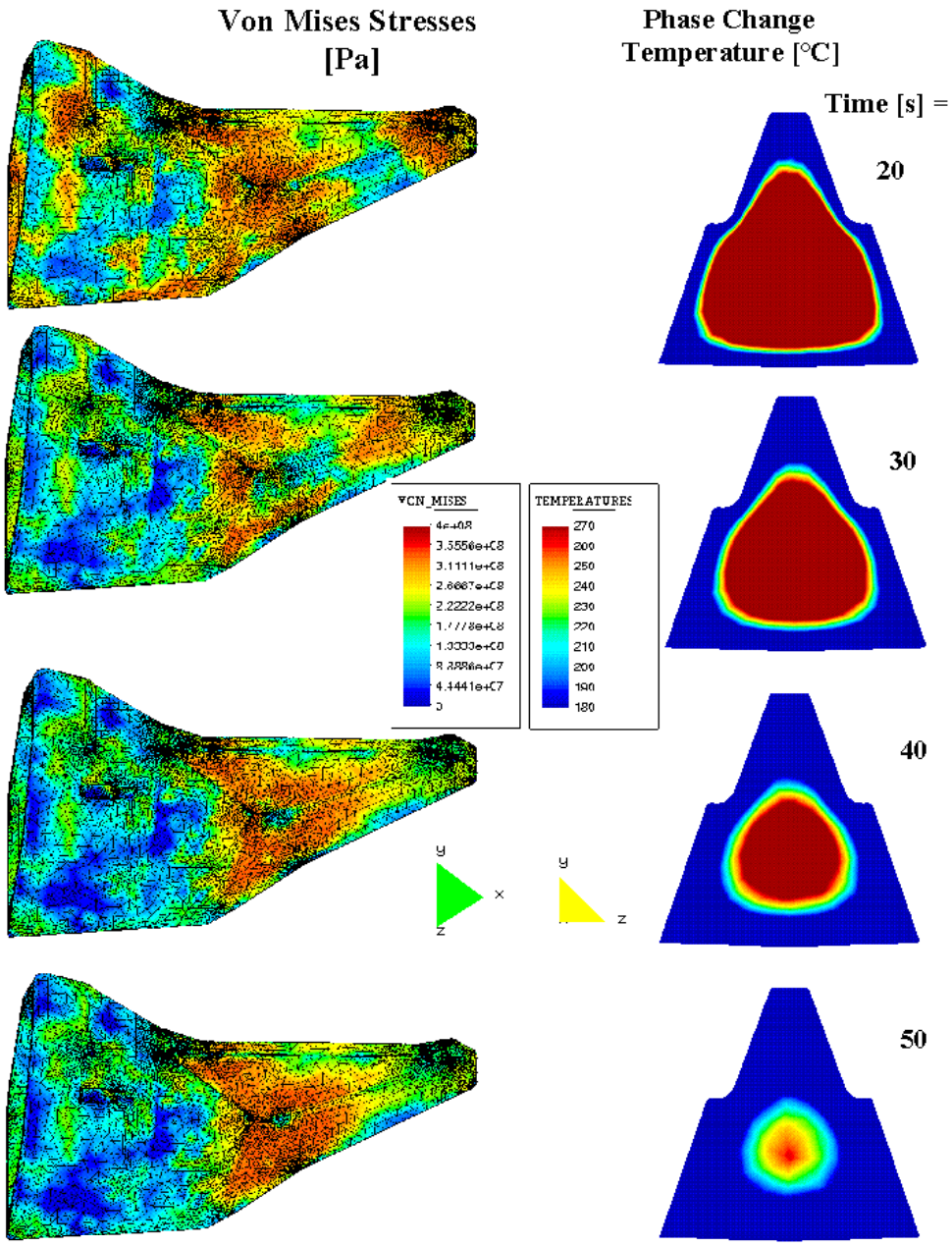

Figure 8.15: Von Mises Stresses (b)

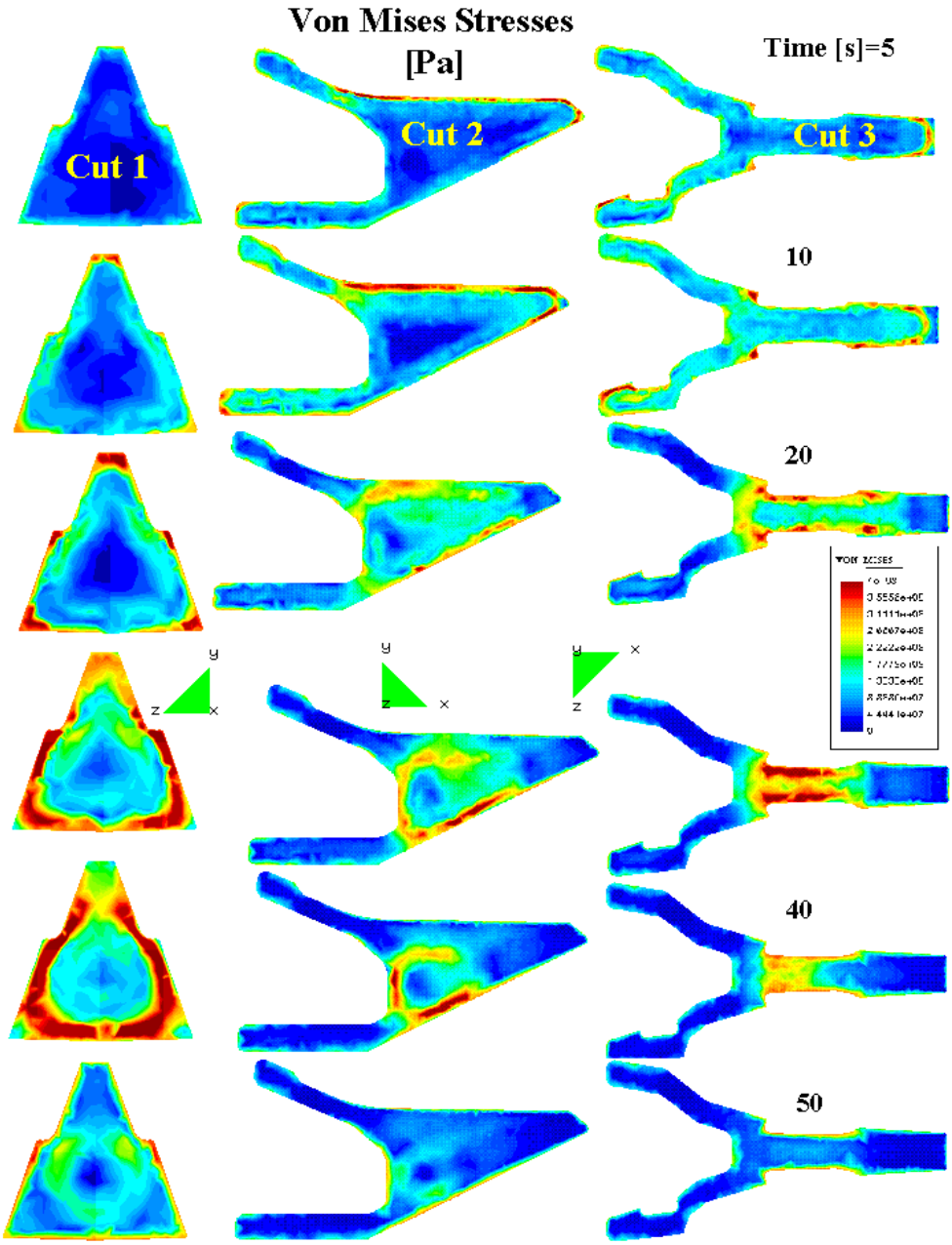

Figure 8.16: Von Mises Stresses (c)

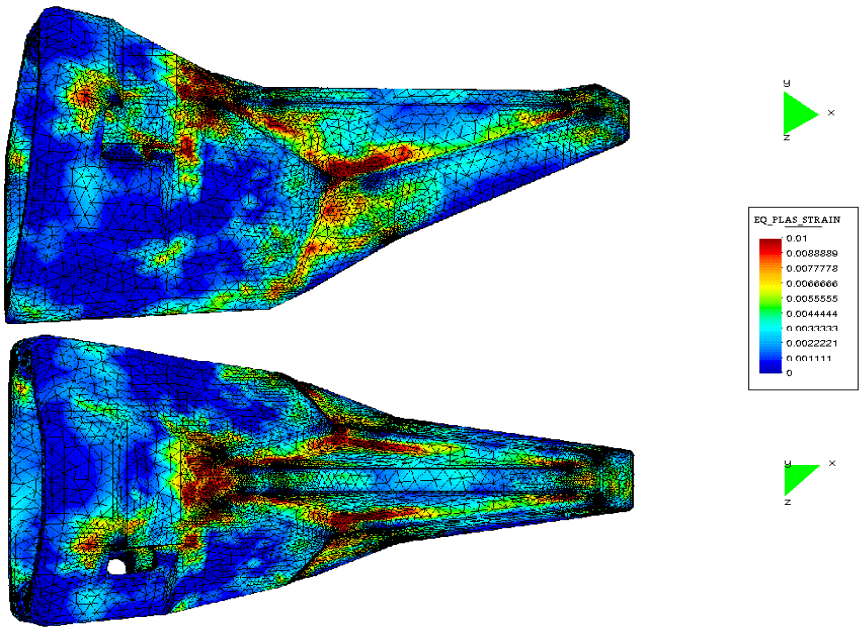

Figure 8.17: Equivalent Plastic Strain

Note that in this example the number of elements is twice as high as in the previous ones. Looking at the GiD-plots it can be noticed that the result-distributions already are a lot smoother although in some critical areas the geometry of the single element can be recognized.

Deformations (Figure 8.12):

As the geometry of this dredger tooth is quite complex, it is difficult to observe the single deformation steps for the whole body. The deformations seem to remain quite small, and hardly any characteristic changes of the shapes become visible. Therefore the evolution of the deformation was examined for three cuts. At the same time the progression of the phase change throughout the cuts was observed.

Examining the cooling progression it strikes that the back part of the tooth cooles down first. As explained in *chapter 7*, thinner parts like the pointed end or the hollow back part pass the cooling process clearly quicker than the massive core. This is because the thinner parts are cooled from more than one side at the same time.

Comparing the three cuts it can also be noticed that the upper, narrow part of the tooth cools much quicker than the lower for the same reason.

Concerning the deformation, the basic developments are similar to the previously examined geometries. Although in this new case some interesting new characteristics can be observed. The plots of *cut 1* show how the upper part of the body reaches a more and more bulbous shape. This is due to the expansion of the body in the center of the cross section while the top area contracts. Moreover it can be remarked how the lower edge of *cut 2* curves in at the t=30s. Looking at the area of the cut which passes the phase change temperature and expands at this time step, it can be noticed that to both sides of this curve the phase change area is bigger than in the center. The sides expand stronger than the center, a re-entrant curvature results.

Temperature Gradient (Figure 8.13):

To observe the progression of the temperature gradient, the same scale as for the previous example is used. The highest temperature gradient appears at the beginning of the process, afterwards the gradient diminuishes with each time step and already at second 5 there are hardly any gradient peaks visible any more. The critical areas appear to be those where the geometry is especially complex as to speak in the areas of re-entrant and protruding edges and corners as well as near the hole. Comparing to the temperature gradient course of the previous example the time development is distinct. While in the previous case the highest temperature gradients appeared at second 5, here the critical time step is already at t=1s. This can be explained by looking at the temperature course of *figures 8.14* and *8.15* in comparison to the one of *figures 8.5* and *8.6*. The surface of the dredge tooth passes the phase change temperature by far quicker than the surface of the previously examined tooth, which has to be related to the distinct surface characteristics. Later on the body cools down slower. It takes more than 50 seconds for the body to pass the phase change, whereas in the case of the standard tooth example it only took about 11 seconds.

Von Mises Stresses (Figures 8.14, 8.15 and 8.16):

The values used in the scale for the plot of the Von Mises stresses are lower than for the last example, which means that the stresses are smaller. This is due to more massive cross sections (compare the cuts of *figure 8.16* with the ones of *figure 8.7*). The first stress peaks (t=1s) appear in the areas where are also the highest temperature peaks (t=1s) are noticed. Later on the

stress distribution becomes quite extensive - the stress peaks near the edges and corners extend over a big part of the surface (t=10). Finally, the stress peaks can be observed in those areas where the core of the body still passes the phase change (t=40s and t=50s), here again the highest concentrations are in the areas of re-entrant angles as the smaller surface is exposed to the same tensions like the more extensive surface near protruding parts of the geometry.

Equivalent Plastic Strains (Figure 8.17):

The equivalent plastic strains are plotted at t=50s for two different perspectives of the body. Like this the critical zones of the whole body become visible. They are situated near re-entrant angles and the hole. Comparing the plastified zones of this geometry with the ones of the standard tooth it strikes that here bigger areas plastify to a higher level. On the other hand the stress plots showed that the stresses of this example reach lower values. This phenomenon can be explained by the temperature dependent material properties: At a later state of the cooling, when the body passes or passed the phase change, the stress limit for plastification (initial yield stress) takes on lower values (see *chapter 5*), the body plastifies more easily. As in this example high stresses remain after having passed the phase change, the plastification is more extensive even though the maximum stresses of the whole process keep lower than in the case of the standard tooth.

Chapter 9

Conclusions and Lines for Future Work

This work documents the application of a finite element program to the solution of the industrial problem of Heat Treatment Processes on Steel Parts. With the results obtained, conclusions are drawn about lines for future work. The realizations can be divided into three sectors:

- the thermo-mechanical *material behaviour*
- information about the *design optimization*
- characteristics of the *finite element numerical program* in relation to the examined cases

9.1 Conclusions

Material Behaviour As a first step the material behaviour is analyzed by focusing in the cooling process in different steps. It is obvious that the combination of high temperature gradients induced by rapid cooling and the straining due to the phase change generate high stresses. A stress wave passes through the body simultaneously to the phase change. Splitting the analysis, the detailed mechanical behaviour can be stated. As a next step plasticity of the material and temperature dependence of the material properties are considered. The result of deformation development, stress distribution and location of plastic strains gives a good insight on the material behaviour in dependence on the given properties.

Design Optimization With the elastic analysis it is possible to show how specific variations in design change the stress development. The plastic analyses of various geometries - cylinder, cube, teeth designs - allow to draw detailed conclusions about the different effects of design variation. Starting with the cylinder and the cube, the basic effects of the analysis are observed. These basic informations help to interprete the complex geometries of the two tooth designs and to compare their results: Deformation development, stress distribution and location of plastic strains are examined in relation to each other and this way give informations about the weak areas of the design. It can be predicted where the body is most likely to break.

Finite Numerical Program It is possible to simulate the quenching process and to visualize the results in various ways. To get a general impression of the process, it is sufficient to use the graphical postprocessing devices. Examining the results closer, it gets evident that above a certain cooling speed overshoots occur in the resulting curves. Due to the convergence of the program to the true value there are two possibilities to improve the results:

- improving the quality of the mesh by increasing the number of elements, and
- application of a smaller time step for the critical initial phase of the process

For the plastic analysis the program enables a split of the resulting strain into its single components. This possibility is used to get an insight about the interactions of elastic, plastic, thermal and viscous influences on the results.

9.2 Lines for Future Work

Material Behaviour To make more detailed statements about the material behaviour, it is necessary to get further informations about the mechanical characteristics. These informations have to be provided by material specialists, who have appropriate experience and knowledge in this field.

Design Optimization For a better analysis of the effects of variations in design, the mesh criteria have to be improved. A first approach already was made by using a twice as fine mesh in the plastic example of the dredge tooth. As a next step it is advisable to use a finer mesh at the surface, where the cooling advances with higher speed. Moreover, it would be interesting to use a mesh of different shaped (i.e. hexahedral) elements.

Further on, more details of the conditions during the quenching process can be applied. Those details are received by the experience of the manufacturing specialists. To name one example, the real cooling temperatures vary over the surface of the bodies: While the outer surface is cooled as applied, inside the cavities, where the water stays in, the cooling takes place much slower.

Principally the examination of different designs has to be continued- many more examples have to examined and the results compared with each other - this way a better understanding of the effects of design variations on the distribution of problem zones and shapes can be reached.

Finite Numerical Program This requirement is also important to reach more informations about the characteristics of the numerical program. Moreover it would be helpful to analyse in a detailed manner the course of result graphs of the plastic cases like it has been done for the elastic cylinder and partly also for the plastic cylinder. This way a better understanding of the interaction of elastic, plastic, thermal and viscous influences on the results can be reached.

To sum up, one can say that the step-by-step analysis provided in this work is a suggestive method, to get a detailed knowledge of the application difficulties and to prevent the user from jumping to conclusions. It is advisable to continue with this method for further examinations.

Like this the application of the program in its whole variety becomes a valuable contribution to a successful, time- and cost-saving manufacturing.